NTNU

Norwegian University of
Science and Technology

Earthquake Response of Different Types of Retaining Walls

Anuj Thapa Magar

Geotechnics and Geohazards
Submission date: June 2016
Supervisor: Gudmund Reidar Eiksund, BAT
Co-supervisor: Amir M. Kaynia, NGI

Norwegian University of Science and Technology
Department of Civil and Transport Engineering

Abstract

Retaining walls are designed to restrain against the lateral earth thrust while keeping its original position intact. During an earthquake, the lateral earth thrust increases and the walls become susceptible to failure which has resulted in frequent damages of the walls. This thesis studies the earthquake response of different types of retaining walls where a comparative study of these walls have been carried out in terms of the stability and performance under the earthquake excitation with the help of a finite element program, PLAXIS 2D. The different walls analyzed are the gravity, gabion and cantilever wall. In addition, parameter studies have been performed for a gravity wall to understand the effect of different parameters.

Prior to the analysis on the retaining walls, two different tests have been performed for analyzing the boundary conditions. To verify the model in PLAXIS, the results have been compared with the test results of the physical shake table test of a scaled retaining wall.

For the parameter studies, there different height of the wall (3.5, 4 and 5 m), three different backfill angles (32°, 35° and 38°) and three different backfill slope (1/15, 1/10 and 1/5) with four different PGA levels (0.05g, 0.1g, 0.15g and 0.2g) have been taken. For the variation of earthquakes, three different earthquakes have been used. The results are compared with the total force on the wall and the permanent displacement of the wall for different cases. The total force and the displacement of the wall increase with the increase of the wall height or backfill slope whereas decreases with the increase in the backfill

friction angle. The total force from the PLAXIS is also compared to that from M-O method which showed a large variation. It again highlighted the fact of M-O method being a conservative design method but with more appropriate input acceleration, the performance of the M-O method can be improved.

The comparative study of different walls showed that the total force for the gabion wall is lower than the gravity wall while the cantilever wall has the lowest total force. Also, the permanent displacement is lower in the gabion wall than the cantilever wall whereas the gravity wall has displaced the most in all the cases. Overall, the cantilever wall provided the better stability and performance under the earthquake excitation for the wall height of 4 m and PGA level up to 0.2g. In addition, considering the cost effectiveness, construction easiness and material volume, cantilever wall could be the most appropriate solution among the three types of retaining walls. Furthermore, the gabion wall also showed good anti-seismic characteristics and performed better than the gravity wall. The future work could be to perform more parameter studies such as the different height of the wall and higher PGA level than 0.2g for analyzing different walls.

Acknowledgment

This Master's thesis was conducted at the Department of Civil and Transport Engineering at Norwegian University of Science and Technology (NTNU) during the spring semester of 2016.

I would like to express my sincere gratitude to my supervisors Adjunct Professor Amir M. Kaynia, Department of Structural Engineering at NTNU and Professor Gudmund Reidar Eiksund, Department of Civil and Transport Engineering at NTNU for their continuous support, guidance and valuable suggestions throughout the thesis.

I would also like to thank Professor Steinar Nordal, Department of Civil and Transport Engineering at NTNU for his moral support and valuable suggestions. Also, the help from all the masters student of the Geotechnical Section at NTNU has been vital in the preparation of this thesis.

I am thankful to my family for their continuous support and love throughout my studies.

Finally, I would like to thank and acknowledge all the people who have helped me directly or indirectly in developing this thesis.

Trondheim, 23 June 2016

Anuj Thapa Magar

Contents

List of Figures

List of Tables

Chapter 1

Introduction

1.1 Background

Retaining walls are susceptible to failure during earthquakes and are damaged frequently. Failure mechanism could be sliding, tilting, bending or bearing which is the result of the shear stresses being greater than the shear strength of the soil. Under the static conditions, the properly designed retaining wall will achieve equilibrium of the forces that are acted upon by the body forces related to the mass of the wall, soil pressures, and other external forces but during an earthquake, it may cause the permanent deformation of the wall due to violation of equilibrium from inertial forces and changes in soil strength (Kramer, 1996). This permanent deformation might cause a failure with at least any one of the above-discussed failure mechanism. Hence, the study of a response of the retaining walls under the earthquake excitation becomes mandatory.

The most commonly adopted retaining walls in practice are gravity walls,

gabion walls and cantilever walls. In the past, the study of earthquake response of these individual walls has been done by many researchers. Veletsos and Younan (1997) illustrate their elasticity-based analytical work on designing a cantilever wall against earthquakes while Green et al. (2003) and Psarropoulos et al. (2005) study the seismic earth pressure on the flexible retaining walls by finite element method. Furthermore, Yang et al. (2010) claims the reinforced gabion retaining walls to be a very good anti-seismic structure based on the different tests carried out. So it would be of great interest to perform a comparative study of these walls under the earthquake excitation.

This thesis studies the earthquake response of different types of retaining walls (gravity, gabion and cantilever wall) where a comparative study of these walls have been carried out in terms of the stability and performance under the earthquake excitation by finite element method. In addition, parameter studies have been conducted to account for the effect of different parameters such as the height of the retaining wall, the friction angle of the backfill and the backfill slope. The results are also compared with the classical design method, Mononobe-Okabe (M-O) method. Previous studies such as Green et al. (2003) and Ostadan (2005) suggest that the M-O method to be nonconservative whereas Gazetas et al. (2004) and Psarropoulos et al. (2005) suggest the method to be conservative. Hence, the results will be useful in analyzing the M-O method as well.

1.2 Objectives

The main objective of this thesis is to perform a comparative study of different types of retaining walls under earthquake excitation. The different types of walls are gravity, gabion and cantilever wall and these retaining walls have a similar factor of safety under static condition. The aim is to find the best solution for the wall among these three walls by analyzing their stability and performance under the earthquake excitation.

In addition, it is of great interest to study the effect of different parameters such as the height of the wall, friction angle of the backfill, backfill slope and different PGA levels of the earthquake on the stability and performance of the retaining wall under the earthquake excitation.

1.3 Approach

All the numerical analysis for the thesis will be performed in the finite element program, PLAXIS 2D. First, before performing any analysis on retaining walls, the analysis of boundary condition will be performed for different boundary conditions provided in PLAXIS 2D. This analysis will help to select the best boundary condition among the different alternatives and also to use it properly in order to get a better output for the further analysis.

Furthermore, a verification of the numerical model with shake table test will be performed. This test will be relevant in verifying and analyzing the performance of the numerical model.

Then, the numerical analysis of a gravity wall with sand backfill will be performed. Four different levels of PGA will be used to analyze the effect of different parameters such as the height of the wall, friction angle of the backfill, backfill slope, on the stability and performance of the gravity wall under earthquake excitation.

Finally, the analysis of three different types of retaining walls: gravity, gabion and cantilever wall will be carried out. The comparison of the results will be done in terms of stability and performance under the earthquake excitation. This comparative study will be helpful in selecting the best option among the three alternatives. The thesis will be concluded with the summary of all the results, conclusion and further recommendations.

1.4 Structure of the report

The thesis is divided into the following nine chapters:

- Chapter 1: Introduction

  This chapter provides the basic introduction to the research topic. The objectives of the research topic and approach to the topic are introduced. A short outline of the thesis is presented to provide an overview for the reader.

- Chapter 2: Literature Review

  This chapter presents the theories and literatures reviewed to carry out all the numerical analysis.

- Chapter 3: Analyzing Boundary Conditions

  The analysis of different boundary conditions available in PLAXIS 2D are presented in this chapter.

- Chapter 4: Verification of Numerical Model with Shake Table Test

  This chapter presents the verification of numerical model with physical shake table test. The verification is done by comparing the PLAXIS 2D results with the real test output.

- Chapter 5: Numerical Modeling of Gravity Wall

  This chapter provides a base case for numerical modeling of retaining wall. All the further analysis of different walls are similar to the analysis that is carried out in this chapter.

- Chapter 6: Parameter Studies

  The effect of different parameters on the gravity wall has been studied in this chapter.

- Chapter 7: Comparison of Different Types of Retaining Walls

  The comparison of different types of retaining walls under earthquake excitation is presented in this chapter.

- Chapter 8: Summary and Conclusions

- Chapter 9: Recommendations and future work

Chapter 2

Literature review

2.1 Earthquake Response

This section discusses the theories regarding basic dynamics and earthquake response. First is the brief description of the Equation of motion and then followed by Earthquake excitation, Damping and Shear modulus.

2.1.1 Equation of Motion

The equation of motion for the undamped free vibration with single degree of freedom (SDOF) is

$$m\ddot{u}(t) + ku(t) = 0 \tag{2.1}$$

where, m and k are the mass and stiffness of a system, $\ddot{u}(t)$ is the acceleration and $u(t)$ is the displacement of the mass. For SDOF system, there is only one

equation of motion and only one parameter is enough to find the response of the system. In the case of multiple degrees of freedom (MDOF) system with 'n' degree of freedom, there will be n numbers of equation of motions with n natural frequencies, modes of vibrations, modal masses and damping ratios and the parameters in Equation 2.1 will be all matrices (Chopra, 2012).

2.1.2 Earthquake Excitation

When an earthquake excitation is given to a system as in Figure 2.1, then the total displacement $u_t(t)$ is the sum of both due to the ground acceleration $u_g(t)$ and column deformation $u(t)$, see Equation 2.2.

$$u_t(t) = u_g(t) + u(t) \tag{2.2}$$

After taking double derivate acceleration can be obtained and making the equation similar to that of Equation 2.1, it becomes

$$m\ddot{u}_g(t) + m\ddot{u}(t) + ku(t) = 0 \tag{2.3}$$

Arranging the Equation 2.3 with excitation on the one side and response on the other side, it becomes

$$m\ddot{u}(t) + ku(t) = -m\ddot{u}_g(t) = P(t) \tag{2.4}$$

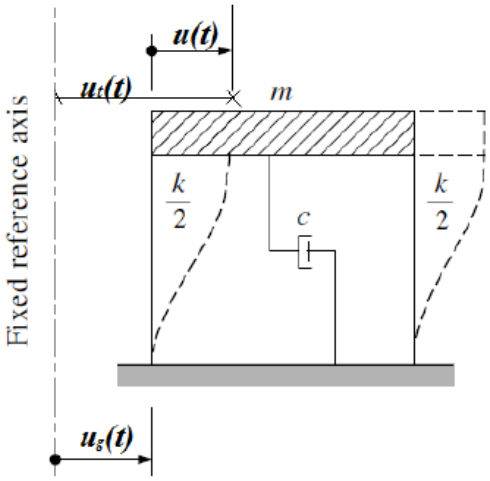

Figure 2.1: Earthquake excitation on a mass spring system (Clough and Penzien, 1993)

Here, $-m\ddot{u}_g(t) = P(t)$ is the external force due to the earthquake excitation. The response of the system can be obtained by integrating step by step.

2.1.3 Damping

'The process by which free vibration steadily diminishes in amplitude is called *Damping* (Chopra, 2012). With the inclusion of damper, the equation of motion becomes

$$m\ddot{u}(t) + ku(t) + cu(t) = P(t) \tag{2.5}$$

where c is the damping coefficient and $u(t)$ is the velocity. For the dynamic analysis, the damping can be introduced as a Rayleigh damping. The Rayleigh damping consist of a damping matrix C composed of the portion of both mass matrix M and stiffness matrix K (Brinkgreve et al., 2014c), see Equation 2.6.

$$C = \alpha M + \beta K \tag{2.6}$$

Here, α and β are the rayleigh coefficients which determines the influence of mass and stiffness in the damping of the system. Brinkgreve et al. (2014c) presents the relation between α and β with damping ratio (ξ) as:

$$\alpha + \beta\omega^2 = 2\omega\xi \tag{2.7}$$

$$\omega = 2\pi f \tag{2.8}$$

Here, ω is the circular frequency and f is the natural frequency. The damping coefficients can be found if the Equation 2.7 is solved for two different target frequencies and corresponding target damping ratios, see Equation 2.9 and 2.10.

$$\alpha = 2\omega_1\omega_2\frac{\omega_1\xi_2 - \omega_2\xi_1}{\omega_1^2 - \omega_2^2} \tag{2.9}$$

$$\beta = 2\frac{\omega_1\xi_1 - \omega_2\xi_2}{\omega_1^2 - \omega_2^2} \tag{2.10}$$

Hudson and Beirkae (1994) and Hashash and Park (2002) explains that the first target frequency can be taken as the first natural frequency f_1 and the second target frequency is taken as the closet odd integer larger than the ration f_p/f_1 i.e. the ratio of predominant frequency of the input motion to the natural frequency of the soil. The natural frequency of the soil of thickness H can be obtained from the Equation 2.11.

$$f_1 = \frac{v_s}{4H} \tag{2.11}$$

where, v_s is the shear wave velocity on the soil deposit.

2.1.4 Shear Modulus

A hysteresis loop as shown in Figure 2.2 might be exhibited by a typical soil subjected to symmetric loading beneath a level ground surface far from adjacent structure. Inclination and its breadth of a hysteresis loop are its two important characteristics. The inclination of the loop at any point during loading is dependent on the stiffness of the soil and can be described by tangent shear stiffness (G_{tan}). This G_{tan} varies throughout a cycle of loading but its average value over the entire loop can be approximated by the secant modulus (G_{sec}) (Kramer, 1996), see Equation 2.12.

$$G_{sec} = \frac{\tau_c}{\gamma_c} \tag{2.12}$$

where, τ_c and γ_c are the shear stress and shear strain amplitudes respectively.

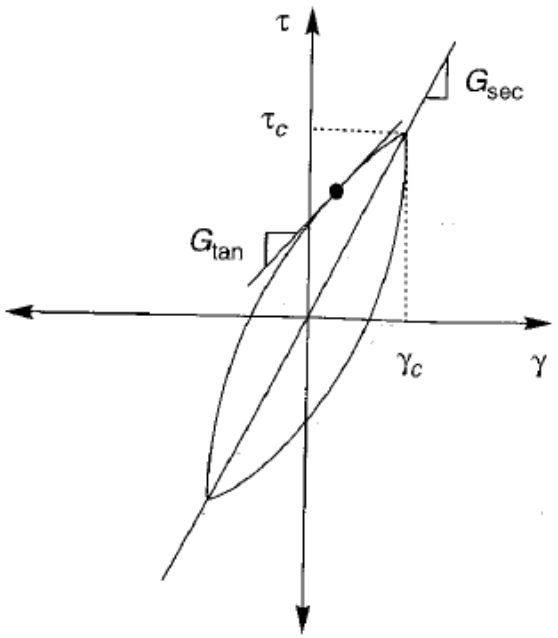

Figure 2.2: Hysteresis loop with Tangent and Shear stiffness (Kramer, 1996)

The damping ratio ξ describes a measure of energy dissipation and can be expressed as:

$$\xi = \frac{1}{2\pi}\frac{A_{loop}}{G_{sec}\gamma_c^2} \tag{2.13}$$

The parameters G_{sec} and ξ are known as *equivalent linear* parameters and considerable attention is given to these parameters as some of the most commonly used methods of ground response analysis are based on the use of their properties (Kramer, 1996).

Figure 2.3 shows the variation of secant shear modulus of an element of soil with cyclic shear strain amplitude. The secant shear modulus is high at low strain

amplitudes but it decreases as the strain amplitude increases.

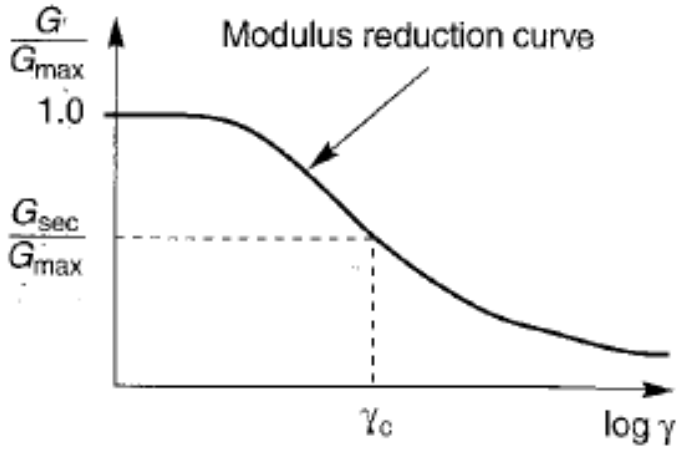

Figure 2.3: Reduction of Secant modulus as a function of shear strain (Kramer, 1996)

Earthquake with large excitation gives larger deformation and it is important to find the new shear modulus for earthquake analysis. It's an iterative process and consumes a lot of time. Hence, there is a provision in EC 8-5 for the reduction of shear modulus as per different ground acceleration, see Table 2.1.

Table 2.1: Reduction in shear modulus (Table 4.1 in EC 8-5)

Ground acceleration ratio, $\alpha.S$	Damping ratio	$\frac{v_s}{v_{s,max}}$	$\frac{G}{G_{max}}$
0,10	0,03	0,90(±0,07)	0,80(±0,10)
0,20	0,06	0,70(±0,15)	0,50(±0,20)
0,30	0,10	0,60(±0,15)	0,36(±0,20)

The maximum shear modulus for a particular soil deposit can be found out from the measured shear wave velocities and is generally the most reliable means of evaluation, see Equation 2.14.

$$G_{max} = \rho v_s^2 \tag{2.14}$$

Kramer (1996) provides estimation of G_{max} in several different ways such as from different laboratory test data when shear wave velocity measurements are not available, see Equation 2.15.

$$G_{max} = 625F(e)(OCR)^k p_a^{1-a}(\sigma'_m)^n \tag{2.15}$$

where $F(e)$ is a function of void ratio, p_a is the atmospheric pressure (100 kPa), OCR is the overconsolidation ratio, n a stress exponent generally taken 0.5 for sand, k is an overconsolidation ratio exponent dependent on plasticity index and σ'_m is the mean principal effective stress. Hardin (1978) suggested that $F(e) = 1/(o.3 + 0.7e^2)$, and Jamiolkowski et al. (1991) proposed that $F(e) = 1/e^{1.3}$.

The maximum shear modulus of sand is often estimated as

$$G_{max} = 1000K_{2,max}(\sigma'_m)^{0.5} \tag{2.16}$$

where, $K_{2,max}$ is estimated from the void ratio or relative density and σ'_m is in lb/ft^2 (Seed and Idriss, 1970), see Table 2.2.

Table 2.2: Estimation of $K_{2,max}$ (Adapted from Seed and Idriss (1970))

e	$K_{2,max}$	D_r(%)	$K_{2,max}$
0.4	70	30	34
0.5	60	40	40
0.6	51	45	43
0.7	44	60	52
0.8	39	75	59
0.9	34	90	70

Some empirical relations can be used to find the shear modulus in terms of undrained shear strength (S_u) for typical clays, see Equation 2.17.

$$G = 1000 S_u \tag{2.17}$$

Depending on the active, direct or passive test, the undrained shear strength (S_u) can also be estimated from different laboratory results in terms of effective vertical stress (σ'_v), see Equation 2.18.

$$S_u = (0.1 - 0.3)\sigma'_v \tag{2.18}$$

2.2 Retaining Walls

Retaining walls are the structures that are built to retain vertical or nearly vertical earth banks or any other materials (Murthy, 2002). Some of the most earliest and fundamental principles of soil mechanics were developed to allow rational design of retaining walls as the problem of retaining soil is one of the

oldest in geotechnical engineering (Kramer, 1996). Retaining walls are usually constructed of masonry or sheet piles and may retain water or earth and also the earth retained may be natural or fill. The different types of retaining walls generally used are shown in the Figure 2.4.

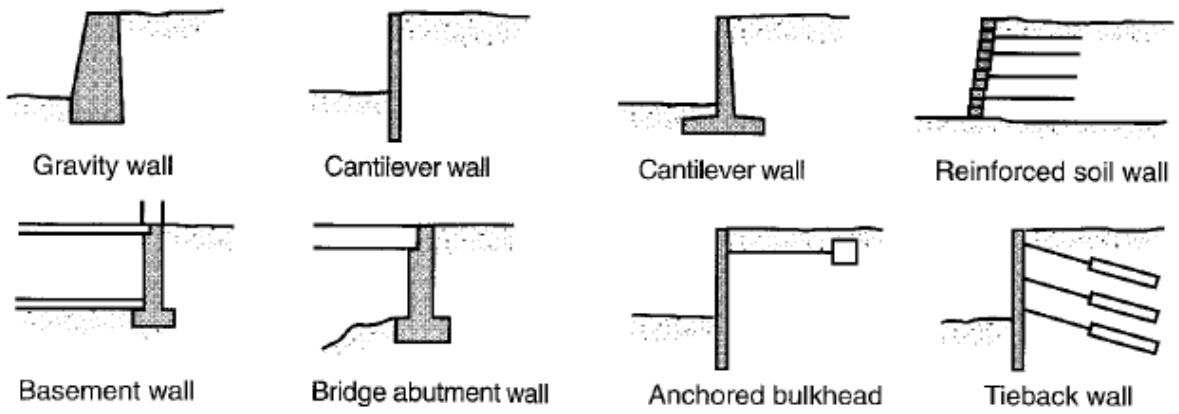

Figure 2.4: Different types of retaining walls (Kramer, 1996)

These walls have to withstand the lateral pressure either from earth or any other materials on the face regardless of whatever may be the type of wall. The pressure due to the soil acting on the wall tries to move the wall away from its position, hence the wall should be designed in such a way that the wall remains stable in the place and do not move from its position (Murthy, 2002).

2.2.1 Types of Retaining Walls

While designing any retaining walls, it is necessary to know how walls can fail hence, it becomes necessary to define failure. Failure mechanism could be sliding, tilting, bending, bearing or some other mechanism which is the result of the shear stresses being greater than the shear strength of the soil. The properly designed retaining wall will achieve equilibrium of the forces that are

acted upon by the body forces related to the mass of the wall, soil pressures and other external forces under the static conditions, but during an earthquake, it may cause the permanent deformation of the wall due to violation of equilibrium from inertial forces and changes in soil strength (Kramer, 1996). This permanent deformation might cause a failure with one or more above discussed failure mechanisms. In general, there are different types of retaining walls as shown in figure 2.4 but in this section the three most common retaining walls; gravity wall, gabion wall and cantilever wall will be discussed, see Figure 2.5.

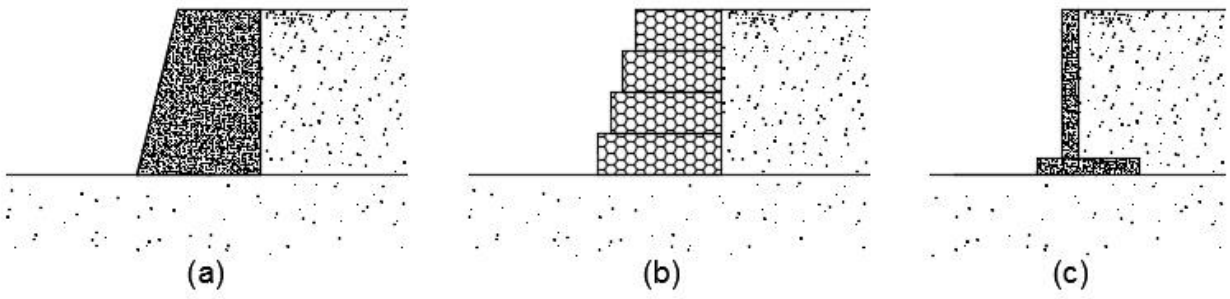

Figure 2.5: Retaining wall types (a) Gravity wall, (b) Gabion wall and (c) Cantilever wall

2.2.1.1 Gravity Walls

Gravity walls are the oldest and simplest type of retaining wall. Their movement occurs generally by rigid-body translation and/or rotation as these walls are thick and stiff enough that they do not bend (Kramer, 1996). They are generally built of stone or brick masonry or mass concrete and it resists movement due to the pressure from the soil by their self-weight (Murthy, 2002). The general failure mechanism of gravity walls such as sliding and/or overturning or gross instability are shown in Figure 2.6.

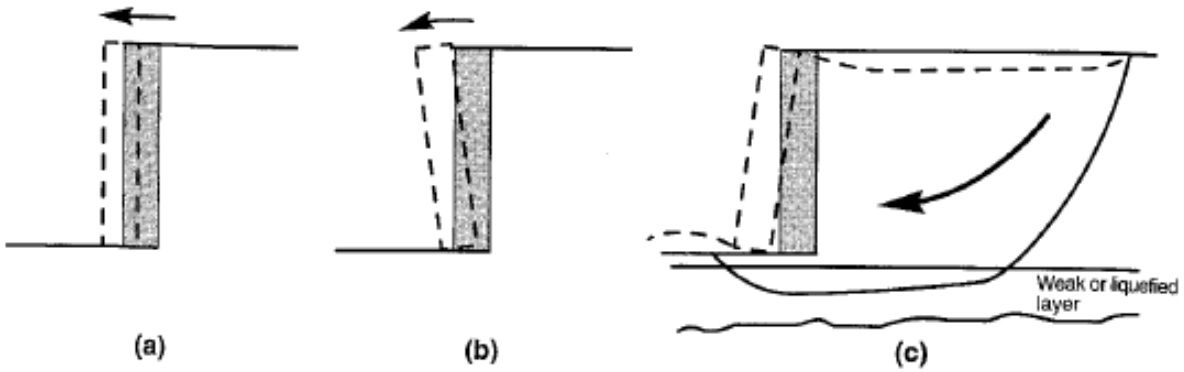

Figure 2.6: Typical failure mechanisms for a gravity walls: (a) sliding: (b) overturning: (c) gross instability failure. (Kramer, 1996)

2.2.1.2 Gabion Walls

Gabion walls are rectangular cages made of zinc-coated steel wire mesh and filled with stones of appropriate size and necessary mechanical characteristics. The zinc coated wire helps to tie the individual units firmly so as to form a monolithic structure, see Figure 2.5. The hexagonal double-twisted wire mesh is generally adopted.

The gabion wall generally functions similar to the gravity wall without considering the contribution of the mesh which in addition provides resistance to tension and further enhances the safety factor (Agostini et al., 1987). Despite many advantages of gabion walls, failure might occur if the wall is subjected to a high magnitude of lateral forces which tends to cause side-shifting of the adjacent gabion units (Ramli et al., 2013).

2.2.1.3 Cantilever Walls

Cantilever walls are generally considered advantageous over gravity walls as it is economic and easy to construct and install (Kloukinas et al., 2014). The stems of a cantilever walls are thinner and the base slab is the cantilever portion (Murthy, 2002). It utilizes the weight of the backfill soil over the footing slab to provide most of the resistance to the sliding and overturning and allows the construction of walls of considerable height (Kloukinas et al., 2014).

The failure mechanisms of the cantilever walls are same as gravity walls and in addition there is flexural failure mechanism as well. Soil pressures and bending moments in cantilever walls depend on the geometry, stiffness and strength of the soil-wall system and also the flexural failure may occur if the bending moment required for the equilibrium exceed the flexural strength of the wall (Kramer, 1996), see Figure 2.7. Note that the Figure 2.7 might resemble more with sheet pile wile but the shown mechanisms are similar for both sheet pile wall and cantilever wall.

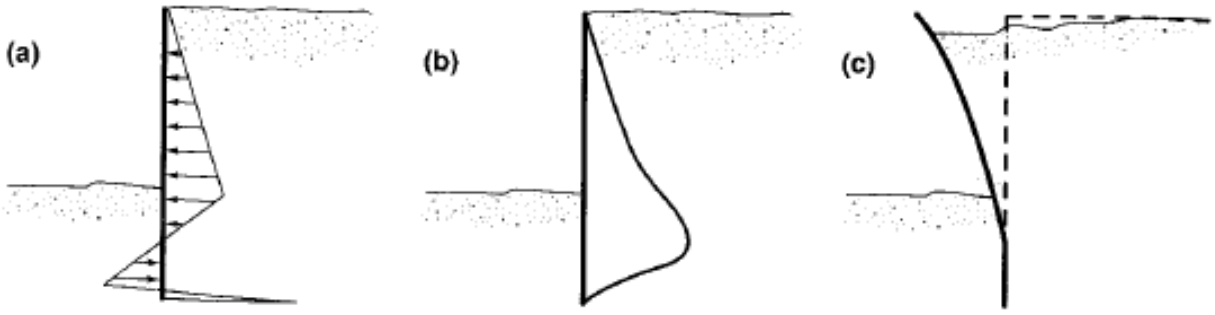

Figure 2.7: (a) Soil pressures: (b) bending moments, and (c) flexural failure mechanism for cantilever retaining wall. (Kramer, 1996)

2.2.2 Backfill

The retained mass of soil is called backfill. When retaining walls are used to contain a backfill, the embankment must be protected from the effect of seasonal weather variations, especially from the surface and deep penetration freezing. Thus, clay backfill must be avoided as far as possible as they absorb water, swell up and give rise to unwanted increase in pressure. Hence, a non-cohesive material, preferably coarse grain sand and gravel are advisable to use as they permit the flow of water. (Agostini et al., 1987)

2.3 Lateral Earth Pressure

In design of different earth retaining structures, its mandatory to compute the lateral pressure exerted by the retained mass of soil (Punmia and Jain, 2005). This retained mass of soil called backfill tries to move the wall from its position which is resisted partly by the soil in front of the wall and party by the wall itself (Murthy, 2002).

Finding out the lateral earth pressure against the retaining walls is one of the oldest in civil engineering and is the common expression for the stress components i.e. normal and shear that act in the interface of soil and structure (Geotechnical Division NTNU, 2014). The preliminary rigorous analysis for the earth pressure done by Coulomb in (1776) and later Rankine in (1857) provided the theories to estimate the magnitude of Active and Passive earth pressures as explained in Chapter 2.3.1 (Murthy, 2002).

2.3.1 Active and Passive Earth Pressure

Active earth pressure occurs when the retaining structure is holding the soil volume in place which otherwise tends to fall. Passive earth pressure occurs when the wall is being pushed into the earth. The pressure is called passive as the weight of the backfill opposes the movement of the wall (Murthy, 2002).

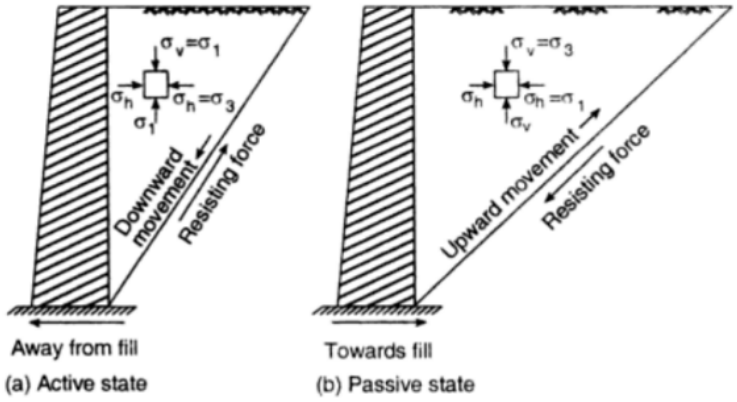

Figure 2.8: Active and Passive earth pressure (Punmia and Jain, 2005)

Figure 2.8 show the active and passive sate of plastic equilibrium with the horizontal ground surface in a non-cohesive soil. The major principle stress σ_1 is vertical and the minor principal stress σ_3 is horizontal in active state whereas major principal stress σ_1 is horizontal and the minor principal stress σ_3 is vertical in passive state. The development of the active and passive earth pressure can also be seen in the Figure 2.9.

In Figure 2.8, σ_v and σ_h are the vertical and horizontal earth pressure. If the backfill is considered to be homogeneous then the ratio of these two gives a constant value called the earth pressure coefficient, k_o (Murthy, 2002) and is shown in Equation 2.19.

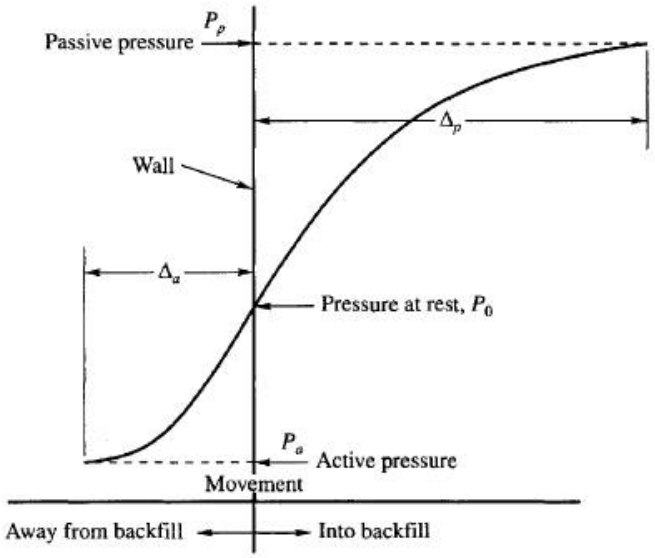

Figure 2.9: Development of active and passive earth pressure (Murthy, 2002)

$$k_o = \frac{\sigma_h}{\sigma_v} \tag{2.19}$$

2.4 Friction between Soil and Wall

Friction between soil and the wall has a significant impact on the size of the earth pressure. The roughness includes the influence of the soil-wall interaction in both active and passive state. Figure 2.10 shows the effect on the size of failure surface for both S_u and $a\phi$ analysis as per the change in roughness when it is positive.

Table B.5 in Appendix B presents the typical friction angle for soil-wall interface as per different types of soil-wall interaction.

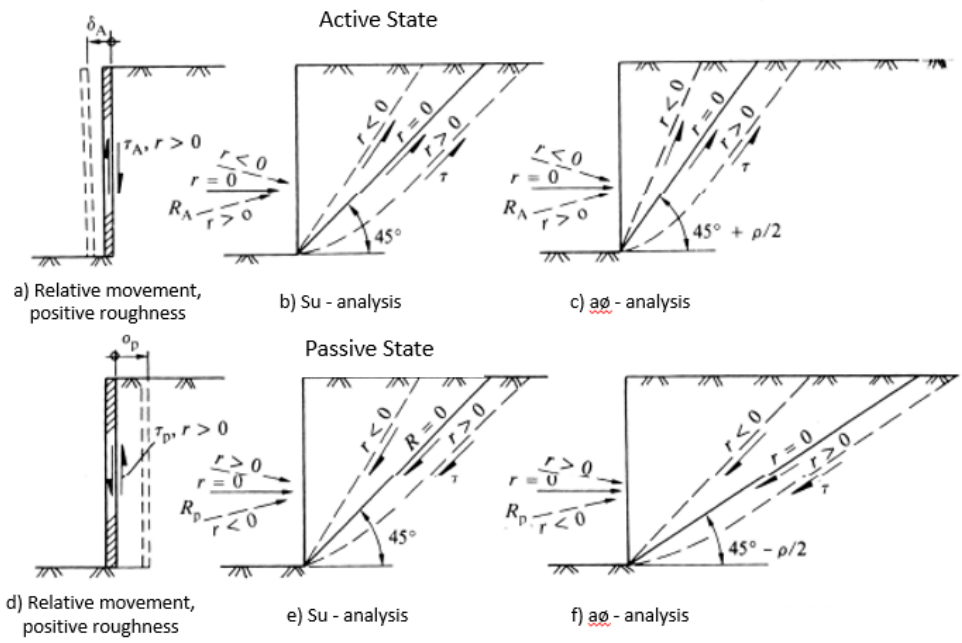

Figure 2.10: Effect of roughness on active and passive state (Aarhaug, 1984)

2.4.1 Roughness and roughness ratio

When there is a soil-wall interaction, it is clear that the active and passive condition will give rise to shear stress τ on the wall (Geotechnical Division NTNU, 2014). In active and passive case, it will cause downwards and upwards respectively.

The roughness ratio (r) is the ratio of the shear stress τ to the critical shear strength τ_c of the soil, see Equation 2.20.

$$r = \frac{\tau}{\tau_c} \tag{2.20}$$

If $r = 0$, $\tau = 0$, which implies that the wall becomes a principal plane (Geotechnical Division NTNU, 2014).

2.4.2 Effective Stress Analysis

In effective stress analysis, the stresses are calculated acting on the soil grains only and later stress due to water is added to get the total stress. The effective normal stress is expressed in the Equation 2.21 and 2.24 for active and passive condition respectively. Similarly, shear stress for active and passive condition are expressed in the Equation 2.23 and 2.26 respectively.

Active Condition:

$$\sigma'_A + a = K_A(\sigma'_v + a) \tag{2.21}$$

$$\sigma'_v = q + \gamma' z \tag{2.22}$$

$$\tau_A = r\,tan\rho(\sigma'_A + a) \tag{2.23}$$

Passive Condition:

$$\sigma'_P + a = K_P(\sigma'_v + a) \tag{2.24}$$

$$\sigma'_v = q + \gamma' z \tag{2.25}$$

$$\tau_P = r\,tan\rho(\sigma'_P + a) \tag{2.26}$$

Here, σ'_A and σ'_P are the effective normal stress for active and passive condition

respectively, a is the attraction, σ'_v is the vertical effective stress, q is the surcharge load, γ' is the effective unit weight of soil, z is depth of soil considered and $tan\rho$ is the mobilized soil friction. K_A and K_P are the earth pressure coefficients for the active and passive condition respectively and depend on the value of r and . The value of K_A and K_P can be estimated from the chart shown in Figure B.1 in Appendix B.

2.5 Analyzing Method

This section provides the basic background about different earthquake analysis methods. First is the description of Time History Analysis then followed by the Mononobe-Okabe (M-O) method, Eurocode 8 and Finite Element Method.

2.5.1 Time History (TH) Analysis

Earthquake analysis of the structures can be performed by applying a time-dependent earthquake excitation known as time history analysis. The applied time history could be any one of acceleration, velocity or displacement time history. Figure 2.11 shows the acceleration time history recorded for the Imperial Valley Earthquake.

Time history analysis provides the exact response but as there are large data sets are involved, the interpretation of these data may become time-consuming. Since applied load by time history analysis varies rapidly with time, the $c-\phi$ reduction cannot be used to find the safety factor for earthquake excitation. For the evaluation of the performance of the structure

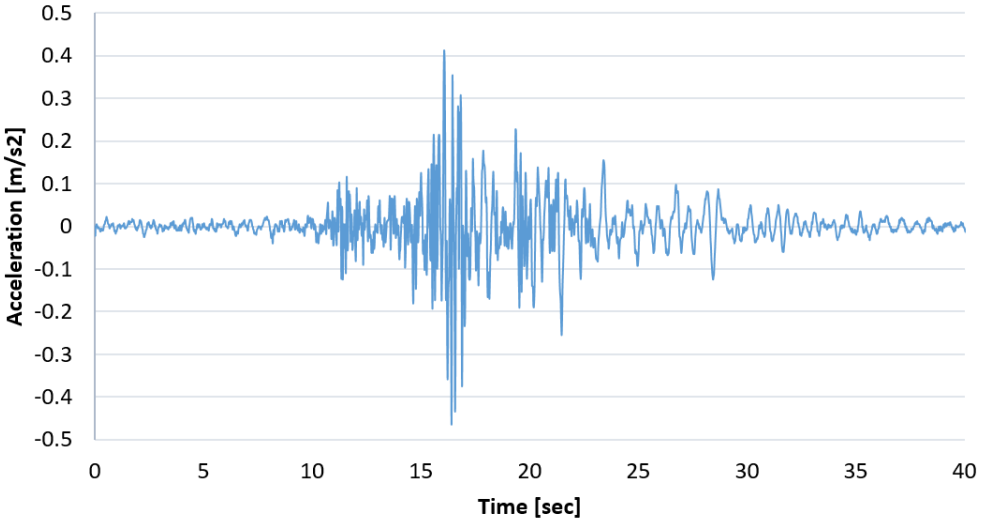

Figure 2.11: Acceleration time history recorded of Imperial Valley Earthquake with PGA 0.05g

under earthquake, the forces and deformations on the structures during and after the earthquake can be analyzed.

2.5.2 Mononobe-Okabe (M-O) Method

The Mononobe-Okabe (M-O) method has been developed as a result of the work of Okabe (1926) and Mononobe and Matsuo (1929) which gave the basis for a pseudo-static analysis of seismic earth pressures on retaining structures. The method is initially developed for the homogeneous backfill with dry, frictionless soil material (Kramer, 1996). The method is a direct modification of a Coulomb wedge method where the earthquake effects are replaced by a quasi-static inertia force whose magnitude is computed on the basis of the seismic coefficient concept (Azad et al. (2008), Cai and Bathurst (1997)). Mononobe-Okabe method which simply provides the total force acting on the retaining wall during an earthquake and the location of the point from which the total force is acting (attack point) is effective in assessing the seismic active

earth pressure and is generally adopted in the current practices for the seismic design of the rigid retaining walls (Azad et al., 2008).

Seed and Whitman suggested in 1970 that the total force (P_{AE}) can be divided into static force (P_A) and dynamic force (ΔP_{AE}) (Kramer, 1996). P_{AE} is estimated by the following equation 2.27.

$$P_{AE} = P_A + \Delta P_{AE} = \frac{1}{2} K_{AE} \gamma H^2 (1 - k_v) \tag{2.27}$$

where, H is the height of the retaining wall, γ is the unit weight of the backfill soil and K_{AE} is the active dynamic earth pressure coefficient and is given by the equation 2.28.

$$K_{AE} = \frac{cos^2(\phi - \theta - \psi)}{cos\psi cos^2\theta cos(\delta + \theta + \psi)[1 + \sqrt{\frac{sin(\delta+\phi)sin(\phi-\beta-\psi)}{cos(\delta+\theta+\psi)cos(\beta-\theta)}}]^2} \tag{2.28}$$

where, $\phi - \beta \geq \psi$, $\gamma = \gamma_d$ and $\psi = arctan[\frac{k_h}{1-k_v}]$. The other parameters ϕ, θ, δ, β and α_{AE} are shown in the figure 2.12. k_h and k_v are the horizontal and vertical seismic coefficients and these values are provided in Eurocode 8-5 (EC 8-5 7.3.2.2 (4)P).

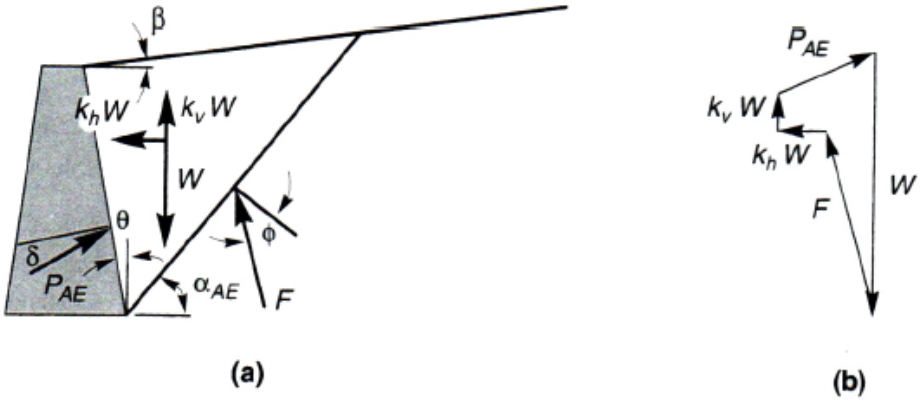

Figure 2.12: (a) Force acting on active wedge in Mononobe-Okabe Analysis, (b) force polygon illustrating equilibruim of forces acting on active wedges (Kramer, 1996)

Zarrabi-Kashani (1979) provided the estimation for the critical failure surface inclined at an angle α_{AE} as

$$\alpha_{AE} = \phi - \psi + arctan[\frac{-tan(\phi-\psi-\beta)+C_{1E}}{C_{2E}}] \tag{2.29}$$

where,

$$C_{1E} = \sqrt{tan(\phi-\psi-\beta)[tan(\phi-\psi-\beta)+cot(\phi-\psi-\theta)][1+tan(\delta+\psi+\theta)cot(\phi-\psi-\theta)]} \tag{2.30}$$

$$C_{2E} = 1 + tan(\phi-\psi-\beta)[tan(\phi-\psi-\beta)+cot(\phi-\psi-\theta)] \tag{2.31}$$

The attack point of the total active thrust can be estimated by taking into

account of both static and dynamic components as seen in Equation 2.27. Kramer (1996) gives the relation to estimate the height (h) of the attack point for the total active thrust with the consideration of the fact that the static component acts at $H/3$ above the base of the wall and taking into the recommendation given by Seed and Whitman (1970) that the dynamic component act at approximately $0.6H$. The relation that provides the attack point (h) above the base of the wall can be seen in the Equation 2.32.

$$h = \frac{P_A H/3 + \Delta P_{AE}(0.6H)}{P_{AE}} \tag{2.32}$$

2.5.3 Eurocode 8

This chapter provides an information about how different parameters required for Mononobe-Okabe (M-O) method are taken from Eurocode 8. EC 8-1 (EN 1998-1: 2004 + NA:2008) is the main part of the design of structures for seismic resistant, for which it provides alternative procedures, values and recommendations. EC 8-5 (EN 1998-5: 2004 + NA:2008) provides geotechnical aspects to the design of structures for seismic resistant and also contains analytical method such as M-O method. EC 8-5 binds the general requirement to the retaining structures that the design should be such that it still fulfill its function after an earthquake.

For the design of the retaining wall using M-O method, it is difficult to find the representative values for the seismic coefficients. Some representative values

for k_h and k_v are provided in the Eurocode (EC 8-5 7.3.2.2 (4)P).

$$k_h = \alpha \frac{S}{r} = (\frac{a_g}{g}) \frac{S}{r} \tag{2.33}$$

$$k_v = \pm 0.33 k_h \tag{2.34}$$

where,

a_g, is the design ground acceleration on type A ground ($a_g = \gamma_I * a_{gR}$)

γ_I, is the Seismic factor, depends on the seismic class, see Table B.3 and B.4 in Appendix B

a_{gR}, is the reference peak ground acceleration on type A ground

g, is the acceleration due to gravity

S, is the soil factor dependent on the soil conditions

r, is the factor used for calculating k_h, shown in Table 2.3.

Table 2.3: Factor for calculating horizontal seismic coefficient (Table 7.1 i EC 8-5)

Type of retaining structure	r
Free gravity walls that can accept a displacement up to $d_r = 300\ \alpha \cdot S$ (mm)	2
Free gravity walls that can accept a displacement up to $d_r = 200\ \alpha \cdot S$ (mm)	1,5
Flexural reinforced concrete walls, anchored or braced walls, reinforced concrete walls founded on vertical piles, restrained basement walls and bridge abutments	1

The amplification factor (S) can be found out for different ground types from the Table B.2 in Appendix B. The different ground types A, B, C, D, E, S_1 and S_2

can be identified from the Table B.1. The r value is taken from the Table 2.3. Hence for a given ground acceleration at the area where the retaining wall stands, horizontal seismic coefficient k_h could be estimated with the further help of the information regarding seismic classes and seismic factors, shown in Table B.3 and B.4 respectively.

2.5.4 Finite Element Method

The Finite Element Method, also called FEM or FE Method, is an approximate numerical method which can be used to solve a number of different problems in engineering sciences (Nordal, 2015). FEM can be used to solve a number of technical problems, while the issue can be described by a partial differential equation or integral equations (Cook et al., 2001).

Basically, the same theoretical method, known as *Displacement method* is applied on which the forces or loads are applied on a structure or soil body and the response is studied in terms of displacements and deformations (Nordal, 2015).

With the help of FEM, one can build a mathematical model of a physical problem including different boundary conditions, material model and input parameters but these are just an idealization of the physical problem with lots of assumptions, hence, it is very important to understand that FEM provides an approximate solution (Cook et al., 2001).

2.5.4.1 PLAXIS 2D

"PLAXIS 2D is a two-dimensional finite element program, developed for the analysis of deformation, stability and groundwater flow in geotechnical engineering" Brinkgreve et al. (2014a). The software helps to simulate the soil behavior but the accuracy of it depends on the expertise of the users regarding the modeling of the problem, understanding and limitations of the soil models, model parameters and the ability to judge the output (Brinkgreve et al., 2014b).

The triangular finite elements which when added up represents the behavior of the whole structure. When this element deforms, the deformations of the element are described by the deformations in a set of nodal points (Nordal, 2015). PLAXIS uses 6 or 15 nodal point triangular elements as shown in Figure 2.13.

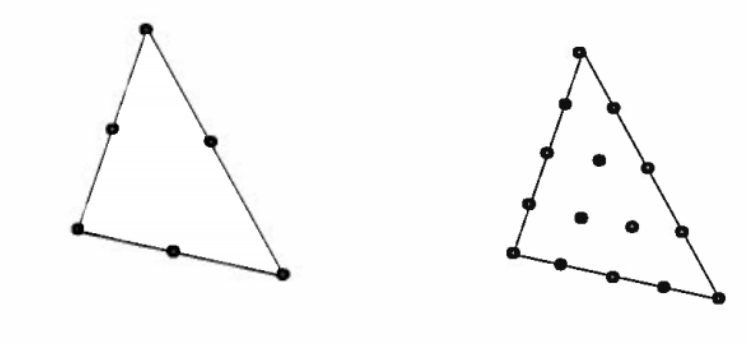

Figure 2.13: Triangular element with 6 and 15 node points (Nordal, 2015)

In all the PLAXIS Analysis, '15 noded elements' with 'Plane strain' condition have been used.

2.6 Soil Model

Different soil models that have been used in the analysis such as Mohr-Coulomb Model and Hardening Soil Model are discussed in the following section:

2.6.1 Mohr-Coulomb (MC) Soil Model

Mohr-Coulomb Soil model is a simple linear elastic perfectly plastic soil model which gives the first approximation of the soil behavior. The Hooke's law of isotropic elasticity governs the linear elastic part of the Mohr-Coulomb model whereas the perfectly plastic part is based on the Mohr-Coulomb failure criterion (Brinkgreve et al., 2014b). The Mohr-Coulomb failure criterion is governed by the Equation 2.35.

$$\tau = c + \sigma' tan\phi \tag{2.35}$$

where, τ is the shear strength, c is the cohesion, σ' is the effective normal stress and ϕ is the friction angle of the soil.

The linear elastic perfectly plastic behavior can be explained from the stress strain plot shown in Figure 2.14. The ε^e and ε^p refers to the elastic and plastic strain respectively.

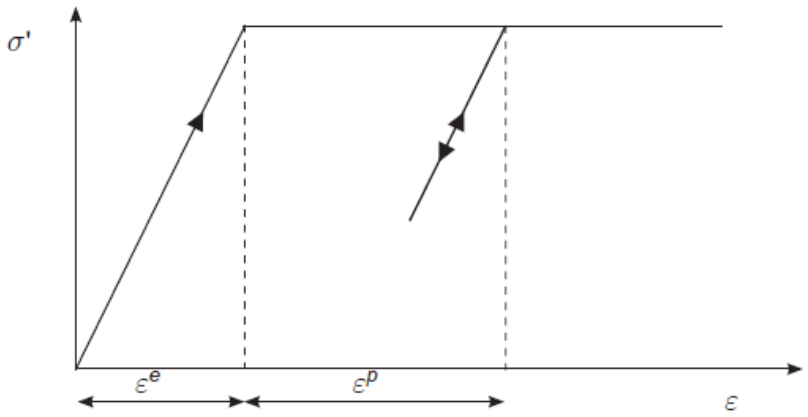

Figure 2.14: Basic idea about linear elastic perfectly plastic behavior (Brinkgreve et al., 2014b)

2.6.2 Hardening Soil (HS) Model

Hardening Soil model was originally proposed for sand but it is now further developed to be used for all types of soil (Nordal, 2015). In reality, soils behave rather non-linear when subjected to change in stress and strains and the stiffness of soil is dependent on the stress level, stress path and the strain level (Brinkgreve et al., 2014b). Hardening Soil model is one of the advanced soil models on which there is a built in formulation that makes the stiffness dependent of the effective stress level (Nordal, 2015). The general expression for the stiffness is shown in Equation 2.36 for deviatoric loading.

$$E_{50} = E_{50}^{ref} \left(\frac{\sigma_3' + a}{p_{ref} + a}\right)^m \tag{2.36}$$

Here, p_{ref} = atmospheric pressure = 100 kPa, a = attraction, Index m is the stress exponent, generally taken 1 for clay and 0.5 for sand. E_{50}^{ref} is the input parameter and the real stiffness E_{50} is calculated as a function of σ_3'. ${E_{50}}^{ref}$, ${E_{oed}}^{ref}$ and

${E_{ur}}^{ref}$ and m are very important input parameters in Hardening Soil model.

Brinkgreve et al. (2010) has provided formulas to estimate the reference stiffness parameters fro sand in terms of Relative Density (RD), considering p_{ref} = 100 kPa:

$$E_{50}^{ref} = 60000RD/100 \tag{2.37}$$

$$E_{oed}^{ref} = 60000RD/100 \tag{2.38}$$

$$E_{ur}^{ref} = 180000RD/100 \tag{2.39}$$

where all the reference stiffness (${E_{50}}^{ref}$, ${E_{oed}}^{ref}$ and ${E_{ur}}^{ref}$) have the unit in kPa. Also, the formulas for other parameters can also be found as given by Brinkgreve et al. (2010):

$$m = 0.7 - RD/320 \tag{2.40}$$

$$\phi' = 28 + 12.5RD/100 \tag{2.41}$$

In a dynamic analysis for both Mohr-Coulomb model and Hardening Soil model, Rayleigh damping may be defined in order to simulate the soil's damping characteristics in dynamic loading (Brinkgreve et al., 2014b).

Chapter 3

Analyzing boundary conditions

This chapter discusses different types of boundary conditions that are used in PLAXIS 2D for dynamic analysis. First, the introduction and general information about these boundary conditions are presented followed by series of two tests. The tests have been very significant in analyzing the different boundaries.

3.1 Introduction

The finite simulation in PLAXIS 2D is done for the analysis of deformation and stability in geotechnical engineering practice. The modeling of soils and structures in a finite element program is done for the actual representation of real case scenario. In reality, these soil extends to infinity in all directions whereas in the finite element program the model is of a finite size and is constrained by a boundary. Hence, the knowledge of these boundaries and its usage as per different cases is very important to perform a proper finite element analysis.

In a dynamic analysis, the waves generated by a vibration propagates to infinity. If modeling is done with standard fixities (none boundary condition) then the waves get reflected from the model boundaries which does not resemble with the reality and consequently results in a poor analysis. This problem can be fixed with the use of quiet boundaries (Viscous, Free field, Tied degree of freedom, Compliant & Fixed base) provided in PLAXIS 2D and also can be fixed with a free lateral boundary (Witasse, 2012). The understanding of these boundaries is mandatory for any dynamic analysis.

3.1.1 Types of Boundaries

3.1.1.1 Viscous Boundary

A viscous boundary consists of viscous dampers applied along the boundary. It is an absorbing boundary and absorbs the incoming wave energy and are used generally for problems where the dynamic source is inside the mesh (Brinkgreve et al., 2014c). It is available at the left, right and bottom side of the model in PLAXIS 2D.

3.1.1.2 Fixed and Complaint Base

A fixed base is a fully reflective boundary. This is used along the base of the model in combination with a line prescribed displacement. The compliant base is made up of a combination of a line prescribed displacement and a viscous boundary. The combination of a load history and a viscous boundary allows for input of an earthquake motion while still absorbing incoming waves and

the prescribed displacement history is transferred into a load history internally (Brinkgreve et al., 2014c).

3.1.1.3 Free field Boundary

It is also an absorbing boundary which enforces laterally free-field motion such that the boundaries still retain their non-reflecting properties (Plaxis bv, 2015). The free field boundary conditions are only available for lateral boundaries. Laterally, they mush be placed at a distance for which free-field conditions are reached. The free-field motion is transferred to the main domain from the free field elements with the application of the equivalent normal and shear forces (Brinkgreve et al., 2014c), see Figure 3.1.

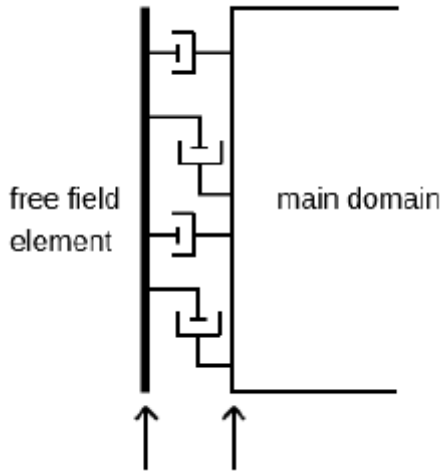

Figure 3.1: Free field boundary condition (Brinkgreve et al., 2014c)

3.1.1.4 Tied degree of freedom

The tied degree of freedom is also only available for the lateral boundaries. The nodes of the left and right model boundaries are tied which will undergo the

exact same displacements when tied boundaries are used (Plaxis bv, 2015), see Figure 3.2. This boundary condition can only be applied if the distribution of nodes along the vertical model boundaries is identical (Brinkgreve et al., 2014c).

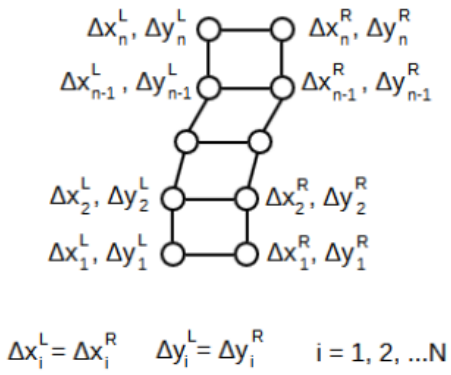

Figure 3.2: Tied degrees of freedom (Brinkgreve et al., 2014c)

3.1.1.5 Free lateral Boundary

Free lateral boundary can be created manually in PLAXIS 2D by a line displacement. These are given to the lateral boundaries in such a way that the lateral boundaries can move horizontally but are fixed vertically. This boundary condition is used in combination with a linearly increasing horizontal stress at the lateral boundaries. For, linear elastic model it does not require the horizontal stress but for non-linear models where the soil has a limited shear strength, a horizontal stress with proper k_o value should be applied.

3.2 Tests on Boundary Conditions

The influence of these boundary conditions on the dynamic analysis should be studied and which boundary condition is most reliable to use for a particular dynamic analysis should also be analyzed prior to any real simulations. For that, two different tests have been performed and discussed below:

3.2.1 Test 1: Comparison of PLAXIS 2D output with Analytical Solution

In this test, dynamic response of a homogeneous soil will be studied under different boundary conditions.

3.2.1.1 Geometry

For simplicity, a soil layer with uniform thickness 25 m and width 150 m is taken, see Figure 3.3.

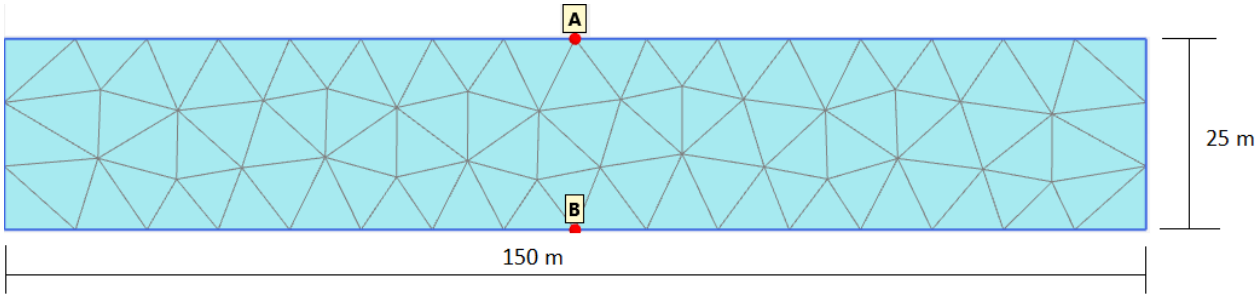

Figure 3.3: Soil layer with node points at top (A) and bottom (B)

3.2.1.2 Parameters

The linear elastic soil with shear wave velocity (v_s) of 100 m/s has been taken for the test. The rayleigh damping of 5 % is applied for frequencies f_1 = 0.5 Hz and f_2 = 5 Hz. The detailed description of the parameters are shown in the Table 3.1.

Table 3.1: Parameters for Test 1 on boundary conditions

Parameters	Remarks
Soil Model	Linear Elastic - Undrained (C)
Unit weight of Soil (γ)	20 kN/m^3
Thickness (H)	25 m
Rayleigh damping (ξ)	5 % (at 0.5 Hz and 5 Hz)
Rayleigh Parameters	$\alpha = 0.289$ and $\beta = 2.89 * 10^{-3}$
Poission ratio (υ)	0.495
Shear wave velocity (v_s)	100 m/s
Mesh Coarseness	Medium

The natural frequency of the soil for a fixed base with thickness (H) can be calculated as:

$$f_n = \frac{v_s}{4H} \tag{3.1}$$

Equation 3.1 gives the natural frequency of the soil layer to be 1 Hz. When the frequency of the input motion is same as the natural frequency of the soil i.e. resonance condition, the response will have the maximum amplitude. The amplification of the response can be measured by means of a factor called Amplitude factor (A). The Amplitude factor is the ratio of amplitude of the response taken at top and bottom layer, provided that the ratio is taken at the steady state.

For a linear elastic model, the Amplitude factor can be calculated analytically as:

$$A = \frac{1}{\sqrt{Cos^2(\frac{\omega H}{v_s}) + (\xi(\frac{\omega H}{v_s}))^2}} \tag{3.2}$$

3.2.1.3 Analysis

A harmonic acceleration of amplitude 0.05g is given to the *fixed base* for 20 seconds and the response at the top level is observed, see Figure 3.4. For the test, the harmonic acceleration is applied frequencies of 0.5 Hz to 5 Hz with an increment of 0.5 Hz for a particular boundary condition. The similar process is repeated for all the boundary conditions i.e. Viscous, Free-field, Tied degree of freedoms and free lateral boundary.

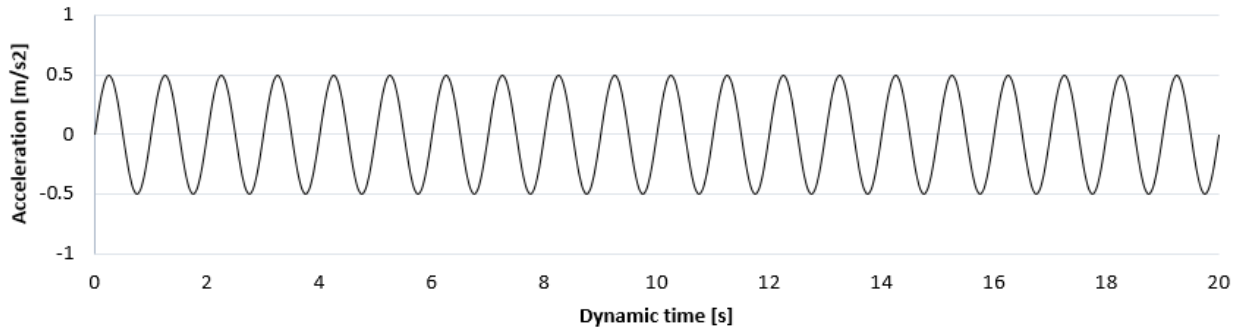

Figure 3.4: Harmonic acceleration of amplitude 0.05g and frequency 1 Hz

3.2.1.4 Results

Figure 3.5 shows output of PLAXIS 2D taken for resonance condition (f_{input} = 1 Hz) with tied degree of freedom as boundary condition. The response is taken at the top of the soil layer (Point A) and at the base (Point B).

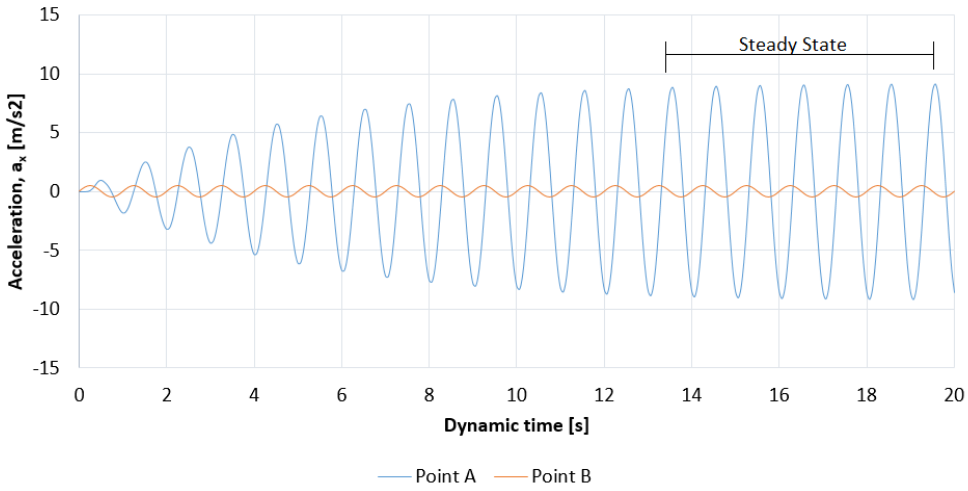

Figure 3.5: Acceleration at the Point A and Point B on the soil model

Figure 3.6 shows the comparison of the obtained values of amplitude factors from the PLAXIS 2D output for different boundary conditions with the analytical solution. The plot of Amplitude factor (A) is plotted against the frequency ratio (r), which is the ratio of a given frequency to the natural frequency of soil. The detailed calculation of amplitude factors is provided in the Table B.6 of Appendix B. The plot provides a tentative idea about how well the applied boundaries are working. As seen from the Figure 3.6, Tied degree of freedom and Free lateral boundary are giving almost exact values as calculated from the analytical solution from Equation 3.2 whereas results from Viscous and Free field boundary are deviating. Hence, for the dynamic analysis with *fixed base*, *Tied degree of freedom* or *Free lateral boundary* should be preferred.

The effect of mesh coarseness has also been studied for the same soil model with Free lateral boundary by changing the mesh coarseness from very coarse to very fine mesh and for each case, the amplitude factor is calculated. The Table 3.2 shows the obtained values of amplitude factor for different mesh coarseness for

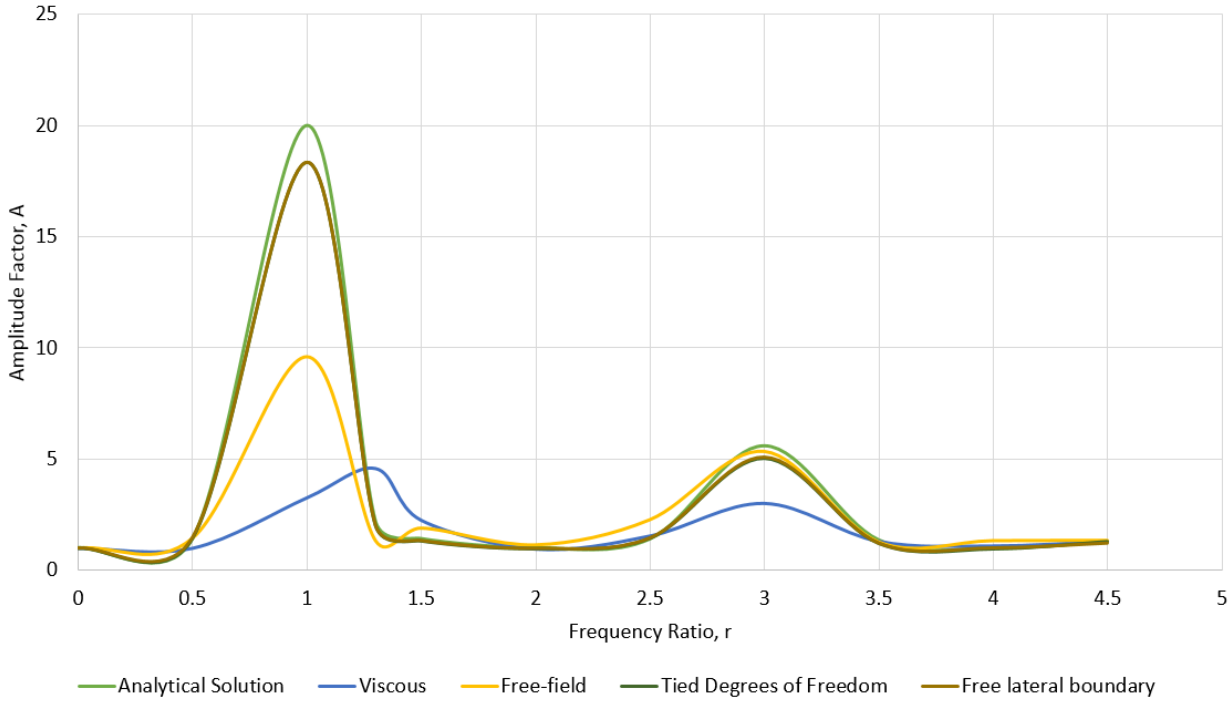

Figure 3.6: Comparison of Amplitude factors for different boundary conditions with Analytical Solution

a particular frequency of 1 Hz. The amplitude factor for all the mesh coarseness did not vary much for a frequency of 1 Hz but one should remember that for higher frequencies, the solution will become mesh dependent.

Table 3.2: Amplitude factor in different mesh coarseness for frequency 1 Hz

Mesh	V. coarse	Coarse	Medium	Fine	V. fine
Amplitude factor (A)	18.18	18.29	18.34	18.35	18.41

3.2.2 Test 2: Slope Test

The effect of boundary conditions is now tested on a slope. As seen from the Test 1 on Section 3.2.1 for linear elastic soil with uniform thickness, both viscous and free field boundary did not work well and provided a very deviating results from the analytical solution. Hence, the result from slope test for both viscous and

free field boundary will not be discussed in detail as the results from the slope test cannot be verified analytically. Instead, a qualitative analysis can only be done based on the output at some desired locations in the soil model. The slope test is performed for two boundary conditions i.e. Tied Degree of Freedoms and Free lateral boundary.

3.2.2.1 Geometry

The slope has a steepness of 1/3 and the width of the soil is 50 m on the left boundary and 30 m on the right boundary. The slope is modeled in such a way that it lies always in the center of model, see Figure 3.7.

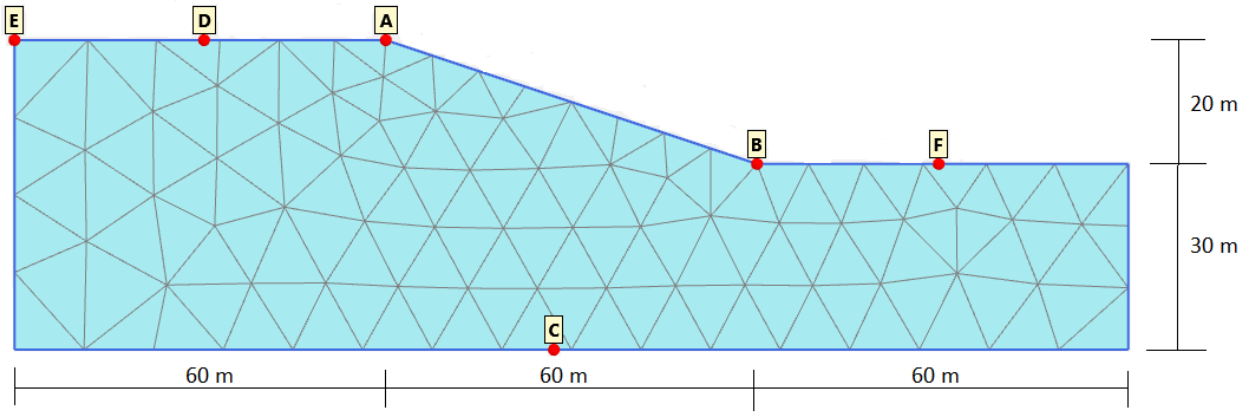

Figure 3.7: Short Model with node points for Free lateral boundary

3.2.2.2 Parameters

The linear elastic model with a fixed base is again used for this test as well. As in Test 1, the rayleigh damping of 5 % for frequencies f_1 = 0.5 Hz and f_2 = 5 Hz are taken for the soil but the shear wave velocity (v_s) is taken as 200 m/s. The detailed parameters used in the slope test are shown in the Table 3.3.

Table 3.3: Parameters for slope test

Parameters	Remarks
Soil Model	Linear Elastic - Undrained (C)
Unit weight of Soil (γ)	20 kN/m^3
Thickness (H)	50 m (left) and 30 m (right)
Damping Ratio (ξ)	5 (at 0.5 Hz and 5 Hz)
Rayleigh Parameters	$\alpha = 0.289$ and $\beta = 2.89 * 10^{-3}$
Poission ratio (υ)	0.495
Shear wave velocity (υ_s)	200 m/s
Natural Frequency (f)	1 Hz for 50 m thickness
Mesh Coarseness	Medium

3.2.2.3 Analysis

The harmonic acceleration with an amplitude of 0.05g and frequency 1 Hz is given as a prescribed displacement to the fixed base for all the slope tests, see Figure 3.4. Input motion with the only frequency of 1 Hz has been used for all the analysis unlike Test 1 of section 3.2.1. First, the test is done for a short model with Free lateral boundary (Trial 1). The soil model has a total length of 180 m where the slope with a horizontal and vertical distance of 60 m and 20 m respectively lies in the center. The overall model with desired node points can be seen in the Figure 3.7.

The node points (output point) are taken almost exactly at the same locations for all the slope tests. The response at all the nodes can be seen in the PLAXIS 2D output. For the qualitative analysis of the result, another test is run for the same free lateral boundary condition (Trial 2) but only extending length of the model by 60 m on each side, making a total length of the model to be 300 m. If the response from both tests is almost equal then the model has no effects from the boundary else additional trials should be performed with extending the

model until the response in the two consecutive trails are almost equal. Similar procedure is carried out for both the boundary conditions i.e. Free lateral boundary: **Case 1** and Tied Boundaries: **Case 2**.

3.2.2.4 Results

Case 1: Free lateral boundary

The output at Point A (top crest point) for both the test (Trial 1 & 2) is presented in the Figure 3.8 . It can be seen that, the response at Point A is very different in two tests which may have been due to the effects of boundary on that particular node. Similarly, the responses in all the node points were found to be varying in two trials (figures not shown).

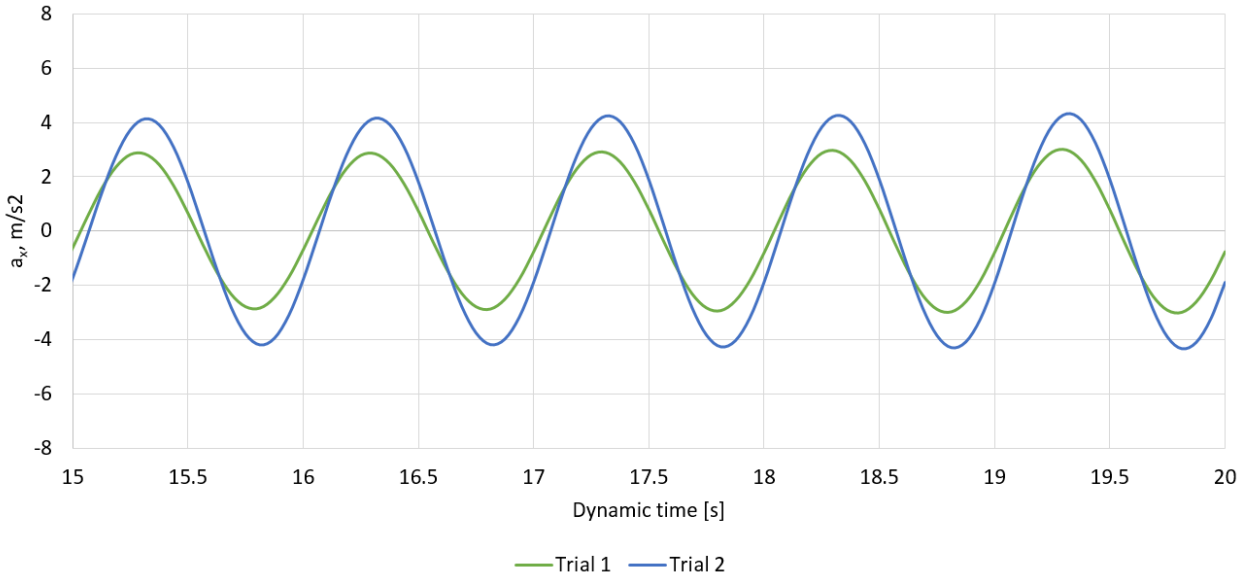

Figure 3.8: Acceleration at Point A in two tests for Free lateral Boundary

Hence, to understand the effect of boundaries, 6 trails have been performed by increasing the boundary on each trial by 60 m on each sides. The over all length

of the soil models for different trails can be seen in the Table 3.4.

Table 3.4: Length of the soil model in different trails

Trial	1	2	3	4	5	6
Length (m)	180	300	420	540	660	780

During all these trials, the slope has been placed in the center of the model. The response from all the trails at point A is presented in the Figure 3.9. It can be seen from the Figure 3.9 that the response at point A is concentrating around some value after a particular trail. After Trial 3, the response is almost the same (reasonably good) even if the length of the model is increased. Hence, it can be said that the response is not influenced by the boundary after third trial (when the soil is extended by 180 m each on both sides for this particular case).

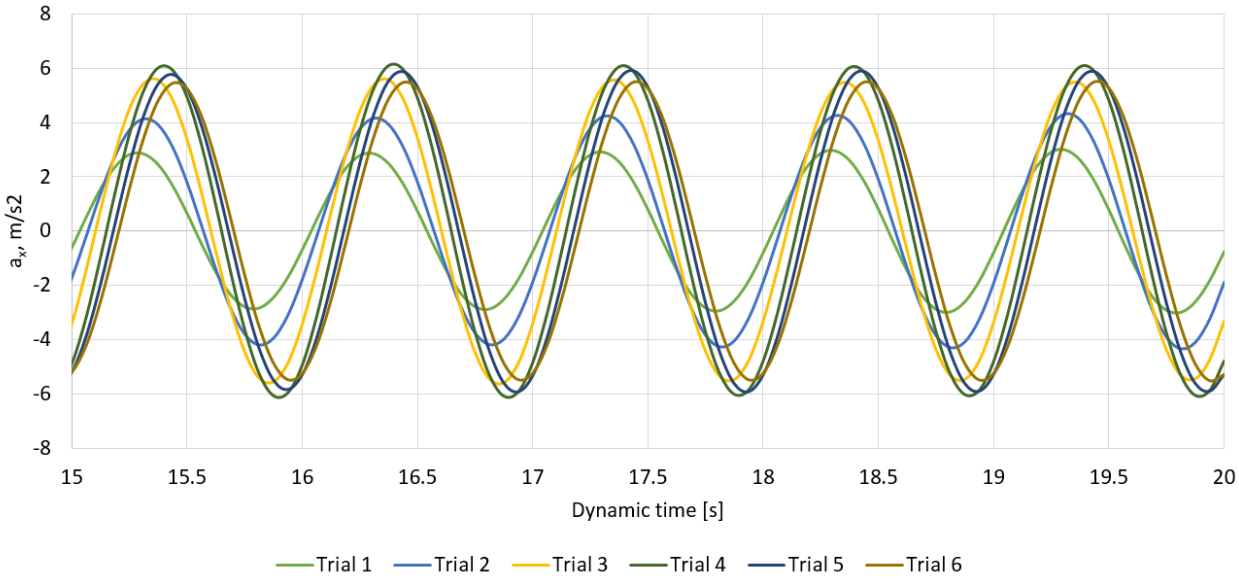

Figure 3.9: Acceleration at Point A in different trial for Free lateral Boundary

As the length of the soil model becomes larger, the finite element size will also increase significantly even if medium mesh coarseness is used for all test. The finite element size for trial 6 is very large as compared to the size of trail 1. To

verify the mesh independence, the trail 6 has been again simulated for the same boundary condition but with refined mesh. The mesh refinement has been achieved by creating horizontal lines in the soil model at a vertical distance of 5 m interval which forces the generated mesh to be refined and have small element size. The comparison of the trail 6 results at point A is presented in Figure 3.10. It can be seen that the response in both cases has been almost equal which again verifies that the analysis in independent of the mesh coarseness or finite element size for the frequency of 1 Hz.

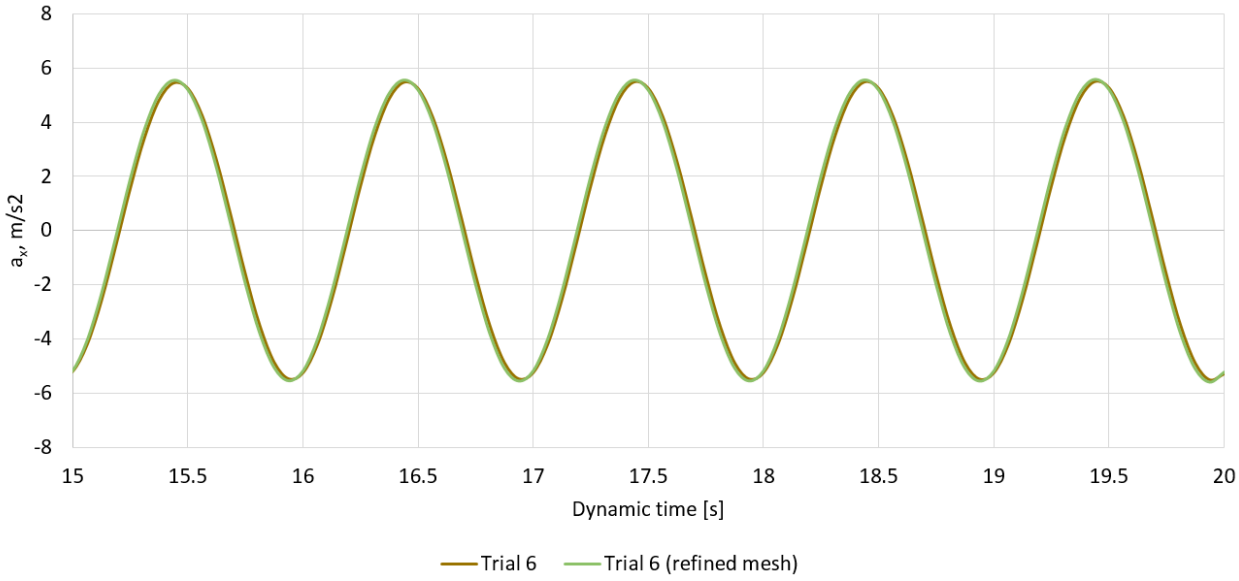

Figure 3.10: Acceleration Comparison at Point A in trial 6 with different mesh refinement

Case 2: Tied Degree of Freedom

For the Tied degree of freedoms, the main requirement for the use of Tied boundaries is that the elevation of lateral boundaries should be exactly same which makes it possible to tie all the lateral nodes of the boundaries. This requirement makes it impossible for Tied boundaries to use the same model as

in the case of free lateral boundary. Hence, to use the tied boundaries in slope test, a symmetric model is created as shown in the Figure 3.11.

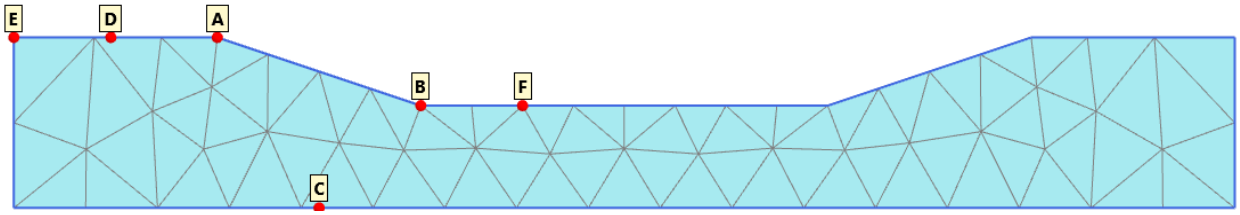

Figure 3.11: Short model with node points for Tied boundary

The output for these tests is taken at exactly same node points as in the case for free lateral boundary. These tests are also done with 6 different trails and some of the results are compared with the previous test on the free lateral boundary as shown in Figure 3.12.

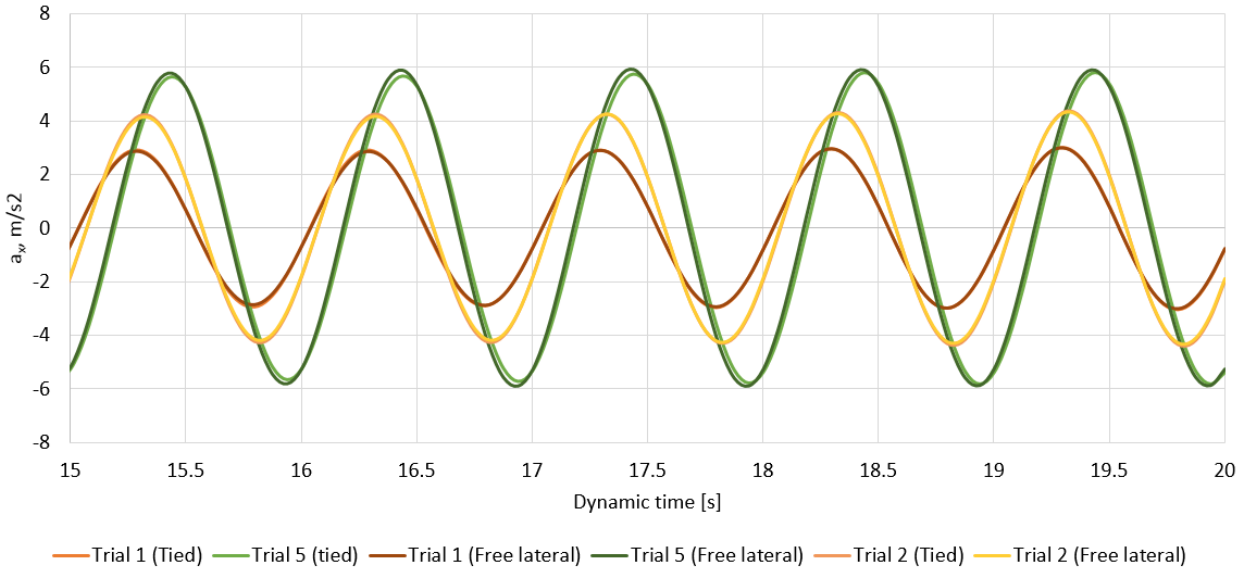

Figure 3.12: Acceleration at Point A with different boundary conditions & different trials

The response is again compared at the Point A for both boundary conditions in three different trials (1,2 and 5). It can be seen from the figure 3.12 that tied boundary is giving very similar responses in all the trials as the free lateral

boundary. Furthermore, there is also an influence from the tied boundary to the output as similar to that from the free lateral boundary. As both boundary conditions are working quite similar, it is more convenient to use the free lateral boundary than tied boundary as it will save plenty of time during model construction and simulations.

The response has been only shown in the Point A (slope crest point) but the response in all the other node points have also been taken for 6 different trials in both boundary conditions. The response in other points for example B, D, E, F etc. also showed a similar trend as Point A for 6 different trials.

Additional Informations

Furthermore, when the model is sufficiently long then the response at point E and F as shown in Figure 3.13 can be roughly compared to the analytical solution for linear elastic soil with uniform thickness. As these points are sufficiently far from both slope and boundary, there would not be much effect from them i.e. free field condition.

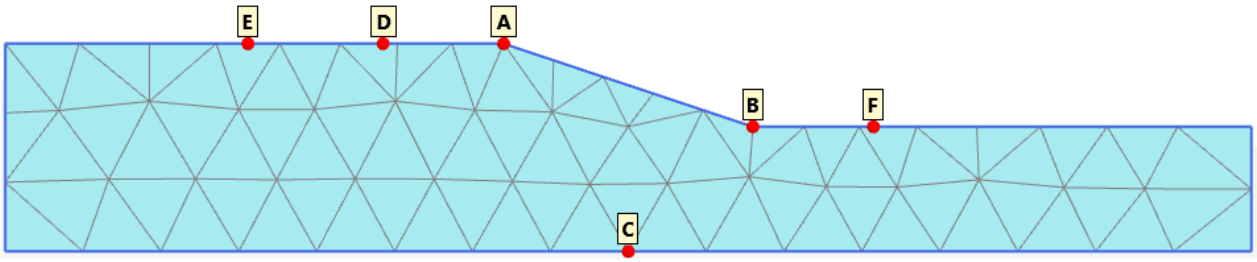

Figure 3.13: Output node E and F for a long soil model

Using the Equation 3.2 and soil parameters from Table 3.3, the amplitude factor (A) for height 50 m (Point E) and 30 m (Point F) is calculated as 20 and

1.7 respectively. The amplitude factor for Point E is very high as it meets the resonance condition. For comparison, the response at point E and F from one of the long model (trial 5) for the free lateral boundary is shown in the Figure 3.14.

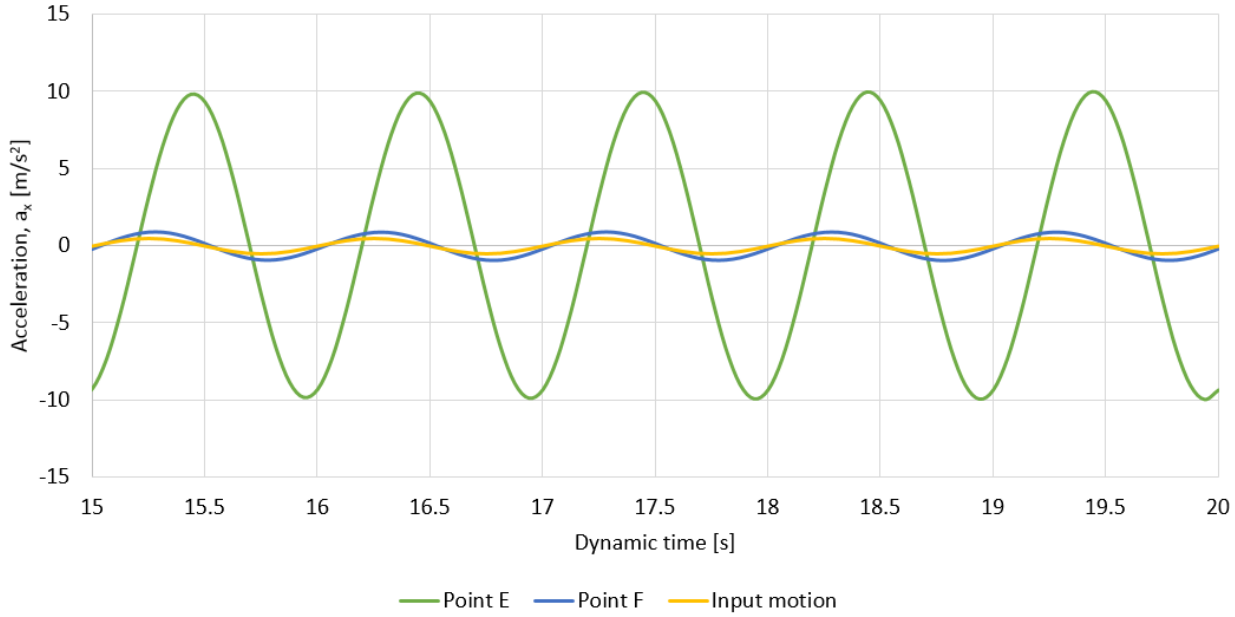

Figure 3.14: Response at node E and F for a long soil model at Trial 5

It can be seen from the Figure 3.14 that, at steady state, the amplitude factor for point E and F can be estimated as 20 and 1.78 respectively which is quite equivalent to the analytical solution.

3.3 Conclusion and Discussion

The effect of boundary conditions on dynamic analysis has been studied in two different tests. In the Test 1, when a harmonic acceleration of amplitude $0.05g$ was applied on the fixed base for linear elastic soil of uniform thickness and the responses were taken at the top and bottom of the soil layer, tied boundary and

free lateral boundary resulted in similar results as compared to the analytical solution whereas viscous and free field boundary provided a very deviating result as presented in Figure 3.6.

In the Test 2 (Slope test), the qualitative analysis was carried out for the harmonic acceleration of 0.05g with frequency 1 Hz applied to a slope with the linear elastic model for free lateral and tied boundary. 6 different trials with different model lengths have been carried out for both boundary conditions. It showed that there was an influence of boundary in the output as the response in a particular node (Point A) varied with the length of the model as shown in Figure 3.8 and 3.9. After the 3rd trails when the boundary was almost 180 m away from the Point A (crest point of the slope), the response remained almost equal even when the length of the model was increased, see Figure 3.9 for free lateral boundary with soil thickness of 50 m (height from the base to the crest point). The similar slope test was again performed for the same soil thickness of 50 m but with different slope steepness (1/2) and different slope height of 30 m. This again resulted in the similar response as in the previous case of the slope test in Section 3.2.2 .i.e. when the boundary was more than 180 m from the crest point, the response remained almost constant, see Figure B.2 of Appendix B. Hence, it can be concluded that for the dynamic analysis to have no effect from the boundary, the boundary should be prolonged 3/4 times (=180/50) the thickness (H) of the soil layer. The tied boundary also provided the similar response as free lateral boundary, see Figure 3.12.

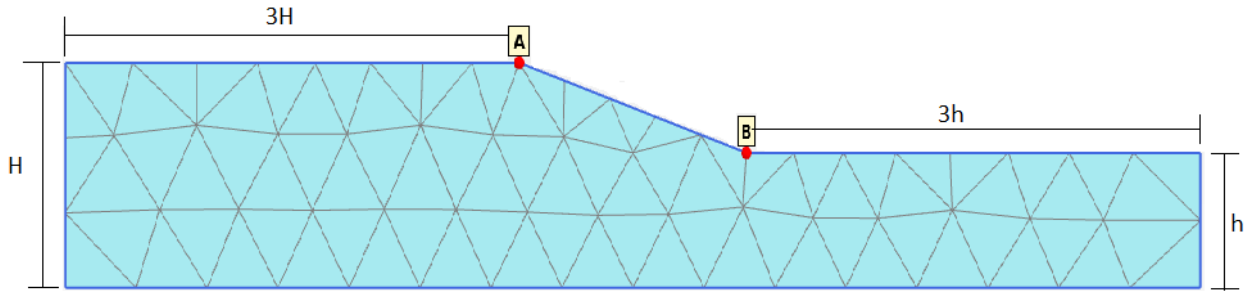

Figure 3.15: Extension of boundary need for dynamic analysis

Hence, for the proper dynamic analysis, free lateral boundaries would be preferred than tied boundary to save the time in model construction and simulations and the boundaries should be kept at least 3 times far than the thickness (H) of the soil layer as illustrated in Figure 3.15.

Chapter 4

Verification of numerical model with shake table test

4.1 Shake table test

This chapter introduces the shake table tests performed at the Bristol Laboratory for Advanced Dynamics Engineering (BLADE), University of Bristol, Uk on 2010. The experiment work was carried out by the Earthquake Engineering Research Center (EERC) in collaboration with the University of Patras (Greece), the University of Federico II Naples Italy and the University of Sannio (Italy). The shake table test results have been relevant in verifying and analyzing the performance of the numerical model.

4.1.1 General

The 1-g shaking table test was performed to explore the dynamic behavior of L-shaped cantilever wall. The experimental investigation was mainly aimed to

better understand the soil-wall dynamic interaction problem, the relationship between design parameters. failure mechanisms and stability safety factors (Kloukinas et al., 2014). The general experimental setup can be seen in the Figure 4.1.

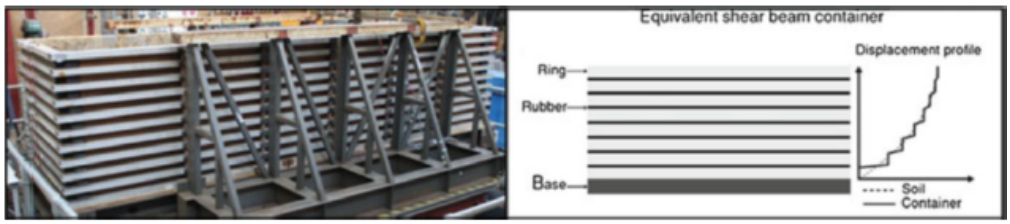

Figure 4.1: Experimental setup of Shake table test (Kloukinas et al., 2014)

4.1.2 Geometry

The apparatus or the Equivalent Shear Beam Container, shown in Figure 4.1 consists of 11 rectangular aluminum rings stacked alternatively with rubber sections. This creates a flexible box with an inner dimension of 4.8 m long, 1 m wide and 1.15 m deep. The apparatus is kept on the shake table of aluminum of size 3 m x 3 m and weighs 3.8 tons. The shaking can be provided with different frequencies from 1 Hz to 100 Hz. The overall apparatus is equipped with 21 1-D accelerometers to measure the accelerations, 4 LVDT (Linear variable differential transducer) transducers to capture the dynamic response and permanent displacement and 32 strain gauges to monitor the bending of the wall. The dimension of the model and the position of different types of equipment in the apparatus can be seen in the Figure 4.2.

Three configurations of retaining walls (Configuration 1, 2 and 3) have been tested during the experiment to provide different responses in sliding and

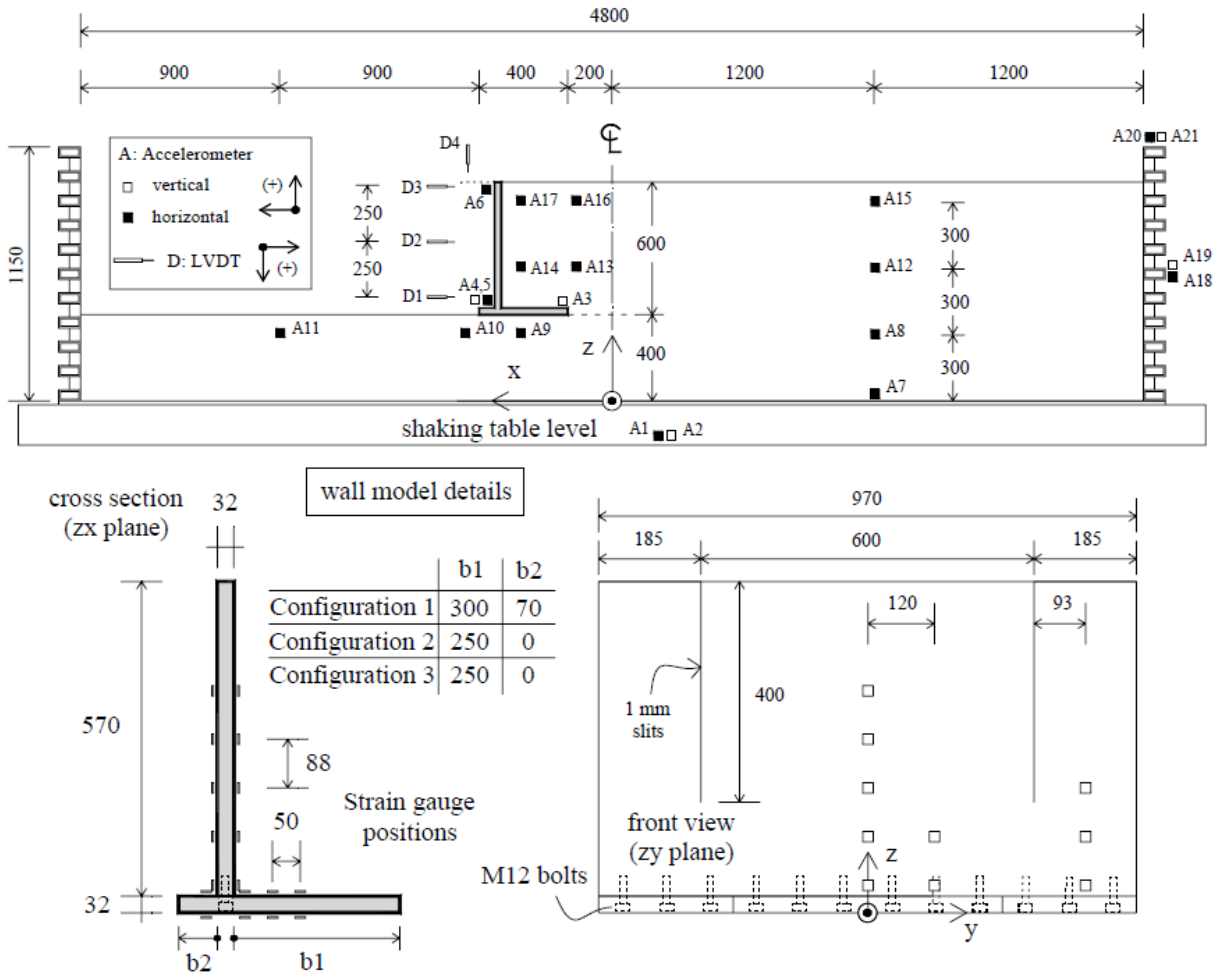

Figure 4.2: Geometry and Instrumentation of Shake test table (Kloukinas et al., 2014)

rocking of the wall. The configuration 1 consists of wall heel of 300 mm with 50 mm toe. In configuration 2 and 3, the wall heel was reduced by 50 mm making it 250 mm in both cases and the toe was completely removed. The model consists of L-shaped retaining walls with 0.6 m thick backfill resting on a 0.4 m thick soil layer as seen in Figure 4.2.

4.1.3 Material properties

The soil material used in the test are a dense supporting layer and a medium dense backfill, both of which are Leighton Buzzard (LB) sand BS 881-131, Fraction B ($D_{50} = 0.82\ mm$, $G_s = 2.64\ Mg/m^3$, $e_{min} = 0.486$, $e_{max} = 0.78$). For the preliminary estimation of the soil strength properties, the empirical correlation between peak friction angle ϕ and relative density D_r has been used from the experimental work of Cavallaro et al. (2001). The base sand was formed by pouring in layers of 150-200 mm from a height of 0.6 m and then densifying by shaking whereas the backfill sand was poured from the height of 0.2 m steadily without further densification.

The overall sand layers have been specified in the three different sections with different eigen frequencies (F_r), Shear wave velocity (V_s) and Shear modulus (G_o) as shown in Figure 4.3.

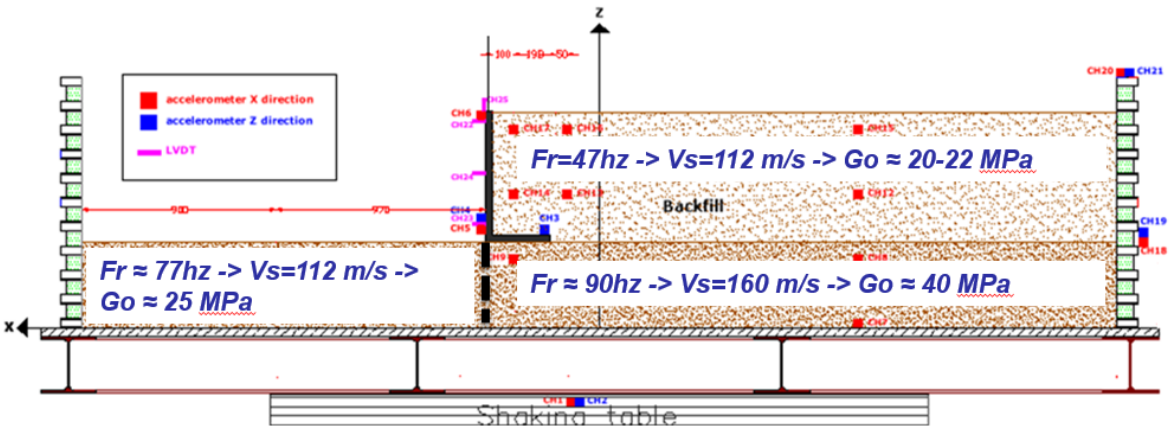

Figure 4.3: Eigen frequencies, Shear wave velocities and Shear modulus for different sand layers (Penna, 2012)

The different soil properties of these 3 different sand layers are provided in detail in Table 4.1.

Table 4.1: Soil properties of different Sand Layers (Adapted from Kloukinas et al. (2014))

Parameters	Bottom Sand	Bottom Sand under backfill	Backfill
Thickness $[mm]$	390	390	600
$e[-]$	0.61	0.61	0.72
Dr [%]	60	60	22
$\gamma\ [kN/m^3]$	16.14	16.14	15.11
$\phi\ [\circ]$	42	42	34

In all the configuration the retaining wall has the same material properties and is given in the Table 4.2.

Table 4.2: Material properties for the retaining wall used in the Shake table test (Adapted from Kloukinas et al. (2014))

Parameters	Retaining Wall
$\gamma\ [kN/m^3]$	27
$E\ [GPa]$	70
υ [-]	0.3

4.1.4 Excitation

Each model configurations were tested with first white noise excitation followed by two different input motions, harmonic and earthquake excitation. The latter excitations were used in the form of sequential, increasing-amplitude time histories. A random noise signal of 1-100 Hz and RMS acceleration of 0.005g was employed during the white noise exploratory testing in order to investigate the dynamic properties of the soil layers and the soil-wall interactive system. The harmonic acceleration was imposed by sinusoidal excitation consisting of 15 steady cycles. The excitation comprises of a 5-cycle ramp up to full test level at the beginning of the excitation and a 5-cycle ramp down to zero at the end to smoothen out the transition between

transient and steady-state response as seen in Figure 4.4. To study the dynamic response of the system, a set of five frequencies 4, 7, 13, 25 and 43 Hz were used at a low acceleration of amplitude 0.05g and then excitation frequency of 7 Hz with increasing amplitude for a series of harmonic excitations was chosen until the failure. (Kloukinas et al., 2014)

Three earthquake records specifically, the Tolmezzo record from the Friuli, 1976 earthquake, the Sturno record from Irpinia, 1980 and the Northridge record from Los Angeles, 1994 earthquake were selected for the earthquake testing. These authentic signals were scaled by a frequency scale factor of 5 in order to be valid for 1-g modelling. (Kloukinas et al., 2014)

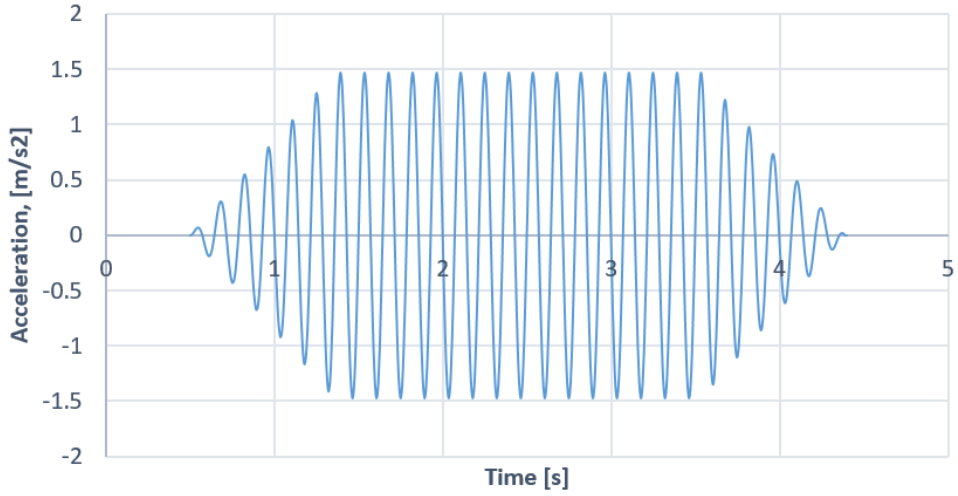

Figure 4.4: Input sinusoidal motion with 7 Hz frequency and amplitude 0.15g

For the verification of the model, the response with only sinusoidal input motion of 15 steady cycles with 7 Hz frequency and PGA of 0.15g as seen in Figure 4.4 has been observed.

4.2 Verification of the numerical model

The verification of the numerical model has been performed in this section. The required information for the creation of the model has been taken from section 4.1. The numerical model of the same size as physical shake table test model has been created in the PLAXIS 2D (version 2015.02). The main aim is to develop a numerical model which confirms that the results are consistent with physical shake table test and then to use the PLAXIS 2D for later analysis.

4.2.1 Geometry

For the numerical model, the same size as the physical shake table test model of 4.8 m wide and 1 m height is created in PLAXIS, see Figure 4.5. The size of retaining wall is taken for Configuration 2 with 600 mm height and 250 mm base. Three node points D1, D2 and D3 along the height of the wall are taken to record the displacement of the wall. The interface has been created in between the sand-wall interaction and prolonged to avoid the numerical problems.

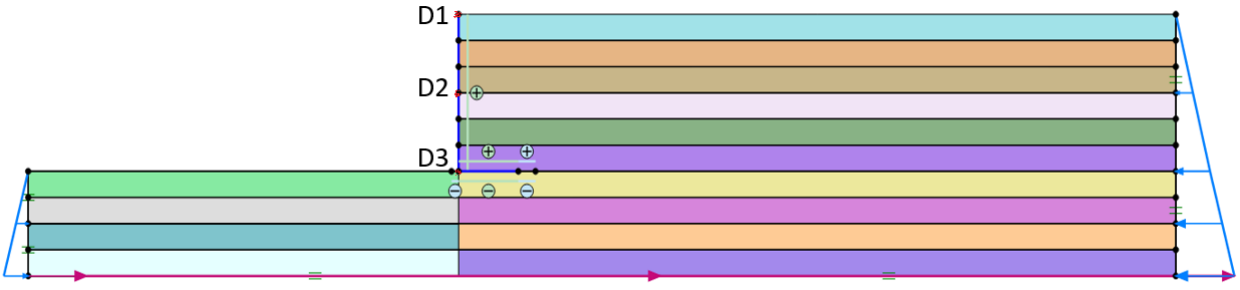

Figure 4.5: Numerical Model in PLAXIS for Shake Table Test for MC Model

4.2.2 Boundary conditions

As discussed in the Chapter 3, the boundaries should be kept at least 3 times the height (3H) of the model to reduce the effect from the boundaries. As the original size of the physical model fulfills this criterion, hence it does not require any prolongation of the boundary.

The *free lateral boundaries* have been used from the result of Chapter 3. The horizontal stress with $k_0 = 1$ has also been added in the lateral boundaries. Few trials were performed with both horizontal stress and no stress condition in the lateral boundaries and the output showed that the results are consistent with the physical model when horizontal stress on the lateral boundaries were applied. At the bottom, the *fixed base* has been applied with a horizontal prescribed displacement to the numerical model.

4.2.3 Material model and material parameters

The numerical analysis has been carried out for 15 noded elements and plane strain condition. The material parameters for the sand and retaining wall has been taken similar to that from the shake table test as described in section 4.1.3. In addition, the values of Poisson ratio, $\upsilon = 0.3$ and cohesion c = 1 kPa has been taken for sand. The overall material properties are summarized in the Table 4.3.

The retaining wall is assumed as a Linear-Elastic non-porous material with $EI = 191 kN/m^2/m$, $EA = 2.24 * 10^6 kN/m$, $w = 0.86 kN/m$ and $\nu = 0.3$ (Gjelseth, 2013). For both sand and wall, the Rayleigh Damping has been given

Table 4.3: Overview of material parameters

Parameters	Bottom Sand	Bottom Sand under backfill	Backfill	Interface soil	Interface wall/soil
ϕ [◦]	42	42	35	42	35
e[−]	0.61	0.61	0.72	0.61	0.72
γ [kN/m^3]	16.14	16.14	15.11	16.14	15.11
G [MPa]	11-31	7-27	30-40	30	20
ψ [◦]	0	0	0	0	0
ν[−]	0.3	0.3	0.3	0.3	0.3
c [kPa]	1	1	1	1	1
$R_{interface}$ [-]	1	1	1	0.6	0.6

as 5% damping for the frequencies 7 Hz and 60 Hz (a_0 = 3.998 and b_0 = 0.000225) as per the study of Penna (2012). For sand, both Mohr-Coulomb and Hardening Soil Model with drained material are used. The analysis is done separately for both models and both the results are compared with the actual shake table output.

For Mohr-Coulomb model, the sand layers are further divided into small layers of each 0.1 m, see Figure 4.5. As the shear modulus does not vary linearly with depth and to account for the stress dependent stiffness, an empirical relation of shear modulus with mean effective stress, Equation 2.16 has been used to estimate the shear modulus. Each layers of sand have been assigned with the computed shear modulus accordingly. The $K_{2,max}$ required in the Equation 2.16 has been assigned corresponding to the void ratio as shown in Table 2.2. The shear modulus calculated from Eigen frequency by Equation 2.11 and 2.14 is different than the shear modulus suggested by Penna (2012) in Figure 4.3, therefore the shear modulus calculated from the empirical relations have been used in the analysis. Figure 4.6 shows the values of shear modulus in different layers for MC model.

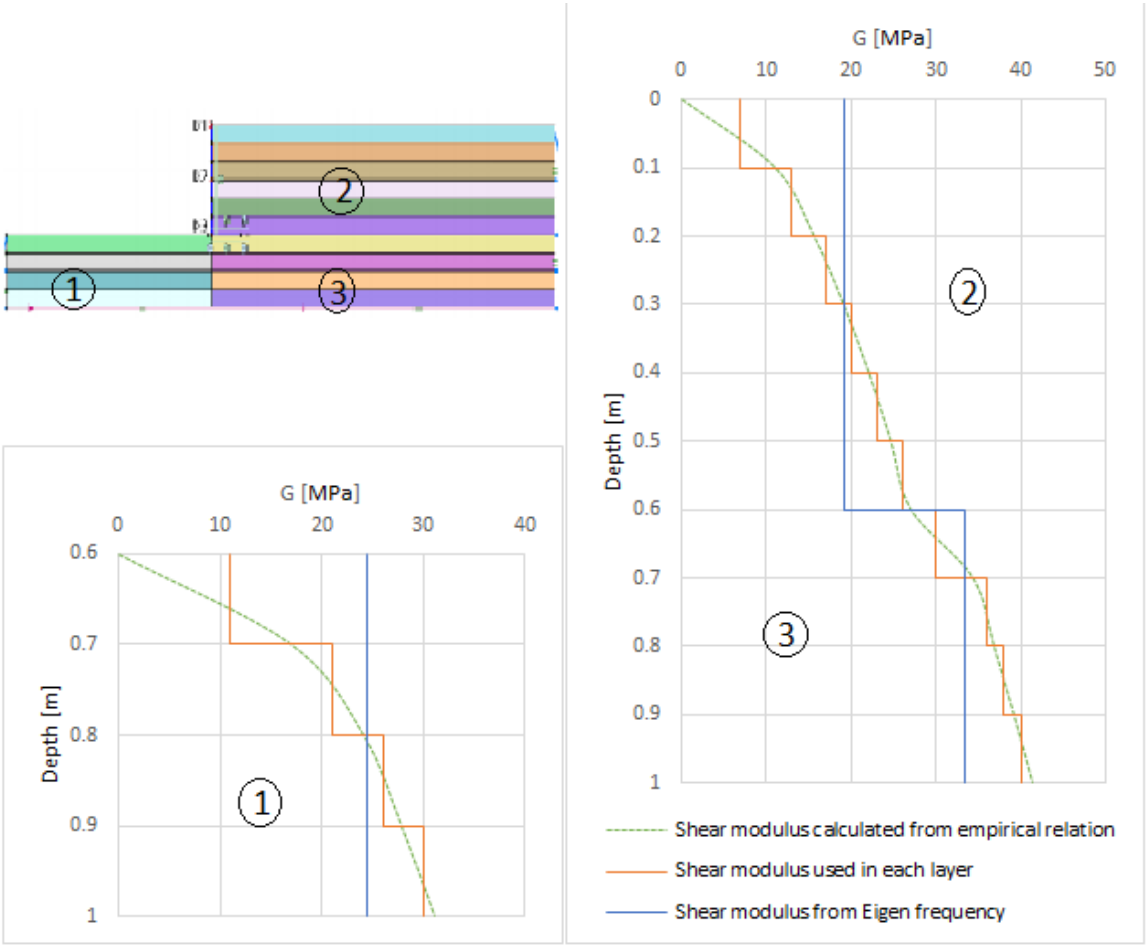

Figure 4.6: Shear Modulus in different layers for MC soil model

For Hardening Soil Model, the particular values of reference stiffnesses ($E_{50}{}^{ref}$, $E_{oed}{}^{ref}$ and $E_{ur}{}^{ref}$) have been assigned for different sand layer. As there was no information provided about these reference stiffnesses in the shake table test papers, these reference stiffnesses along with the m value have been estimated from the formula provided by Brinkgreve et al. (2010) for sands in Equation 2.37, 2.38, 2.39 and 2.40 respectively. The formulas are dependent on the relative density (RD) of the sand and the RD values for different sand layers are taken from Kloukinas et al. (2014). The estimated values have been assigned to each of three different sand layers, see Table 4.4. For the bottom sand under

backfill, the stiffnesses used are bit higher than calculated so as to take into account of the backfill layer above it.

Table 4.4: Reference stiffnesses for different sand layers

Parameters	Bottom Sand	Bottom Sand under backfill	Backfill
${E_{50}}^{ref}$ $[kPa]$	36000	40000	13200
${E_{oed}}^{ref}$ $[kPa]$	36000	40000	13200
${E_{ur}}^{ref}$ $[kPa]$	108000	40000	39600
m	0.51	0.5	0.63

4.2.4 Element size

For a 15-noded element, the element height should be less than the one-quarter of the minimum wavelength in order to get a good results (Kramer, 1996). The model with a medium mesh is shown in the Figure 4.7. The wavelength can be estimated as

$$\lambda_{min} = \frac{V_{s,min}}{f_{max}} \tag{4.1}$$

For the shake table test model, $V_{s,min}$ = 72 m/s and f_{max} = 90 s^{-1}, that gives λ_{min} = 0.8 m and the one quarter of the wavelength becomes 0.2 m. The model has a element size of 0.1 m which should be sufficient to provide a better output.

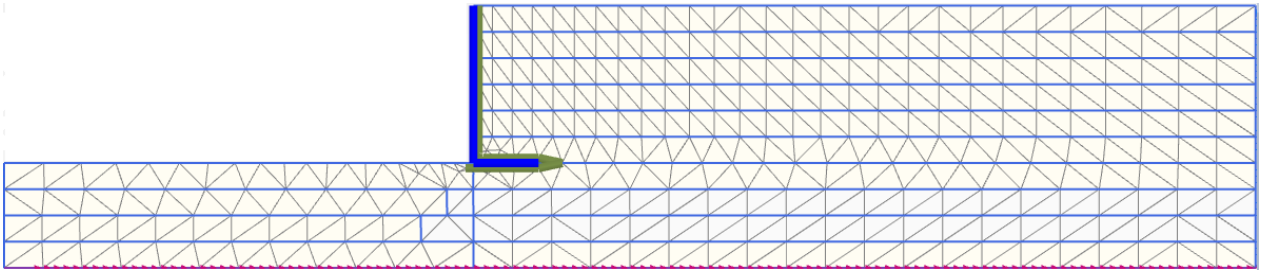

Figure 4.7: Model with 612 elements

4.2.5 Excitation

The acceleration time history of the sinusoidal motion of 7 Hz frequency with amplitude 0.15g presented in Figure 4.4 is integrated and converted into the displacement time history, see Figure 4.8. The displacement time history has been used as an input excitation in the numerical model.

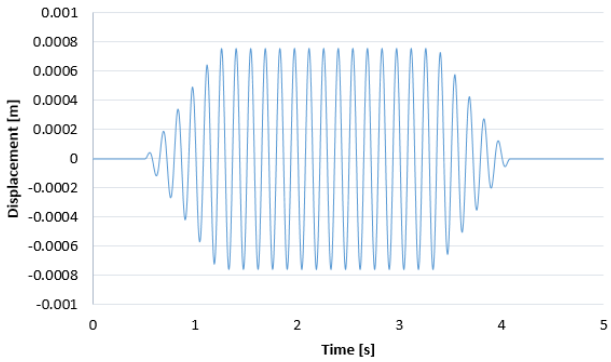

Figure 4.8: Displacement time history of sinusoidal motion of 7 Hz and PGA 0.15g

4.2.6 Analysis

All the analysis have been performed in PLAXIS 2D. The dynamic analysis for both MC model and HS model has been performed with same time steps of 500 with sub steps = 1. The output from the PLAXIS 2D for both the soil models are

compared with actual shake table test results. The results are only compared for the response when sinusoidal motion of frequency 7 Hz and amplitude of PGA 0.15g have been applied for 5 seconds.

4.2.7 Results

The comparison of the PLAXIS 2D analysis with shake table tests has been done for the maximum dynamic moment on the wall and displacement of the wall as a function of time.

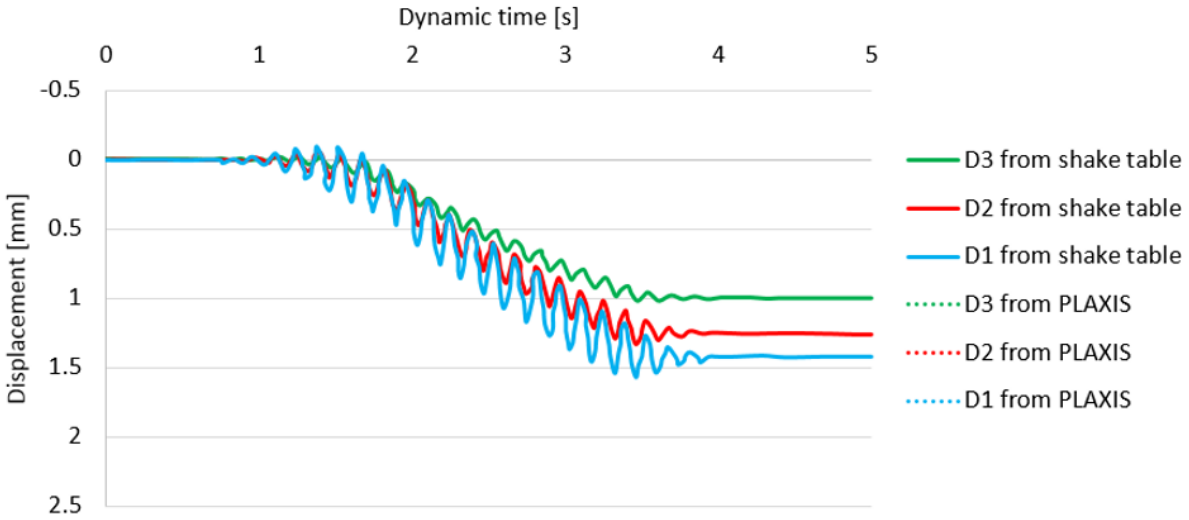

(a) Response in terms of displacement time history for shake table test

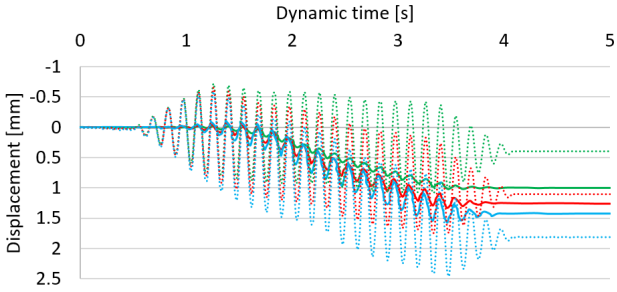

(b) Comparison with MC model

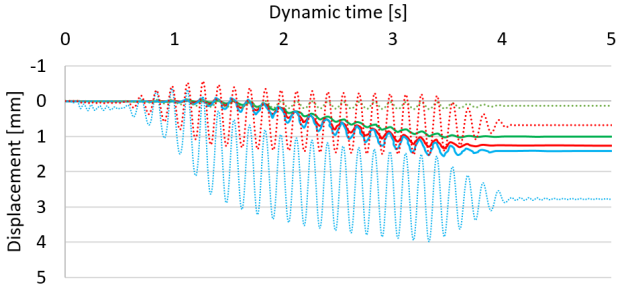

(c) Comparison with HS model

Figure 4.9: Response in terms of displacement time history and its comparison with different soil model

Figure 4.9a shows the actual response in terms of displacement time history of the wall from the Shake table test. D1, D2 and D3 are the output points taken at the wall on top, middle and bottom respectively, see Figure 4.5. Figure 4.9b and 4.9c show the comparison of the displacement time history with MC model and HS model respectively. The result from the shake table test is shown in solid line while the result from the PLAXIS is shown in dotted line. As seen from the Figure 4.9, the amplitude in the PLAXIS out is very large as compared to that from the shake table test. This could have been due to the improper selection of the frequency range for the rayleigh damping provided in the software which resulted in the amplification factor at the top point D1 to be 2.3. Hence, in the numerical model, the wall moves too much in back and forth direction than in actual test.

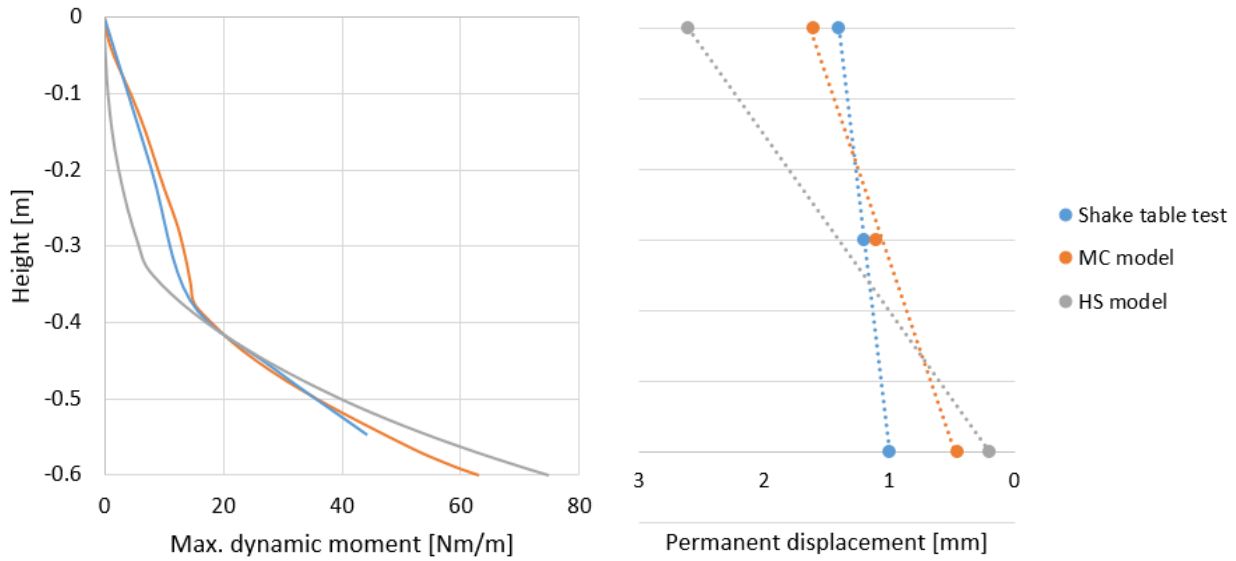

(a) (b)

Figure 4.10: (a) Maximum dynamic moment in the wall and (b) Permanent displacement of wall

The analysis has been again performed with the rayleigh damping of 5 % for f_1 = 7 Hz and f_2 = 20 Hz. This resulted in the displacement of wall of 0.2 mm which

is very deviating from the actual test results. Hence, the chosen damping of 5 % might be low for the analysis.

Furthermore, Figure 4.10a and 4.10b shows the comparison of the maximum dynamic moment on the wall and permanent displacement of the wall respectively for the shake table test, PLAXIS analysis with MC model and HS model. The maximum dynamic moment is calculated by subtracting the static moment from the total moment on the wall.

4.2.8 Conclusion and Discussion

From the results, it can be seen that MC model provided the consistent result with the shake table test than the HS model. The displacement of the wall and also the maximum dynamic moment on the walls as shown in Figure 4.9 and 4.10 are consistent with MC model whereas the HS model gives a very large displacement and rotation of the wall. The main reason behind this could be the parameters provided in the shake table test papers were not sufficient for the HS model and other empirical relations had to be used to estimate the input parameters.

The shear modulus (G), shear wave velocity (v_s), frequency (f) provided in the shake table test papers can be directly used as an input for the MC model whereas for the HS model, the reference stiffnesses and m parameter have been estimated by the empirical formulas provided by Brinkgreve et al. (2010). Also, the friction angle for the sand which have been used in the test i.e. Leighton Buzzard (LB) was estimated by the formula provided by Cavallaro

et al. (2001). For the relative density of 60% it gives the friction angle of 42° but the formula provided by Brinkgreve et al. (2010) in Equation 2.41 gives the friction angle of 35.5°.Hence, the reference stiffnesses estimated by the formula given by Brinkgreve et al. (2010) also may not have been representative for the Leighton Buzzard (LB) sand which ultimately resulted in the deviating results for HS model.

Thus, with the proper input parameters, MC model can provide the consistent result as compared to the actual test output. The applied damping of 5 % might have been low which resulted in more amplification and a bit deviation in the results. To get the better results with HS model, one can perform more trials with different reference stiffnesses and m parameter. Finally, the verification of the numerical model has been performed successfully and the further dynamic analysis performed in PLAXIS 2D should provide a reasonable output.

Chapter 5

Numerical modeling of a gravity wall

This chapter provides a numerical modeling of a gravity wall under earthquake excitation. The gravity wall of height 4 m with a backfill sand having friction angle of 35° is excited with an earthquake of PGA 0.05g. Geometry, Element size, Boundary conditions, material model and material parameters and the results from the analysis of this particular case are illustrated in detail here. It is of great interest to know how the total stresses and forces vary behind the wall and the displacement of the wall due the earthquake excitation. The comparison of the PLAXIS 2D output with the M-O method has also been carried out. This Chapter provides a base case for all the further analysis to be carried out for different types of wall.

5.1 Geometry

The model used has a length of 200 m and height of 34 m. The retaining wall is 4 m high and located nearly at the center of the model, see Figure 5.1.

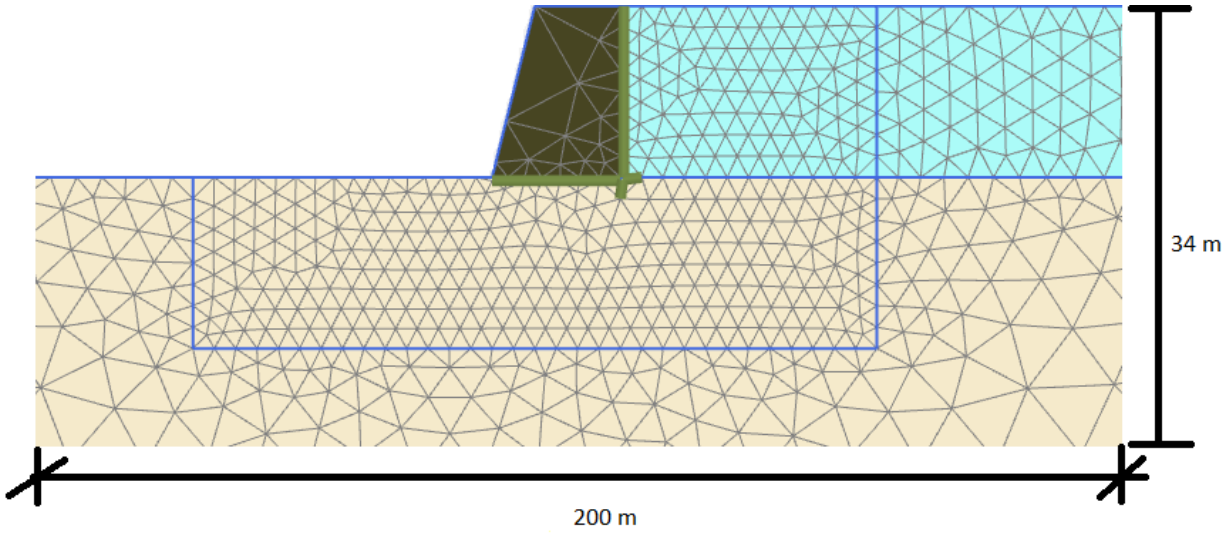

Figure 5.1: Numerical Model for Gravity Wall (figure not to scale)

The backfill material is a dry sand and the underneath the wall is a clay layer of 30 m height. The concrete retaining wall has a height of 4 m and a width of 3 m. To study the response under the earthquake, 10 stress points and few node points are taken as shown in the Figure 5.2. The stress points K to T are taken behind the wall from top to bottom of the wall to study the variation of the earth pressure and total force with time. The node points A and B are taken to study the deformation that the wall undergoes due the earthquake excitation.

Figure 5.2: Stress points (left) and Node points (right)

5.2 Element size

As discussed in the Section 5.1 that the numerical model has a very large size. Hence, a proper element size should be assigned for the better results. For that, the element size near the retaining wall is taken much smaller that the other parts, see Figure 5.3.

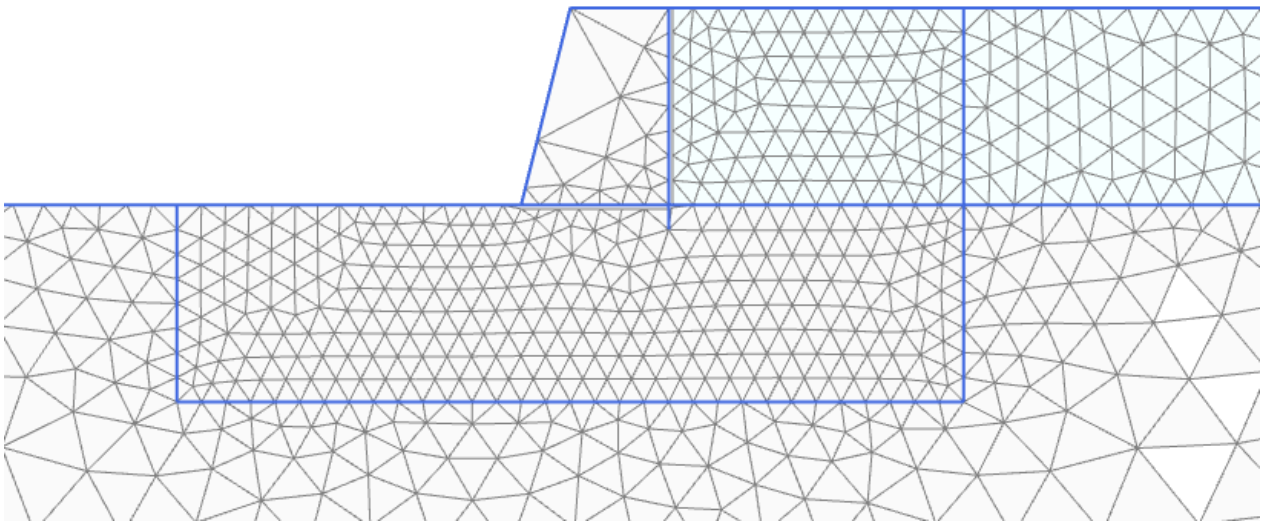

Figure 5.3: Numerical Model with elements

A $c-\phi$ reduction has been carried out for the retaining wall with different mesh coarseness as shown in Table 5.1.

Table 5.1: c-ϕ reduction for different mesh coarseness

Case	Mesh Coarseness	Relative element size	Factor of safety
1	Coarse	1.33	1.457
2	Medium	1	1.443
3	Fine	0.667	1.436
4	Very fine	0.5	1.412
5	Expert setting	0.33	1.411

Figure 5.4 shows the factor of safety for different mesh coarseness. As the factor of safety does not converges even when very fine mesh been used, an expert

setting in PLAXIS 2D with relative element size as minimum as possible i.e. 0.33 has been used which gives the almost equal factor of safety as very fine mesh. Hence, for the better output, all the further analysis has been carried out with an expert setting and relative element size of 0.33, Case 5 shown in Table 5.1.

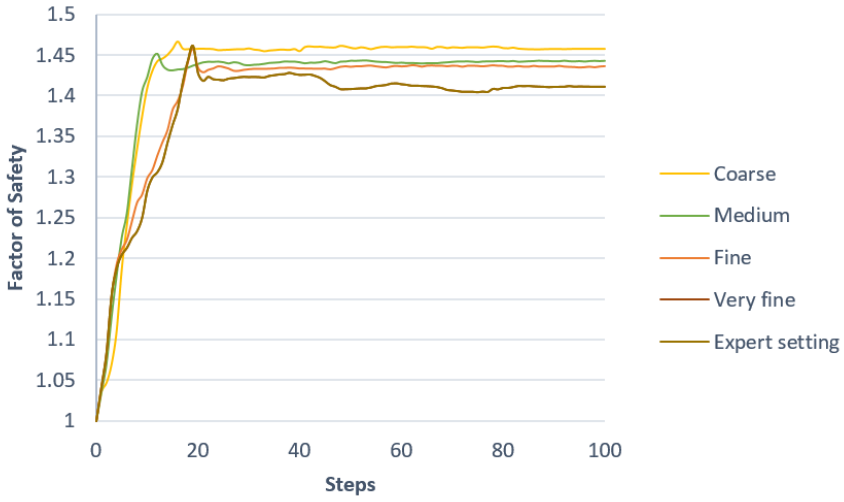

Figure 5.4: Factor of safety for different mesh coarseness

5.3 Material model and material parameters

The analysis is carried out with a 15-noded element in plane strain condition. For a gravity wall, linear elastic material model has been chosen while Mohr-Coulomb has been chosen for both sand backfill and clay. The backfill material can be also clay but because the soil behind the wall should be excavated and replaced by sand, the whole backfill is assumed sand for simplicity. The shear modulus of the sand backfill has been estimated form the Equation 2.16 and Table 2.2, with a relative density of 30 %. Table 5.2 shows the material properties taken for the sand. The rayleigh damping of 5 % for frequencies f_1 = 0.2 Hz and

f_2 = 5 Hz has been taken for all the system. For the friction between wall and soil, interfaces are constructed with a roughness of $R_{vertical}$ = 0.6 for wall-sand interaction whereas $R_{horizontal}$ = 1 has been used for better wall-clay interaction.

Table 5.2: Material properties for Sand

Parameters	Sand backfill	Interface sand
material model	MC-Drained	MC-Drained
ϕ [$\circ$]	35	35
D_r [%]	30	30
γ [kN/m^3]	18	18
G [MPa]	45	45
ψ [$\circ$]	0	0
ν[$-$]	0.3	0.3
c [kPa]	1	1
$R_{interface}$ [-]	1	0.6

For the clay layer, the undrained shear strength(S_u) and shear modulus (G) are estimated from the Equation 2.18 and 2.17 respectively. The Equation 2.17 gives shear modulus dependent on S_u and Equation 2.18 provides S_u dependent on effective vertical stress (taking $S_u = 0.2\sigma'_v$) and linearly increasing with depth. Therefore, the shear modulus used for the analysis is linearly increasing with depth i.e no stress dependent stiffness. For the analysis, a minimum S_u of 30 kPa is taken. Hence, the clay layer is divided into two layers.

The upper layer has the constant S_u of 30 kPa from the ground surface to the depth where S_u estimated from Equation 2.18 becomes 30 kPa and the lower clay layer has a S_u linearly increasing with depth from 30 kPa, see Figure 5.5. The overall depth of the clay layer taken is 30 m. The ground water level is at the top of the upper clay layer. The material properties of the clay are described in the Table 5.3.

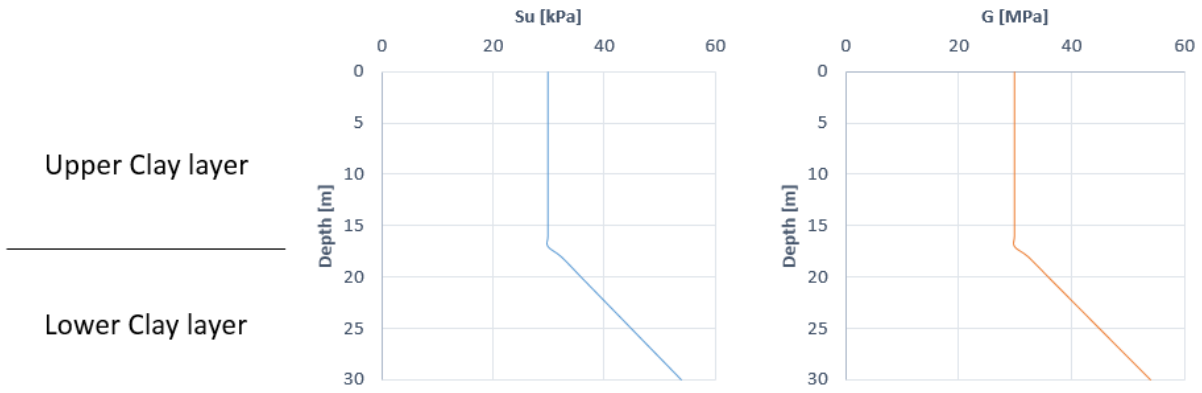

Figure 5.5: S_u and G value for upper and lower clay layer

Table 5.3: Material properties for Clay

Parameters	Upper clay	Lower clay	Interface clay
material model	MC-Undrained	MC-Undrained	MC-Undrained
$Depth[m]$	17	13	-
S_u $[kPa]$	30	30-54	30
γ $[kN/m^3]$	20	20	20
G $[MPa]$	30	30-54	30
$\nu[-]$	0.3	0.3	0.3
$R_{interface}$ [-]	1	1	1

The gravity wall has a unit weight of 24 kN/m^3 with Young's modulus of Elasticity (E) of 3*10^{10} kPa and Poisson ratio (ν) of 0.15.

5.4 Boundary conditions

From the discussion in the Section 3.3 of Chapter 3, the boundaries should be kept at least 3 times the height (3H) of the model to have minimal effect from the boundaries. Thus, for the height of soil layers 30 m and 34 m in front and back of the retaining wall respectively, the lateral boundaries are kept at 100 m distance far at each end from the retaining wall which makes the total length of the model of 200 m.

The *free lateral boundaries* have been used from the result of Chapter 3. At the boundaries, horizontal stress with a k_o = 1 has been added in the model due to the limited shear strength of the soil. At the bottom, the *fixed base* has been applied with a horizontal prescribed displacement to the numerical model.

5.5 Excitation

Figure 5.6 shows the acceleration time history of the earthquake of PGA 0.05g applied to the fixed base of the numerical model. The time history has an overall duration of 40 seconds and is provided at 0.02 second interval. Hence, the number of steps used in PLAXIS for the simulation is 2000 (40/0.02 = 2000).

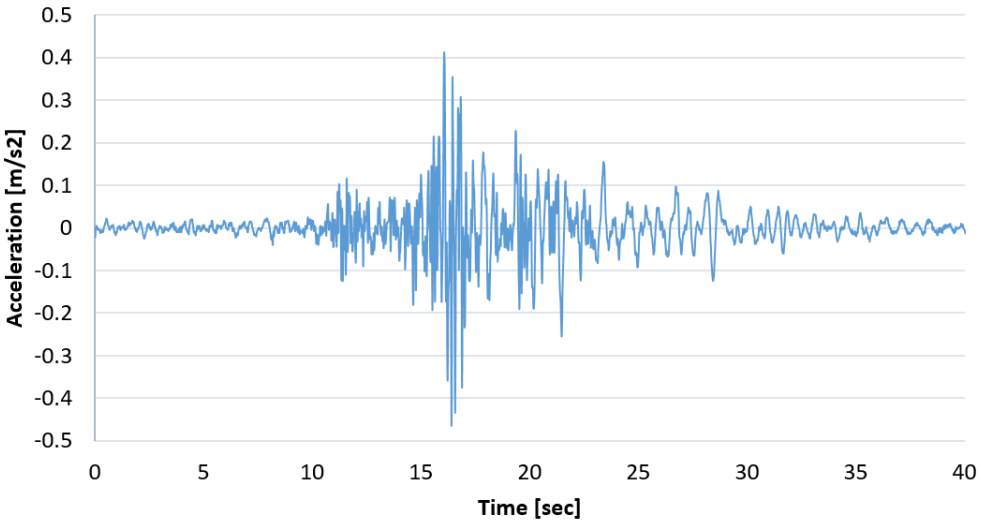

Figure 5.6: Acceleration time history with PGA of 0.05g

5.6 Analysis

The analysis is carried out in the PLAXIS 2D. The different analysis performed at the different phases are shown in the Table 5.4.

Table 5.4: Different phases of analysis in PLAXIS 2D

Phase	Enabled	Calculation	Start from
1	Clay layer	K_o Procedure	-
2	Retaining wall	Plastic	Phase 1
3	Sand Backfill	Plastic	Phase 2
4	Safety	Safety	Phase 3
5	Excitation	Dynamic	Phase 3

5.7 Results

The safety analysis (c-ϕ reduction) done in Phase 4 as shown in Table 5.4, gives a safety factor of 1.451. It satisfies the criteria that the design safety factor should be greater than 1.4 for $c-\phi$ reduction as per EC 7 Design Approach 1/2. Figure 5.7a shows the incremental strain after the safety analysis in Phase 4 where behind the wall there is an active earth pressure failure and underneath a shallow bearing capacity failure. The deformed shape after the earthquake excitation is presented in the Figure 5.7b where some backfill sand mass falls down near the top of the wall.

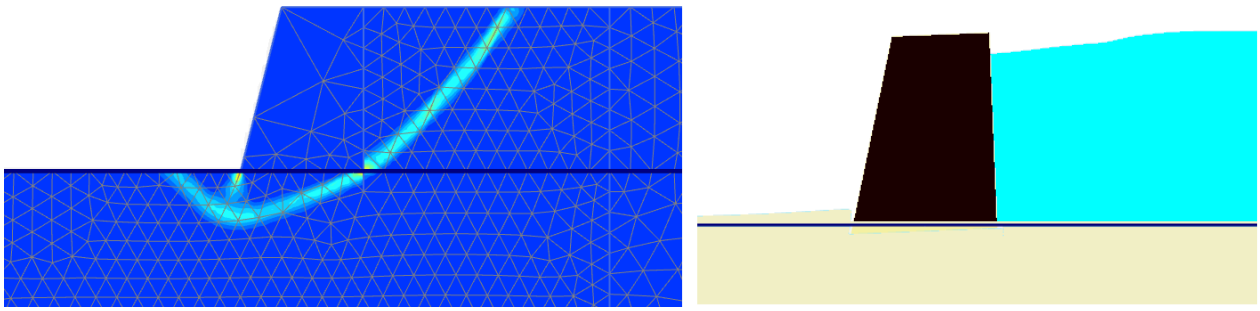

(a) (b)

Figure 5.7: (a) Incremental strain after safety analysis (b) Deformed shape after earthquake excitation (scaled up 100 times)

During dynamic analysis in Phase 5, horizontal stresses (σ'_{xx}) at the wall are obtained through the 10 stress points (K to T) taken behind the wall and the

displacement of the wall is recorded at node point A and B as shown in the Figure 5.2.

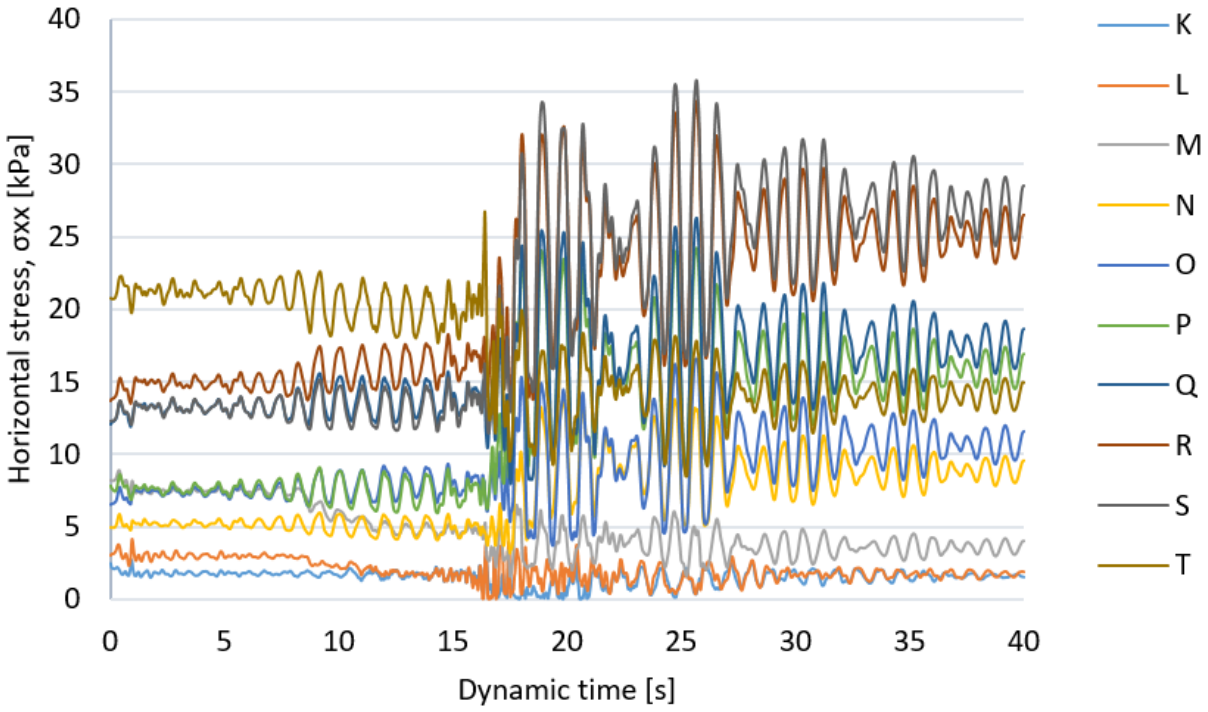

Figure 5.8: Horizontal stress variation at different stress points

The stress variation during the earthquake at these points for K to T is shown in the Figure 5.8. The stress time history from the PLAXIS output is exported to a spread sheet and further integrated to get the total force time history during the earthquake. Figure 5.9 shows the total force variation during the earthquake for the PGA of 0.05g and sand backfill of friction angle 35°.

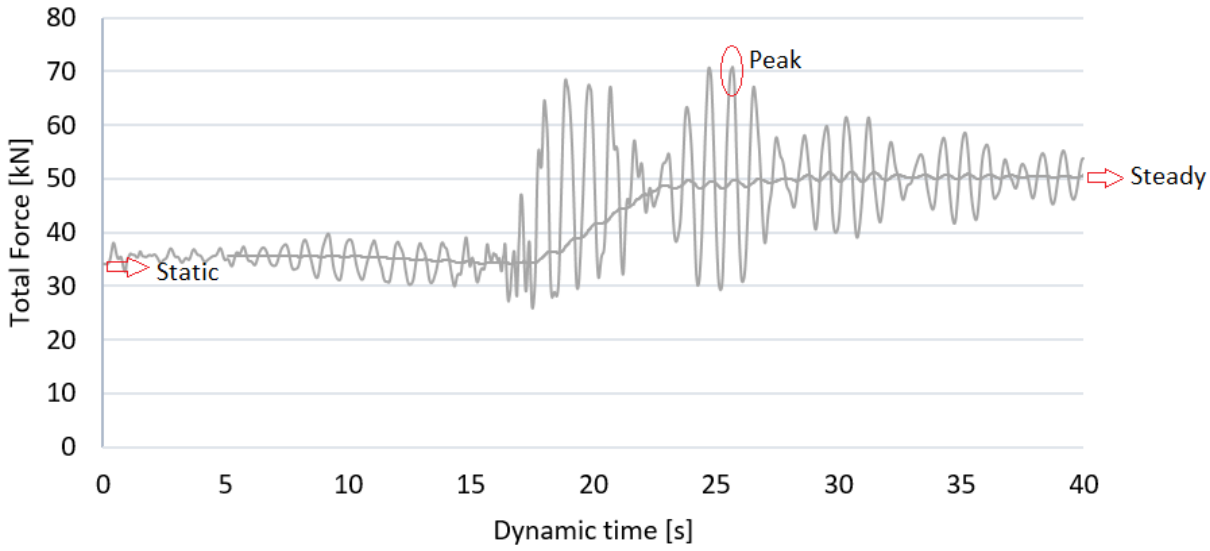

Figure 5.9: Total force variation during earthquake of PGA 0.05g and sand with phi = 35°

The total force is the contribution of both static and dynamic force. From the result, it can be seen that in the static condition both M-O method and PLAXIS gives nearly equal horizontal force acting on the wall i.e. 35.28 kPa and 34.22 kPa respectively which provides a solid ground for the comparison during the dynamic analysis.

For the M-O method, the k_h and k_v are calculated from Equation 2.33 and 2.34 respectively. The amplification factor, S is taken as 1.7 for the ground type E, see Table B.2 in Appendix B. The r value is taken as 1.5 from the Table 2.3 which gives the maximum allowable horizontal displacement of wall for seismic class 2 as $d_r = 200\alpha S = 17$ mm. The horizontal displacement time history of the wall is presented in the Figure 5.10.

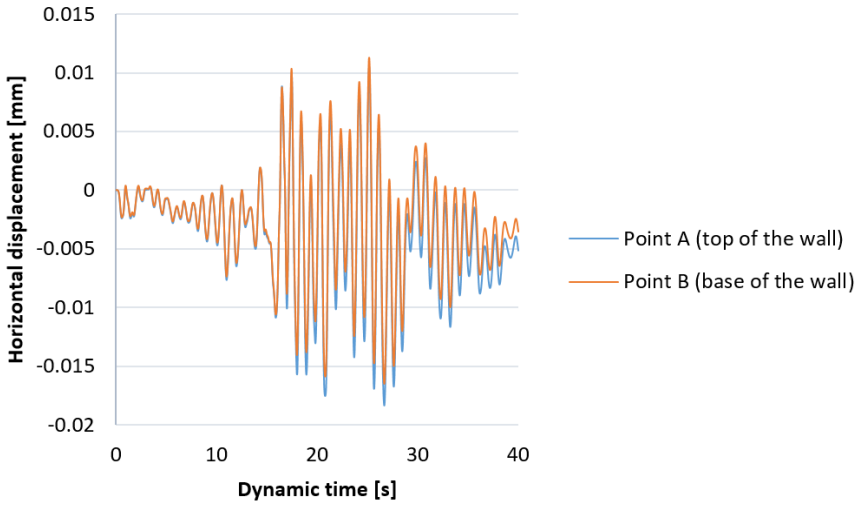

Figure 5.10: Horizontal displacement time history during earthquake of PGA 0.05g and sand with $\phi = 35°$

From the analysis, the total force at peak and steady state are found to be 70.91 kN and 51 kN respectively while M-O method gives 39.31 kN. The permanent horizontal displacement of the wall at point A and B are obtained as 5 mm and 4 mm respectively which shows that there is just a translation of the wall with negligible rotation.

The variation in the total force from PLAXIS and M-O method is also governed by the input acceleration. For the cross check, the input acceleration at the base of the model, base of the wall (left of the wall at Point C) and top of the wall (right of the wall at Point D) are taken from the PLAXIS, see Figure 5.2. The point C and D are taken in between the wall and the boundaries such that there is not much effect from both of them i.e. free field condition. Figure 5.11 shows the acceleration at these different node points. It can be seen that at point C and D, the peak acceleration is ca. 1 m/s^2 and 0.9 m/s^2 which gives the amplification factor of 2.05 and 1.82 respectively. Both the amplification factor (S) is higher

that the value taken in M-O calculation i.e. $S = 1.7$. Hence, if the acceleration is taken at the base of the wall i.e. $S = 2.05$ in the M-O method, it will give the total force a bit closer to the steady state.

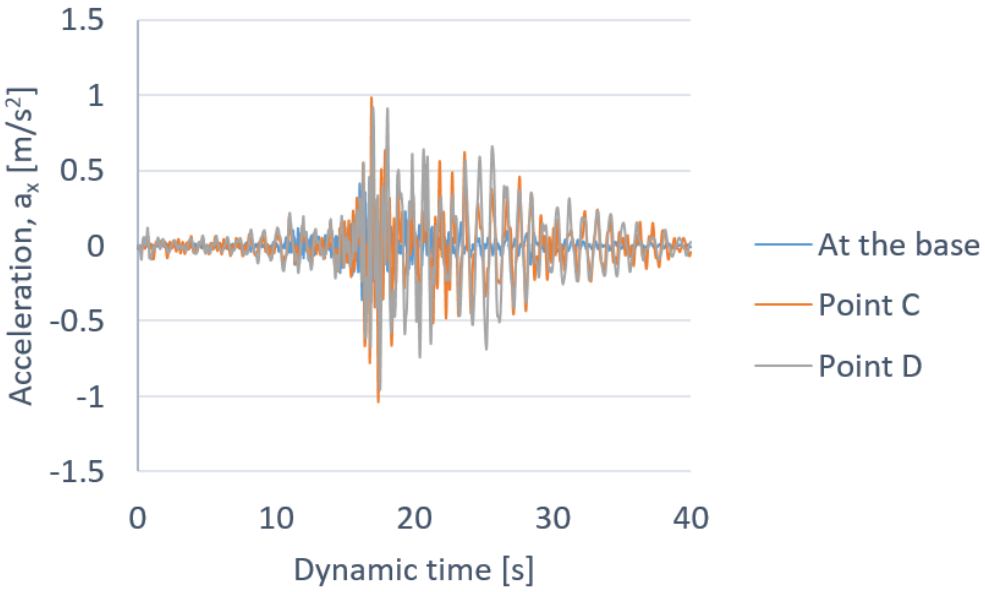

Figure 5.11: Input acceleration at different points

5.8 Conclusion and Discussion

The total forces at peak and steady state is very different than the total force calculated from M-O method. The results show that the total force from M-O method is lower than both peak and steady value but closer to the steady value. The displacement of the wall is within the acceptable limit and there is a just translation of wall which shows resemblance with what M-O method suggests.

In general, this chapter provided a general procedure for the dynamic analysis in gravity wall. All the further analysis of retaining walls with earthquake excitation will be similar to what it has been done in this chapter.

Chapter 6

Parameter studies

This chapter provides the effect of different parameters on the stability and performance of the gravity wall under the earthquake excitation. The stability and performance of the wall are governed by the total force acting behind the wall and deformations of the wall. Parameters studied are the different height of the wall (3.5, 4 and 5 m), the different friction angle of the backfill (32°, 35° and 38°) and different PGA levels of the earthquake (0.05g, 0.1g, 0.15g and 0.2g). In addition, the effect of three different earthquakes but with equal PGA of 0.05g has been studied. Furthermore, the effect of the sloped backfill has also been studied.

6.1 Analysis

The analyzing procedure for all the cases is similar to that of Chapter 5. The analysis has been carried out for different topics as described below:

6.1.1 Effect of wall height and friction angle of the backfill

Table 6.1 shows all the cases analyzed for the effect of the wall height and friction angle of the backfill. In each case, a constant friction angle of the backfill and the height of the wall has been excited by an earthquake with different PGA levels. For the MC model, the shear modulus (G) of the soil has been reduced with the increase in PGA as per the provision in EC 8-5, see Table 2.1. The shear modulus has been reduced by 80 % for $\alpha = 0.1$, 60 % for $\alpha = 0.15$ and 50 % for $\alpha = 0.2$, where $\alpha = a_g/g$.

Table 6.1: Different cases for analyzing effect of wall height and friction angle of backfill

Case	ϕ (°)	Height (m)	F_{safety}	α	G_{sand} (MPa)	G_{clay} (MPa)
				0.05	45	30
				0.1	36	24
1	32	4	1.411	0.15	27	18
				0.2	22.5	15
				0.05	45	30
				0.1	36	24
2	35	4	1.451	0.15	27	18
				0.2	22.5	15
				0.05	45	30
				0.1	36	24
3	38	4	1.481	0.15	27	18
				0.2	22.5	15
				0.05	45	30
4	38	3.5	1.703	0.1	36	24
				0.15	27	18
				0.05	45	30
5	38	5	1.166	0.1	36	24
				0.15	27	18

The first three cases (1, 2 and 3) provides the analysis for the effect of backfill friction angle (32°, 35° and 38°) when the height of the wall is 4 m. Four different PGA levels of Imperial Valley earthquake (0.05g, 0.1g, 0.15g and 0.2g) have been

used for these three cases. The case 3, 4 and 5 refers to the analysis of the effect of the wall height (3.5, 4 and 5 m) when friction angle of the sand backfill is 38°. Three different PGA levels of Imperial Valley earthquake (0.05g, 0.1g and 0.15g) have been used for the case 4 and 5. All the cases shown in Table 6.1 have safety factor more than 1.4 except for the case 5 when the height of the gravity wall is 5 m. Hence, the design of the gravity wall for case 5 is not safe statically.

6.1.2 Effect of different earthquakes of same PGA 0.05g

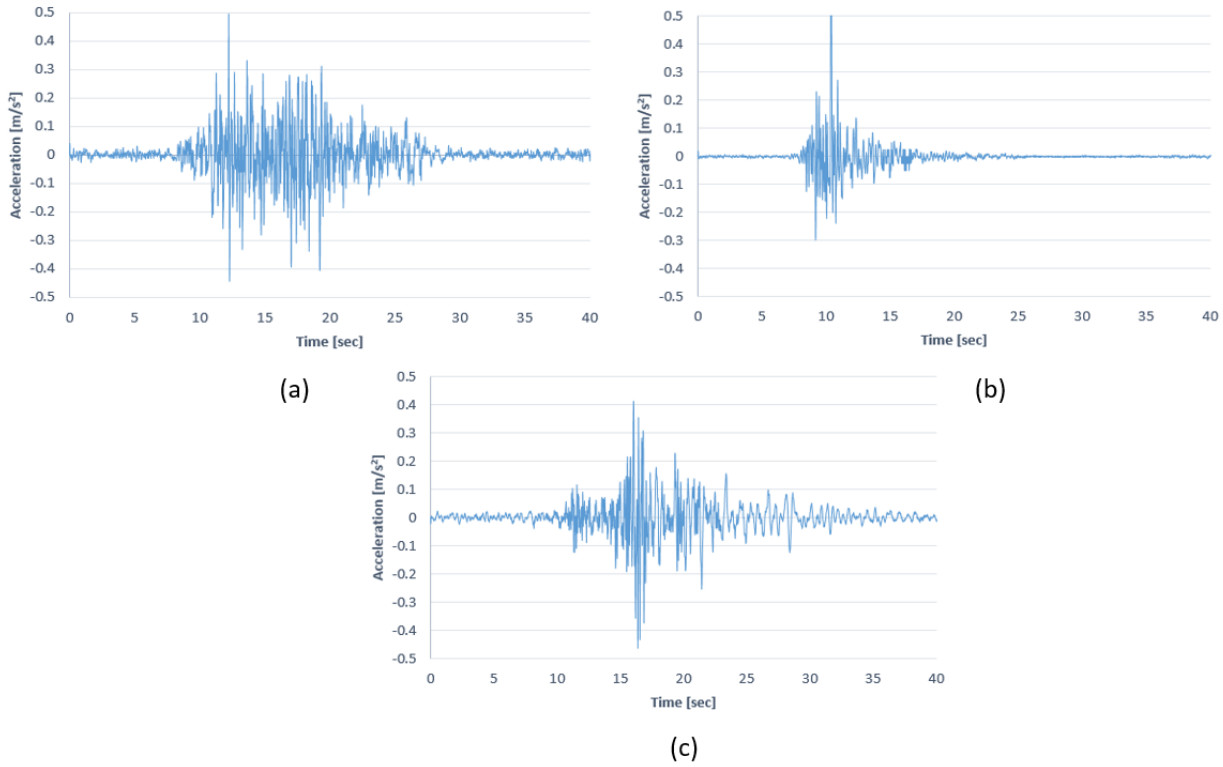

Figure 6.1: Three different earthquakes of same PGA 0.05g (a) Nahani, Canada, Comp. 270 deg., 1985, (b) Friuli, St. Tarcento, Italy, Comp. NS, 1976 and (c) Imperial Valley, St. Superstition Mt., USA, Comp. 135 deg., 1979

Figure 6.1 shows the three different earthquakes; (a) Nahani, Canda (EQ1), (b) Friuli, St. Tarcento, Italy (EQ2) and (c) Imperial Valley, St. Superstition Mt. (EQ3)

with equal PGA of 0.05g. The analysis has been carried out for same ground conditions, gravity wall with a sand backfill of friction angle 35° but with three different earthquakes (EQ1, EQ2 and EQ3) of the same PGA of 0.05g.

6.1.3 Effect of the sloped backfill

The effect of the sloped backfill under the earthquake excitation has also been studied, see Figure 6.2. The analysis has been carried out similarly as in previous cases but with different backfill slopes. Three different slopes (1/15, 1/10 and 1/5) of the backfill along with no slope of backfill have been analyzed. The largest friction angle of backfill of 38° has been taken for the analysis in order to maintain a good safety factor. The analysis has been carried out for the Imperial Valley earthquake with three level of PGA (0.05g, 0.1g and 0.15g). Table 6.2 shows the overview of the different cases analyzed for the sloped backfill. The design of gravity wall for all the cases (6, 7, 8 and 9) are statically safe i.e. in all the cases, the safety factor is more than 1.4.

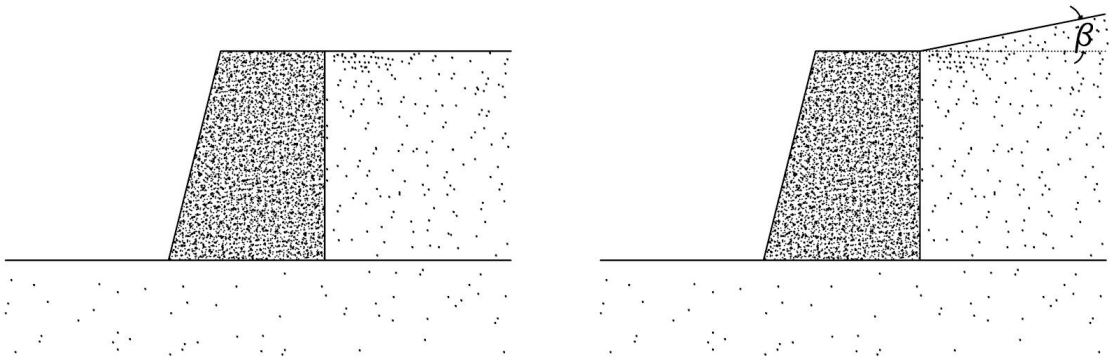

Figure 6.2: Gravity wall with no backfill slope (left) and with backfill slope angle β

Table 6.2: Overview of different cases for sloped backfill

Case	Slope inclination or β	Friction angle of backfill (°)	Height (m)	F_{safety}	α
6	no slope ($\beta = 0$)	38	4	1.481	0.05 0.1 0.15
7	1/15 ($\beta = 3.814$ °)	38	4	1.468	0.05 0.1 0.15
8	1/10 ($\beta = 5.71$ °)	38	4	1.453	0.05 0.1 0.15
9	1/5 ($\beta = 11.31$ °)	38	4	1.426	0.05 0.1 0.15

6.2 Results

As discussed in the previous section 5.7 of Chapter 5, the peak and steady total forces from T-H analysis (PLAXIS 2D) are compared to the total force calculated using M-O method and the displacement of the wall has also been compared for the different cases in order to analyze the stability and performance under the earthquake excitation.

6.2.1 Effect of wall height and friction angle of the backfill

Figure 6.3 shows the variation of total force with different friction angle of the backfill at different PGA for the wall height of 4 m. In all the results, the total force decreases as the backfill friction angle increases. The M-O method gives lower total force than both peak and steady value from the PLAXIS for PGA of 0.05g. The total force from M-O method gets closer to steady value as the PGA increases but there is always a significant difference of almost 30 KN between

the peak value and the value calculated from M-O method.

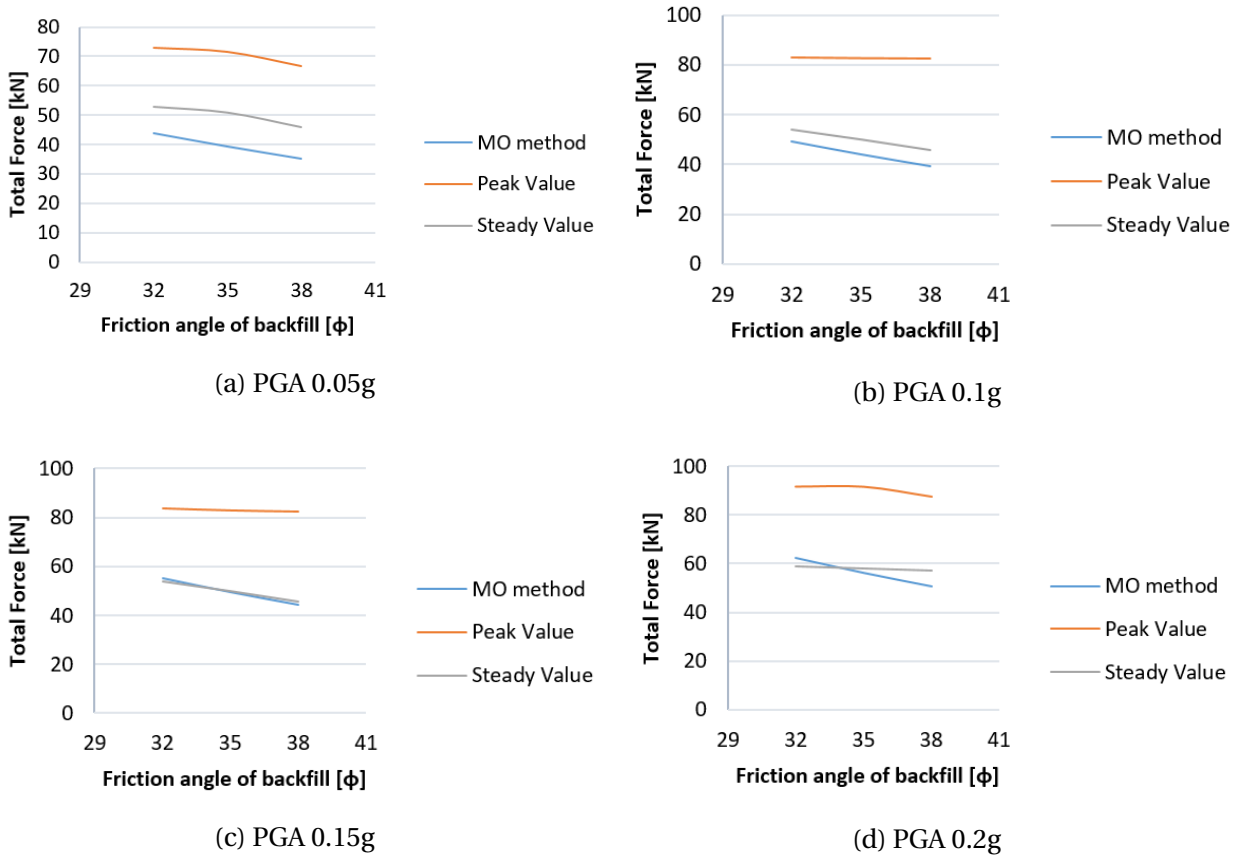

(a) PGA 0.05g

(b) PGA 0.1g

(c) PGA 0.15g

(d) PGA 0.2g

Figure 6.3: Total Force Vs Friction angle of the backfill at different PGA and H = 4 m

Figure 6.4 shows the variation of total force as per different PGA levels of the earthquake. The variation is shown for different friction angles i.e. 32°, 35° and 38° with gravity wall of height 4 m. The results are representative of the case 1,2 and 3 of the Table 6.1. It can be seen that the total force increases as the PGA increases but there is an insignificant increase (almost equal) in total force for peak values from PGA of 0.1g to 0.15g.

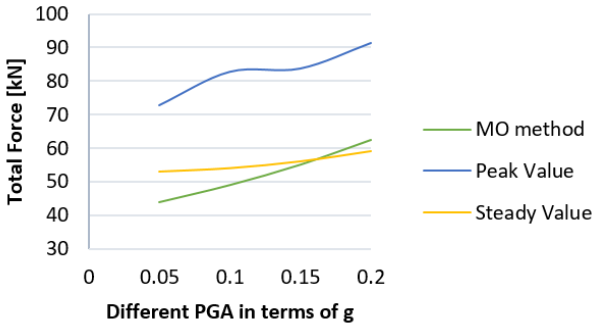

(a) phi = 32°

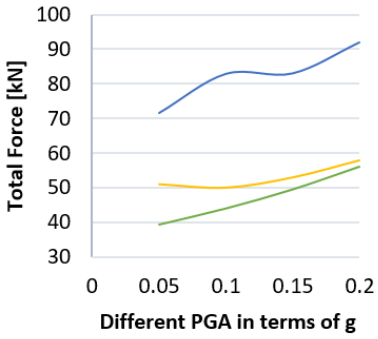

(b) phi = 35°

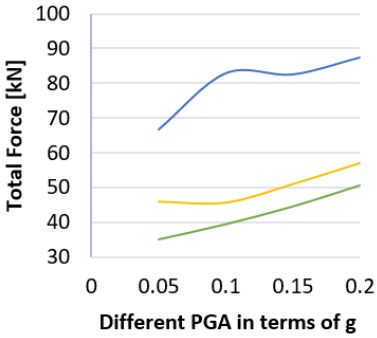

(c) phi = 38°

Figure 6.4: Total Force Vs different PGA at different friction angle of the backfill and H = 4 m

Figure 6.5 shows the horizontal displacement of the wall with respect to different PGA levels of the earthquake. The displacement of the 4 m wall has been measured at the top (Point A) and base (Point B) for different friction angle of the backfill. It can be seen that the displacement of the wall increases as the PGA level increases. The horizontal displacement of the wall is within the permissible limit up to the PGA level of 0.1g. At PGA level of 0.1g, for the backfill of friction angle 32°, the maximum horizontal displacement becomes 26 mm which is lower than the maximum allowable horizontal displacement (for seismic class 2) of $d_r = 200\alpha S = 34$ mm where $\alpha = 0.1$, $S = 1.7$ for the ground type E, see Table B.2 in Appendix B and $r = 1.5$ from the Table 2.3. When the

PGA reaches 0.15g, the horizontal displacement increases significantly and have the values beyond the permissible limit. Hence, the gravity wall fails for the PGA higher than 0.1g.

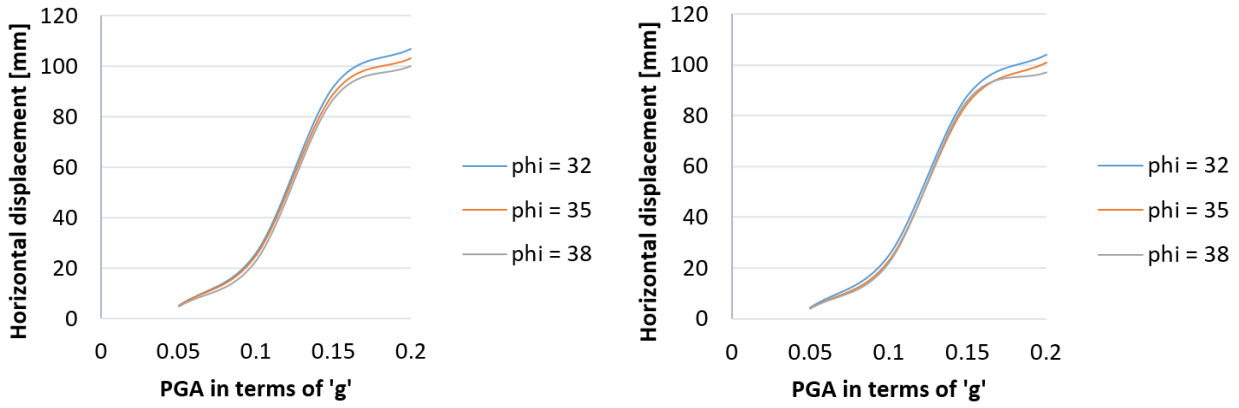

(a) Point A (top of the wall)

(b) Point B (base of the wall)

Figure 6.5: Horizontal displacement of the wall at different PGA for different friction angle of backfill and H = 4 m

Furthermore, the horizontal displacement of the wall decreases as the friction angle of the backfill increases but the change in horizontal displacement with respect to friction angle of the backfill is very insignificant in comparison to the change with respect to the PGA level. Also, the displacement of the Point A (top) and Point B (base) are almost equal for all the cases which explain that there is just a translation of the wall with negligible rotation.

Figure 6.6 shows the variation of the total force with respect to the height of the wall. The graphs are shown for different excitation levels (0.05g, 0.1g and 0.15g). The results are representative of the cases 3, 4 and 5 of the Table 6.1. It shows that the total forces for peak, steady and M-O value are all increasing with the increase of the height of the wall. The peak total force is always larger than the steady and M-O method total forces and the total force from M-O method is

closer to the steady value of total force in all cases.

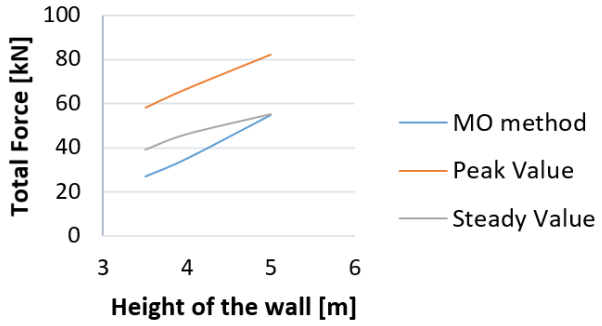

(a) PGA 0.05g

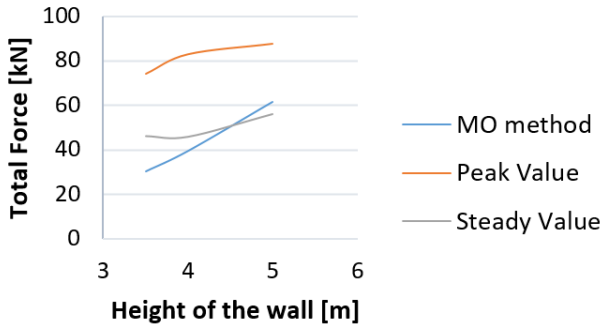

(b) PGA 0.1g

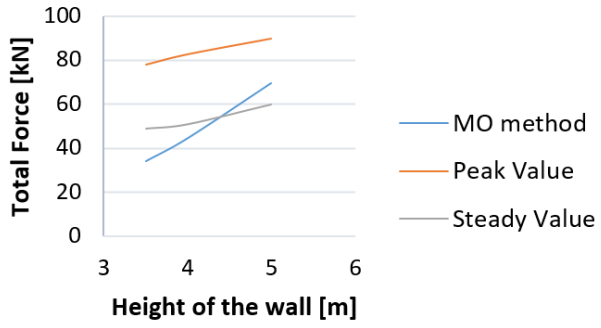

(c) PGA 0.15g

Figure 6.6: Total Force variation at different height of the wall and backfill phi = 38°

Figure 6.7 shows the horizontal displacement of the wall at different excitation levels with a backfill of friction angle 38°. It can be seen that, for the wall of height 3.5 m and 4 m, the horizontal displacement of the wall is within the permissible limit up to PGA 0.1g but fails at PGA 0.15g. The 5 m gravity wall which has a very marginal safety factor of 1.166 (improper design), fails (exceeds the horizontal displacement limit) even in the PGA level of 0.05g and goes under very large horizontal displacement for higher PGA levels. Hence, it highlights the importance of proper design of the walls to perform better under earthquake excitation. As in previous cases, there is just a translation of wall and negligible rotation in all the cases.

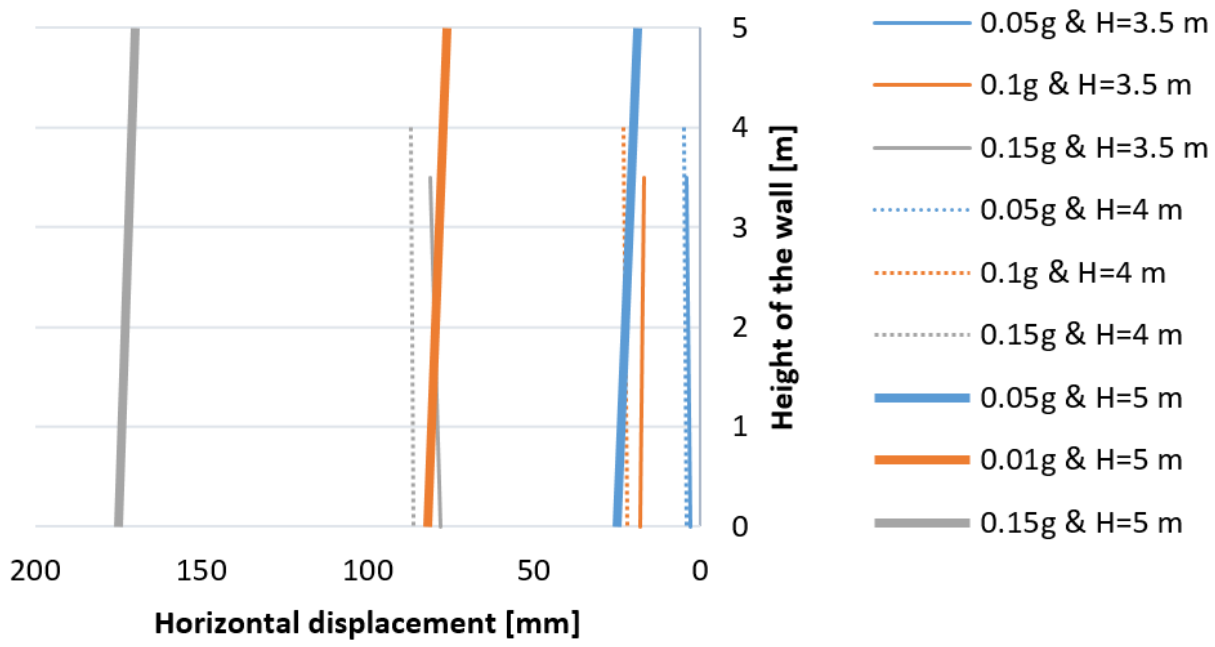

Figure 6.7: Horizontal displacement of the wall of different height at different PGA and phi = 38°

6.2.2 Effect of different earthquakes of same PGA 0.05g

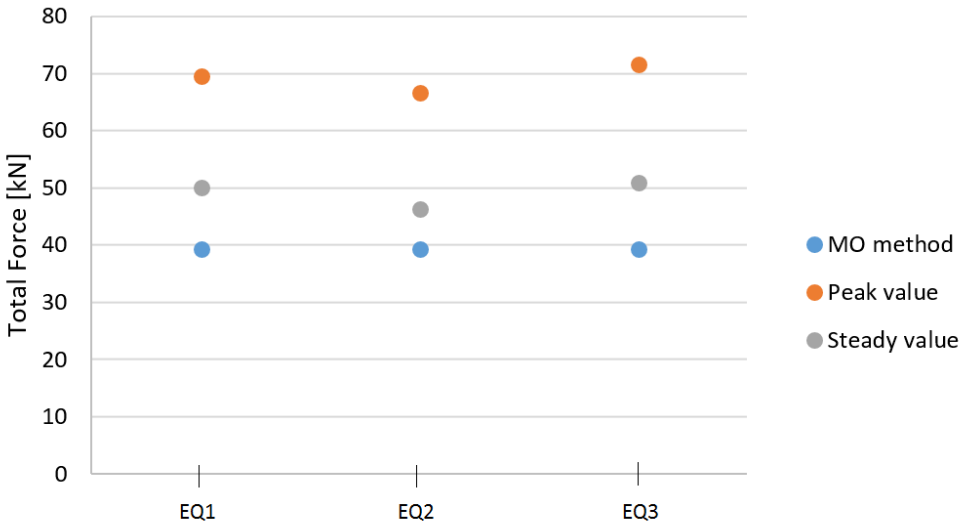

Figure 6.8: Total force for different earthquakes of same PGA 0.05g and phi = 35°

The total force variation for the different earthquakes but with same PGA level of 0.05g, backfill friction angle of 35° and the wall height of 4 m is presented in

the Figure 6.8. For all the three different earthquakes, M-O method gives exactly same total force whereas the time history analysis gives three different total forces at both peak and steady state. The M-O method values are closer to the total force at steady state.

6.2.3 Effect of the sloped backfill

The effect of the sloped backfill is presented in the Figure 6.9 and 6.10. The results are representative of all the cases (6, 7, 8 and 9) shown in the Table 6.2. Figure 6.9 illustrates the total force variation with different slopes of the backfill at different PGA levels. The height of the wall is taken as 4 m with a backfill of friction angle 38°. As in the previous cases, the total forces increases with the increase in PGA level. Also, when the slope of the backfill increases, the total force (peak, steady and MO values) increases for the same PGA level as well.

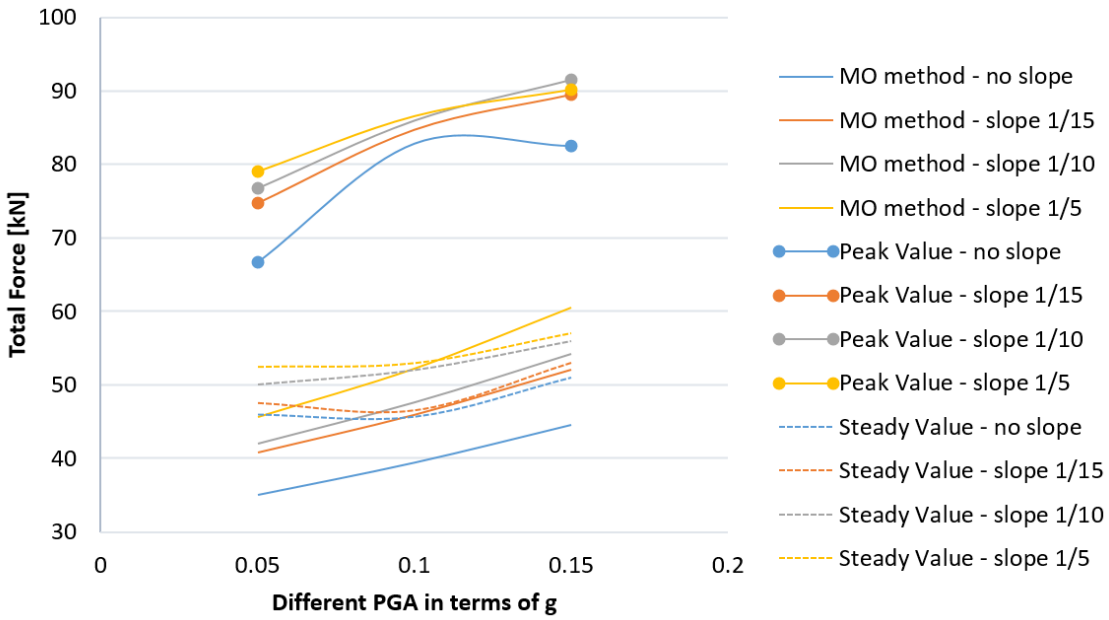

Figure 6.9: Total force variation at different backfill slope at different PGA, phi = 38° and H = 4 m

Figure 6.10 illustrates the horizontal displacement of the wall at point A and point B for different backfill slopes. As in the previous cases, the horizontal displacement of the wall also increases with the PGA levels. Also, as the slope of the backfill increases, the horizontal displacement increases for the same PGA level as well. For all the cases, the horizontal displacement is within the permissible limit up to PGA 0.1g but fails at PGA 0.15g. The displacement of the Point A (top) and Point B (base) are almost equal which explains that there is just a translation of the wall with negligible rotation.

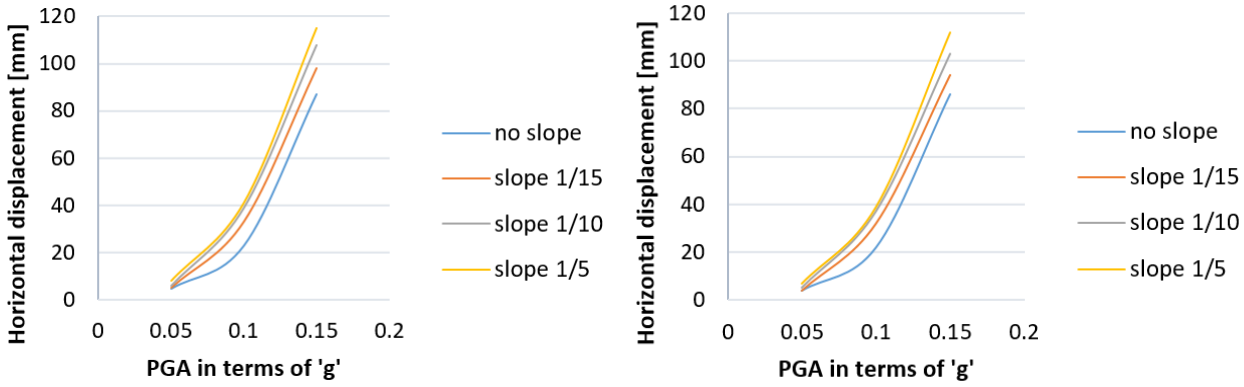

(a) Point A (top of the wall)

(b) Point B (base of the wall)

Figure 6.10: Horizontal displacement of the wall at different PGA for different slope of the backfill, phi = 38° and H = 4 m

Acceleration at different locations in the PLAXIS 2D output

From the result of the Section 6.2.1, it can be seen than there is an insignificant increase (almost equal) in peak total force from PGA of 0.1g to 0.15g which does not seem realistic, see Figure 6.4. Hence, a cross check on the input acceleration has been performed at some desired node points .i.e at the base of the wall (Point C) and at the top of the wall (Point D), see Figure 5.2 on Chapter 5.

The maximum peak acceleration for both PGA level of 0.1g and 0.15g has been obtained at the Point C. The peak accelerations were obtained as 2.3 m/s^2 and 2.6 m/s^2 for the PGA level of 0.1g and 0.15g respectively. This provides the amplification factor (S) of 2.3 and 1.77 respectively. Hence, this could have resulted in the insignificant increase of the resulting total force when the PGA level increased from 0.1g to 0.15g. If the S value of 2.3 (at the base of the wall) is taken in MO method then it will provide the total force which is in between the peak and steady value.

6.3 Conclusion and Discussion

The effect of the different parameters on the stability and performance of the gravity wall under the earthquake excitation has been studied. In all the analysis M-O method gives the value closer to the steady state value whereas the peak value was almost 30 KN higher than the M-O method.

When the friction angle of the backfill increases, the total force decreases, see Figure 6.3 while with the increase in PGA levels the total force also increases, see Figure 6.4. The horizontal displacement of the wall also holds the similar relation with the friction angle of the backfill and PGA level. The total force also increases with the increase in wall height, see Figure 6.6. For the wall height of 3.5 m, there is a huge difference between the M-O value and the peak value. As the height of the wall increases the difference between these value gets reduced and M-O gives the total force between peak and steady value for the wall height of 5 m in all the PGA levels.

In addition, the M-O method estimates the equal value of total forces for three different earthquakes but of same PGA 0.05g while the time history analysis (PLAXIS) provides different total forces for both peak and steady values, see Figure 6.8. This again highlights the fact that the MO method is conservative as a design method.

Furthermore, The total force also increases when the slope of the backfill increases as illustrated in Figure 6.9. The increment of the total force with increase in slope angle is higher for M-O method than peak and steady values. The displacement of the wall also increases with increase in backfill slope, see Figure 6.10.

The M-O method is very sensitive to the amplitude factor S. The values obtained for S at the base of the wall in the PLAXIS output is higher than it was used in the M-O method. Hence, if the S values obtained from the PLAXIS output is used in the M-O method then the total force calculated by M-O method will get closer to the PLAXIS results. The difference in the S values obtained for different PGA levels could be due to the non-linearity of the soil.

In all the cases expect for the case 5 of the Table 6.1 when the height of the wall was 5 m, the horizontal displacement of the wall is within the permissible limit ($d_r = 200\alpha S$) up to the PGA level of 0.1g. For the higher PGA level than 0.1g, the wall undergoes a very large displacement i.e. beyond permissible limit, see Figure 6.5, 6.7 and 6.10. For the case 5 when the height of the wall is 5 m, even an earthquake of PGA 0.05g is sufficient to slide the wall beyond its permissible limit as it has a very low safety factor (improper design statically) as compared

to other cases. It shows the importance of proper design during the static condition to perform better under earthquake excitation.

It can also be seen that there is just a translation of the wall and negligible rotation as the horizontal displacement at the top and base of the wall is almost equal. This may have been due the reason that the designed gravity wall has a marginal safety factor against sliding and a high safety factor against overturning. Thus, when the earthquake of higher PGA than 0.1g has been used, the wall slides laterally beyond the permissible limit and gives a shallow bearing capacity failure as similar to the Figure 5.7a of Section 5.7.

Chapter 7

Comparison of different types of retaining walls

This chapter provides the comparison of different types of retaining walls in terms of the stability and performance under the earthquake excitation. Three different types of retaining walls: gravity wall, gabion wall and cantilever wall having an equal height of 4 m are excited with four PGA levels (0.05g, 0.1g, 0.15g and 0.2g) for three different backfill friction angles (32°, 35° and 38°). The Element size, Boundary Conditions and Excitation used for all the analysis in this chapter are exactly same as described in the Chapter 5.

7.1 General

The three types of the walls have their own characteristics. The gravity walls are simple and most common to build while the gabion walls are simpler and cheaper to construct. The cantilever walls are more economic and easy to construct and it performs better by utilizing the weight of the backfill soil over

the footing slab which provides more resistance.

There has been many studies for the earthquake response of the gravity and cantilever walls but a very little research has been done for the earthquake response of the gabion wall which has raised a big question about its suitableness in the society. Hence, the comparative study of these walls under the earthquake excitation will be very useful.

7.2 Geometry

The model used for different types of the wall has a length of 200 m and height of 34 m. The retaining wall is 4 m high and located nearly at the center of the model for all the types of wall. To study the response under the earthquake excitation, 10 stress points from K to T are taken behind the wall and few node points at desired locations are taken for all the walls.

For **gravity wall**, the geometry and the stress points and nodes points are taken exactly same as in the Chapter 5, see Figure 5.1 and 5.2.

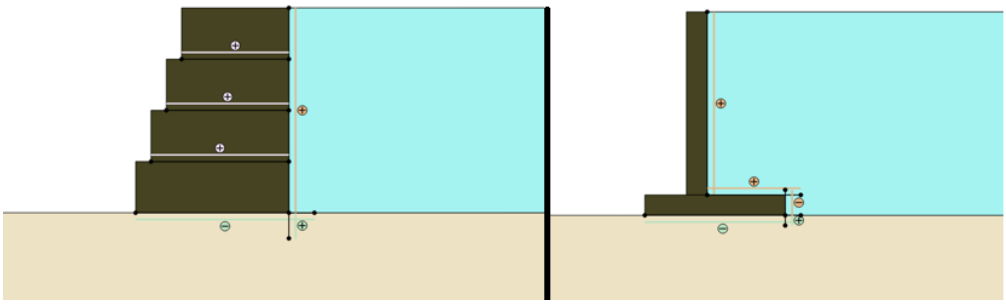

Figure 7.1: Gabion wall (left) and Cantilever wall (right)

For **gabion wall**, the geometry is shown in the Figure 7.1. Four blocks of walls with different sizes (2.1*1.0 m, 2.4*1'0 m, 2.7*1.0 m and 3.0*1.0 m) are placed

together to form a gabion wall of total height 4 m where each block has a height of 1 m. 10 different stress points (K to T) are taken behind the wall as similar to gravity wall and 5 node points (A to E) are taken from top to bottom of the wall, see Figure 7.2.

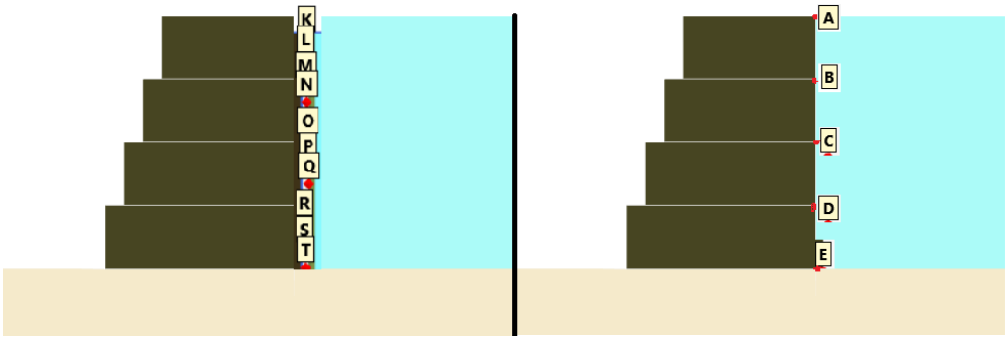

Figure 7.2: Stress points (left) and node points (right) for gabion wall

The **cantilever wall** of height 4 m is shown in the Figure 7.1. The stress points (K to T) and node points (A, B and C) taken are shown in the Figure 7.3.

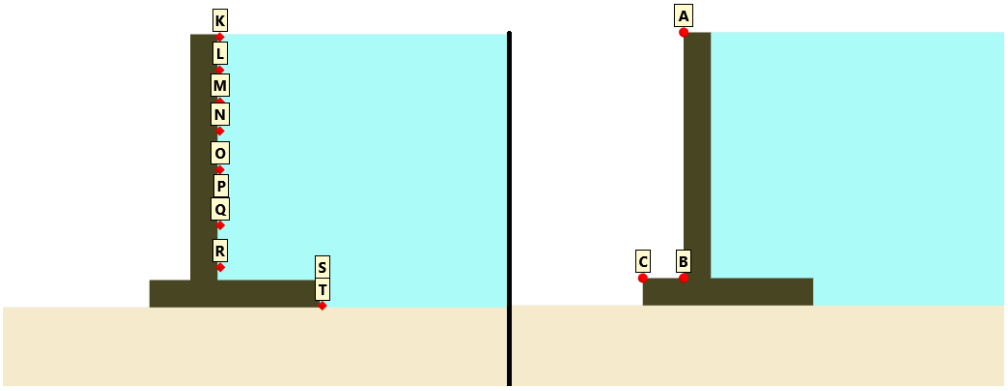

Figure 7.3: Stress points (left) and node points (right) for cantilever wall

The overall dimensions of both the gabion and cantilever wall are shown in the Figure 7.4. All the dimensions are in meters.

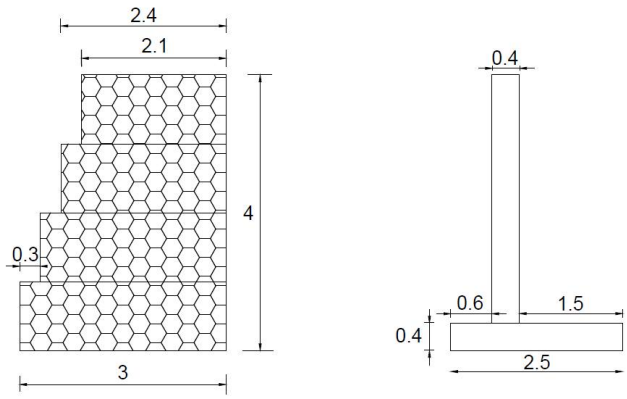

Figure 7.4: Overall dimensions (in meters) of gabion wall (left) and cantilever wall (right)

7.3 Material model and Material parameters

All the analysis are carried out with a 15-noded element in plane strain condition. A linear elastic material model has been chosen for all the types of retaining walls while Mohr-Coulomb has been chosen for the sand backfill and clay. The material properties of the clay and the sand backfill are taken same as described in the Section 5.3 of Chapter 5. The rayleigh damping of 5 % for frequencies f_1 = 0.2 Hz and f_2 = 5 Hz has been taken for all the system.

Section 5.3 describes the material properties for the gravity wall that are taken for the analysis here as well. The material properties for the cantilever wall are also taken same as that for gravity wall, see Table 7.1.

Table 7.1: Material properties for the gravity and cantilever wall

Parameters	Gravity wall	Cantilever wall
Material model	Linear elastic	Linear elastic
γ $[kN/m^3]$	24	24
E $[kPa]$	$3*10^{10}$	$3*10^{10}$
$\nu[-]$	0.15	0.15
$R_{\text{interface}}$ [-]	1	1

The gabion walls are rectangular cages made of wire mesh and filled with stones (granite, limestone etc) of appropriate size and have a porosity of 30-40 % which makes the unit weight to be ca. 17 kN/m^3. The gabion wall is a flexible structure and its shear modulus is estimated to be 75 MPa from the Equation 2.16 and Table 2.2 assuming the relative density equivalent to 60 % of sand. As the blocks can slide on top of each other, the blocks are modeled with a gabion interface with Mohr-Coulomb material model. The different parameters for modeling gabion wall have been taken from the study of Yang et al. (2010) and Lin et al. (2010). Table 7.2 illustrates the different parameters for the gabion wall and gabion interface.

Table 7.2: Material properties for gabion wall and gabion interface

Parameters	Gabion wall	Gabion interface
Material model	Linear elastic	Mohr-Coulomb
ϕ [$\circ$]	-	35
γ [kN/m^3]	17	17
G [MPa]	75	75
ν[$-$]	0.3	0.3
c [kPa]	-	1
$R_{\text{interface}}$ [-]	1	0.7

7.4 Analysis

The overall analysis performed for the comparison of different walls are summarized in the Table 7.3.

Table 7.3: Overview of all the analysis for different types of retaining wall

Case	Wall type	ϕ (°)	Height (m)	F_{safety}	α	G_{sand} (MPa)	G_{clay} (MPa)
1	Gravity wall	32	4	1.411	0.05	45	30
					0.1	36	24
					0.15	27	18
					0.2	22.5	15
2	Gravity wall	35	4	1.451	0.05	45	30
					0.1	36	24
					0.15	27	18
					0.2	22.5	15
3	Gravity wall	38	4	1.481	0.05	45	30
					0.1	36	24
					0.15	27	18
					0.2	22.5	15
4	Gabion wall	32	4	1.580	0.05	45	30
					0.1	36	24
					0.15	27	18
					0.2	22.5	15
5	Gabion wall	35	4	1.646	0.05	45	30
					0.1	36	24
					0.15	27	18
					0.2	22.5	15
6	Gabion wall	38	4	1.704	0.05	45	30
					0.1	36	24
					0.15	27	18
					0.2	22.5	15
7	Cantilever wall	32	4	1.41	0.05	45	30
					0.1	36	24
					0.15	27	18
					0.2	22.5	15
8	Cantilever wall	35	4	1.474	0.05	45	30
					0.1	36	24
					0.15	27	18
					0.2	22.5	15
9	Cantilever wall	38	4	1.521	0.05	45	30
					0.1	36	24
					0.15	27	18
					0.2	22.5	15

7.5 Results

Figure 7.5 shows the variation of the total force with friction angle of the backfill for different walls. The graphs are plotted for four different PGA levels. It can be seen that for all the wall types the total force at peak and steady state decreases with the increase in the backfill friction angle at all PGA levels. The total force at peak state for the gabion wall is similar to the gravity wall and have the values always lower than the gravity wall. At peak state, the cantilever wall has the least total force among the three alternatives at all PGA levels.

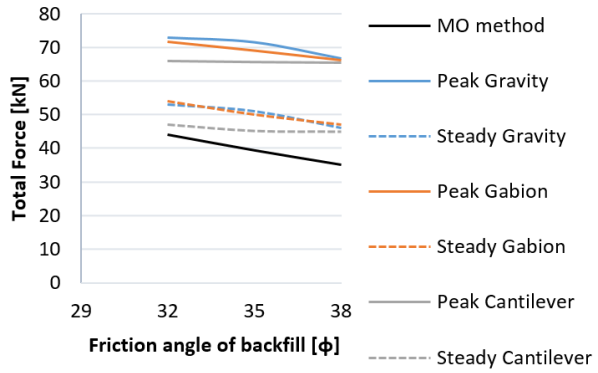

(a) PGA 0.05g

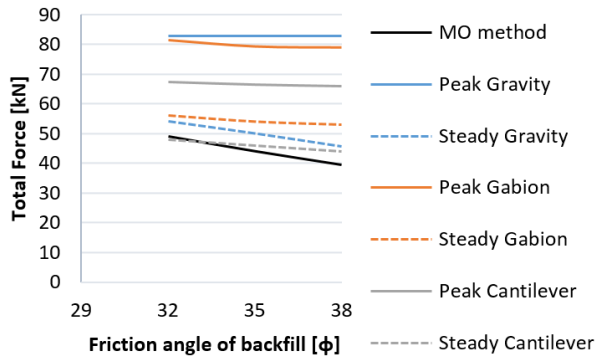

(b) PGA 0.1g

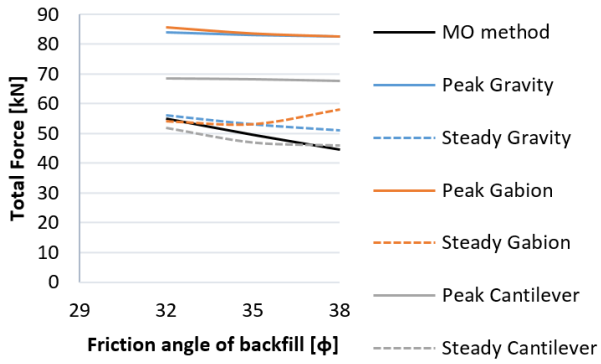

(c) PGA 0.15g

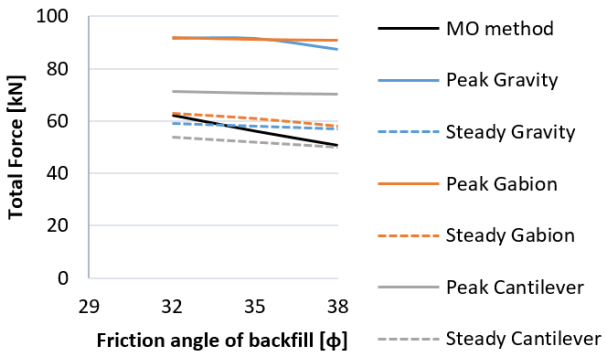

(d) PGA 0.2g

Figure 7.5: Total Force Vs Friction angle of the backfill for different walls of height 4 m

At steady state, the total force for all the walls converges into the same value when the friction angle of the backfill increases and also the values are equivalent to the total force estimated from the M-O method.

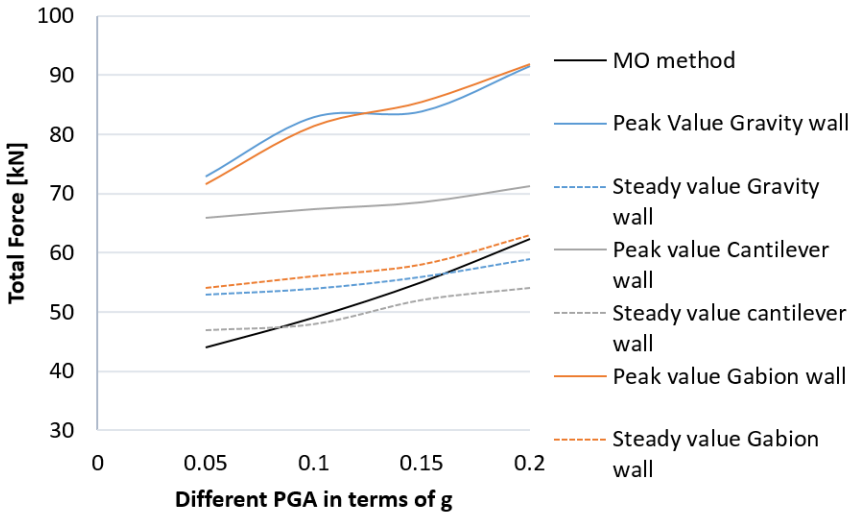

(a) phi = 32°

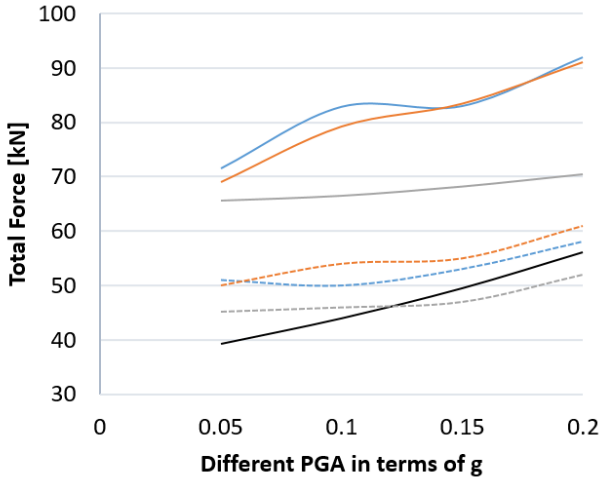

(b) phi = 35°

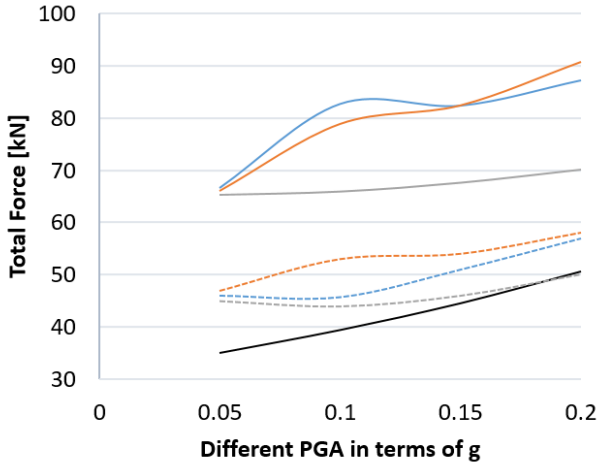

(c) phi = 38°

Figure 7.6: Total Force Vs different PGA at different friction angle of the backfill for H = 4 m

Figure 7.6 shows the variation of total force at different PGA levels for different types of wall. For all the cases, the total force at both peak and steady state increases with the increase in PGA levels however, the increment of the total

force at peak state is quite insignificant in cantilever wall as compared to the gravity and gabion wall. The total force from M-O method is again more consistent with the steady state value for all wall types.

The displacement of the different retaining walls has also been taken from the analysis. Figure 7.7a shows the displacement of the gabion wall at five different points for the backfill friction angle of 35°. The point A is at the top of the wall whereas point E is at the base, shown in Figure 7.2. It can be seen the displacement of the wall increases as the PGA level increases. The horizontal displacement at the top is more than that at the base but the difference in the displacement between the top and the base of the wall is negligible. Hence, the gabion boxes are not sliding over each other rather acting like a rigid block.

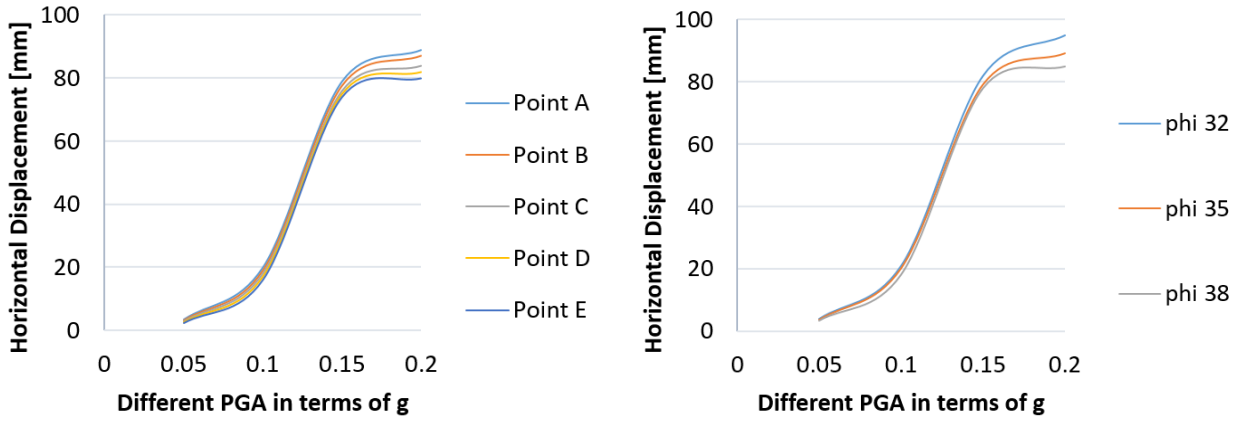

(a) Horizontal displacement at different points for phi = 35°

(b) Horizontal displacement of Point A at different friction angle of backfill

Figure 7.7: Horizontal displacement of the gabion wall

Figure 7.7b shows the horizontal displacement of the gabion wall at point A for different friction angle of the backfill. It can be seen that the horizontal displacement of the wall decreases as the backfill friction angle increases but there is a very slight variation in the displacement. Hence, the horizontal

displacement of the wall is mainly associated with the different PGA levels and the horizontal displacement of the different retaining walls at different PGA levels will be shown only for a particular friction angle.

The comparison of the horizontal displacement of the different types of retaining walls is presented in the Figure 7.8. The horizontal displacement is shown for the four PGA levels (0.05g, 0.1g, 0.15g and 0.2g) and the backfill friction angle of 35°. It can be seen that there is a large increment in the horizontal displacement of all the walls when the PGA level increases from 0.1g to 0.15g.

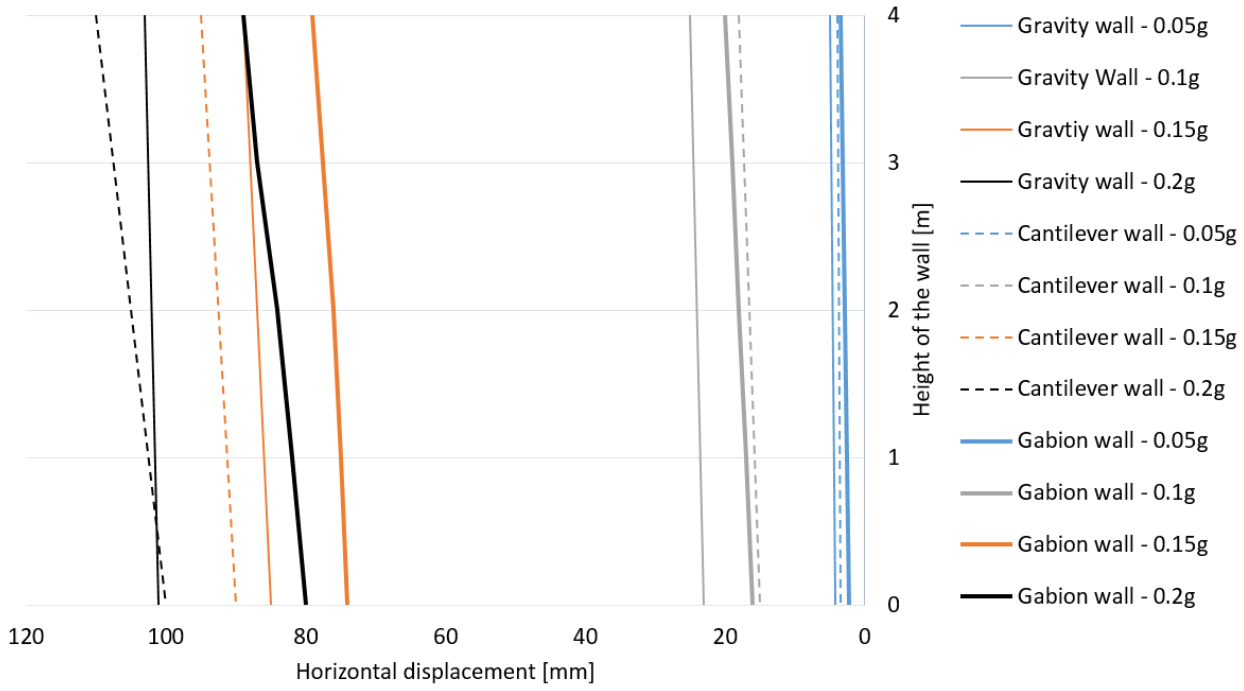

Figure 7.8: Horizontal displacement of different types of walls for backfill friction angle 35°

It can be also seen that there is just a horizontal translation of all the walls. Even though the walls are trying to rotate in the counter-clock direction, there is a very minimal rotation which can be considered as negligible. In all the analysis, the gabion wall has a lower displacement than both the gravity and cantilever

wall and the gravity wall has displaced the most at all PGA levels.

7.6 Conclusion and Discussion

The retaining walls are designed to restrain against the lateral earth thrust while keeping its original position intact. Hence, the study of stability and performance of the different types of walls have been performed by the comparison of the total force on the wall and the displacement of the wall due to the earthquake excitation.

For all the types of retaining walls, the total force decreases as the backfill friction angle increases while the total force increases as the PGA level increases, see Figure 7.5 and 7.6. The total force at peak state is similar for the gravity and gabion wall. The gabion wall has lower total force at peak state than the gravity wall in all the cases as it is more flexible amongst the two. The total force at peak state for cantilever wall is significantly low and has the values closer to the M-O method than other two walls.

The horizontal displacement of all the retaining walls increases with the increase in PGA level while there is not much variation of the displacement with the change in the backfill friction angle, even though, the displacement decreases slightly with the increase in backfill friction angle, see Figure 7.7. For all the PGA levels, the gabion wall has the least displacement as compared to other walls while the gravity wall has the largest displacement. The gabion wall showed a behavior of a rigid block up to the PGA level of 0.15g but a slight shift of the top of the gabion boxes can be seen at 0.2g PGA, see Figure 7.8.

Both the gravity and gabion wall have a wide base of 3 m which gives the very large section for both the walls. The volume of the material used for the construction of these walls would also be very larger than the cantilever wall.

In conclusion, for a PGA level up to 0.2g and height of 4 m wall, the cantilever wall provides better stability and performance under the earthquake excitation. Hence, the cantilever wall could be the most appropriate solution among the three types of retaining walls if the cost effectiveness, construction easiness and material volume are also considered. Furthermore, the gabion wall also showed good anti-seismic characteristics and performed better than the gravity wall under the earthquake excitation.

Chapter 8

Summary and Conclusions

The earthquake response of the different types of retaining walls has been studied in this thesis. The retaining walls studied are gravity wall, gabion wall and cantilever wall. The comparative study of these walls has been done in terms of their stability and performance under the earthquake excitation. All the analysis have been carried out in the finite element program, PLAXIS 2D (version 2015.02).

The analysis of different boundary conditions has been performed prior to the analysis on the retaining walls. Two different tests have been carried for that purpose. This analysis was helpful to select the best boundary condition among the different alternatives and to use it properly in order to get a better output for the further analysis. The tests were equally consistent with both the *free lateral boundary* and *tied boundary* but the *free lateral boundary* was chosen in order to save the time in model construction and analysis.

The verification of the numerical model with the physical shake table test has

been relevant in verifying and analyzing the performance of the numerical model. Both Mohr-Coulomb and Hardening Soil model have been used to model the sand. The results from both soil model have been compared to the actual shake table test results. It showed that the results were more consistent with the Mohr-Coulomb model.

Furthermore, the effect of different parameters on the stability and performance of the retaining wall have been analyzed. For that, a gravity wall with a sand backfill and a clay underneath was taken. Four PGA levels (0.05g, 0.1g, 0.15g and 0.2g) were used to analyze the effect of different parameters which were different height of the walls (3.5, 4 and 5 m), different friction angle of the backfill (32°, 35° and 38°) and different backfill slope (no slope, 1/15, 1/10 and 1/5). In general, the total force and the displacement of the wall increase with the increase in PGA level and decreases with the increase in friction angle of the backfill. For a particular PGA level, the total force and the displacement of the wall increase with the increase in height of the wall or the backfill slope. In all the analysis, the total force calculated from the M-O method was closer to the total force at steady state while the total force at peak state was always ca. 30 KN higher than the M-O value. Also, for the three different earthquakes of same PGA level of 0.05g, the M-O estimated the same total force while the PLAXIS 2D resulted in different total forces. Hence, it highlights the fact that the M-O method is conservative as a design method. In addition, there was just a translation of the wall with negligible rotation at all PGA levels. The possible reason could be due to the fact that the gravity wall had a marginal safety factor against sliding whereas a very high safety factor against overturning and when

an earthquake of PGA higher than 0.1g was applied, the wall displaced beyond its permissible limit and resulted in a shallow bearing capacity failure.

Finally, the study of stability and performance of the different types of walls have been performed by the comparison of the total force on the wall and the displacement of the wall due to the earthquake excitation. In all the analysis, the total force at peak state was similar in the gravity and gabion wall but the total force at peak state was lower in gabion wall as it is more flexible than the gravity wall. The total force at peak state for cantilever wall was significantly low as compared to the other walls. The horizontal displacement of the wall was least for the gabion wall at all PGA levels. The displacement was maximum for the gravity wall whereas the cantilever wall displaced similar to the gabion wall up to the PGA level 0.1g but at higher PGA level (0.15g and 0.2g), the displacement was a bit more than the gabion wall. Also, there was a slight shift on the gabion boxes at the top for the PGA level of 0.2g. Hence, for a retaining wall of height 4 m and the PGA level up to 0.2g, the cantilever wall provides the better stability and performance under the earthquake excitation. In addition, considering the cost effectiveness, construction easiness and material volume of the cantilever wall, it could be the most appropriate solution among the three types of retaining walls. Furthermore, the gabion wall performed better than the gravity wall under the earthquake excitation.

Chapter 9

Recommendations and future work

As it was seen from the results that the retaining wall displaced horizontally beyond its permissible limit for the PGA level higher than 0.1g. This was probably due the fact that the designed wall had a marginal safety factor against sliding and a high safety factor against overturning. Hence, a better design of the retaining wall at static condition could be done.

All the analysis have been performed up to the PGA level of 0.2g but the strong earthquakes generally have higher PGA than 0.2g. For the future work, it is recommended to perform the analysis at higher PGA level than 0.2g as well. Also, the advanced soil models such as HS small model can be used which assigns the stress dependent stiffness and the material damping itself.

Furthermore, for the better comparison of the different types of retaining walls under the earthquake excitation, more parametric studies considering the different height of the walls and higher PGA levels should be performed.

Bibliography

Aarhaug, O. (1984). *Geoteknikk og fundamentering*. NKI-forlaget.

Agostini, R., Cesario, L., Conte, A., and SpA, O. M. (1987). *Flexible gabion structures in earth retaining works*.

Azad, A., Yasrobi, S. S., and Pak, A. (2008). Seismic active pressure distribution history behind rigid retaining walls. *Soil Dynamics and Earthquake Engineering*, 28(5):365–375.

Brinkgreve, R., Engin, E., and Engin, H. (2010). Validation of empirical formulas to derive model parameters for sands. *Numerical methods in geotechnical engineering (eds T. Benz and S. Nordal)*, pages 137–142.

Brinkgreve, R., Swolfs, W., and Engin, E. (2014a). *PLAXIS 2D General Information*.

Brinkgreve, R., Swolfs, W., and Engin, E. (2014b). *PLAXIS 2D Material Model*.

Brinkgreve, R., Swolfs, W., and Engin, E. (2014c). *PLAXIS 2D References*.

Cai, Z. and Bathurst, R. (1997). Seismic-induced permanent displacement of geosynthetic-reinforced segmental retaining walls. *Canadian Geotechnical Journal*, 33(6):937–955.

Cavallaro, A., Maugeri, M., and Mazzarella, R. (2001). Static and dynamic properties of leighton buzzard sand from laboratory tests.

Chopra, A. K. (2012). *Dynamics of structures: Theory and Applications of Earthquake Engineering*, volume 4. Prentice Hall New Jersey.

Clough, R. W. and Penzien, J. (1993). *Dynamics of structures*, volume 2. McGraw-Hill Inc.

Cook, R., Malkus, D., Plesha, M., and Witt, R. (2001). *Concepts and Applications of Finite Element Analysis*. John Wiley & Sons.

Gazetas, G., Psarropoulos, P., Anastasopoulos, I., and Gerolymos, N. (2004). Seismic behaviour of flexible retaining systems subjected to short-duration moderately strong excitation. *Soil Dynamics and Earthquake Engineering*, 24(7):537–550.

Geotechnical Division NTNU (2014). *Theoretical Soil Mechanics*. NTNU Geotechnical Division.

Gjelseth, S. L. (2013). *Numerisk og analytisk analyse av støttekonstruksjoner ved jordskjelvbelastning*. NTNU Masteroppgave.

Green, R. A., Olgun, C. G., Ebeling, R. M., and Cameron, W. I. (2003). Seismically induced lateral earth pressures on a cantilever retaining wall. *Earthquake Engineering*, pages 946–955.

Hashash, Y. M. and Park, D. (2002). Viscous damping formulation and high frequency motion propagation in non-linear site response analysis. *Soil Dynamics and Earthquake Engineering*, 22(7):611–624.

Hudson, M., I. I. and Beirkae, M. (1994). *QUAD4M User's manual.* .

Kloukinas, P., Penna, A., di Santolo, A. S., Bhattacharya, S., Dietz, M. S., Dihoru, L., Evangelista, A., Simonelli, A. L., Taylor, C. A., and Mylonakis, G. (2014). Experimental investigation of dynamic behavior of cantilever retaining walls. pages 477–493.

Kramer, S. L. (1996). *Geotechnical earthquake engineering*. Pearson Education India.

Lin, D.-G., Lin, Y., and Yu, F. (2010). Deformation analyses of gabion structures. *INTERPRAEVENT 2010*, pages 512–526.

Mononobe, N. and Matsuo, H. (1929). On the determination of earth pressures during earthquakes. In *Proceedings, World Engineering Congress*, volume 9, pages 179–187.

Murthy, V. (2002). *Geotechnical engineering: principles and practices of soil mechanics and foundation engineering*. CRC Press.

Nordal, S. (2015). *Geotechnical Engineering Advanced Course*. NTNU Geotechnical Division.

Okabe, S. (1926). General theory of earth pressure. *Journal of the Japanese Society of Civil Engineers*, 12(1):311.

Ostadan, F. (2005). Seismic soil pressure for building walls: An updated approach. *Soil Dynamics and Earthquake Engineering*, 25(7):785–793.

Penna, A. (2012). Dyncrew project (ta-1) meeting: data analysis results.

Plaxis bv (2015). On the use of dynamic boundary conditions. http://kb.plaxis.com/tips-and-tricks/use-dynamic-boundary-conditions.

Psarropoulos, P., Klonaris, G., and Gazetas, G. (2005). Seismic earth pressures on rigid and flexible retaining walls. *Soil Dynamics and Earthquake Engineering*, 25(7):795–809.

Punmia, B. and Jain, A. K. (2005). *Soil mechanics and foundations*. Firewall Media.

Ramli, M., Karasu, T., and Dawood, E. T. (2013). The stability of gabion walls for earth retaining structures. *Alexandria Engineering Journal*, 52(4):705–710.

Seed, H. B. and Idriss, I. M. (1970). Soil moduli and damping factors for dynamic response analyses.

Veletsos, A. S. and Younan, A. H. (1997). Dynamic response of cantilever retaining walls. *Journal of Geotechnical and Geoenvironmental Engineering*, 123(2):161–172.

Witasse, R. (2012). Workshop on the use of plaxis 2d for earthquake geotechnical analysis.

Yang, G.-L., Huang, X.-J., and Lin, Y.-L. (2010). Test study on engineering properties of gabion structures. In *Advances in Environmental Geotechnics*, pages 805–811. Springer.

Appendix A

Acronyms

EC Eurocode

HS Hardening Soil

MC Mohr Coulomb

M-O Mononobe-Okabe

PGA Peak ground acceleration

TH Time history

Appendix B

Appendix

Seismic Zones (EC 8-1 NA.3.2.1)

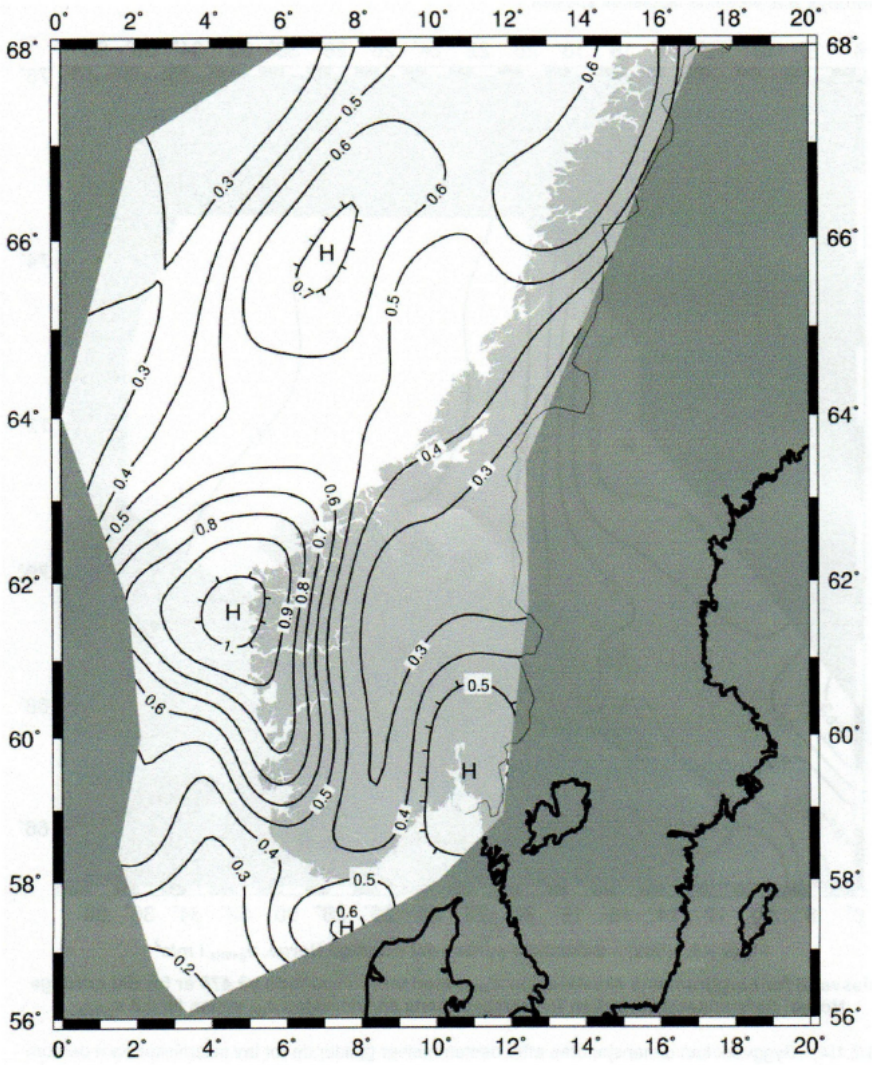
0° 2° 4° 6° 8° 10° 12° 14° 16° 18° 20°
68° 66° 64° 62° 60° 58° 56°
H
H
H
H
0.3
0.4
0.5
0.6
0.7
0.8
0.9
1.

Table B.1: Ground Types (Table NA.3.1 i EC 8-1)

Ground type	Description of stratigraphic profile	Parameters		
		$v_{s,30}$ (m/s)	N_{SPT} (blows/30cm)	c_u (kPa)
A	Rock or other rock-like geological formation, including at most 5 m of weaker material at the surface.	> 800	–	–
B	Deposits of very dense sand, gravel, or very stiff clay, at least several tens of metres in thickness, characterised by a gradual increase of mechanical properties with depth.	360 – 800	> 50	> 250
C	Deep deposits of dense or medium-dense sand, gravel or stiff clay with thickness from several tens to many hundreds of metres.	180 – 360	15 - 50	70 - 250
D	Deposits of loose-to-medium cohesionless soil (with or without some soft cohesive layers), or of predominantly soft-to-firm cohesive soil.	< 180	< 15	< 70
E	A soil profile consisting of a surface alluvium layer with v_s values of type C or D and thickness varying between about 5 m and 20 m, underlain by stiffer material with v_s > 800 m/s.			
S_1	Deposits consisting, or containing a layer at least 10 m thick, of soft clays/silts with a high plasticity index (PI > 40) and high water content	< 100 (indicative)	–	10 - 20
S_2	Deposits of liquefiable soils, of sensitive clays, or any other soil profile not included in types A – E or S_1			

Table B.2: Amplification factor S for different ground types (Table NA.3.3 i EC 8-1)

Grunntype	S
A	1,0
B	1,25
C	1,4
D	1,6
E	1,7

Table B.3: Selection of Seismic Classes (Table NA.4(902) i EC 8-1)

Byggverk	I	II	III	IV
Byggverk der konsekvensene av sammenbrudd er særlig store				X[1)]
Viktig infrastruktur: sykehus, brannstasjoner, redningssentraler, kraftforsyning og lignende			(X)	X
Høye bygninger, mer enn 15 etasjer		(X)	X	
Jernbanebruer [2)]			X	(X)
Veg- og gangbruer [2)]		(X)	X	(X)
Byggverk med store ansamlinger av mennesker (tribuner, kinosaler, sportshaller, kjøpesentre, forsamlingslokaler osv.)		(X)	X	
Kaier og havneanlegg		X	(X)	
Tårn, master, skorsteiner, siloer	(X)	X	(X)	
Industrianlegg		X	(X)	
Skoler og institusjonsbygg		(X)	X	
Kontorer, forretningsbygg og boligbygg		X	(X)	
Småhus, rekkehus, bygg i én etasje, mindre lagerhus osv.	X	(X)		
Landbruksbygg	(X)			
Fiskerihavner	(X)			
Kaier og fortøyningsanlegg for sport og fritid	(X)			

[1)] For byggverk der konsekvensene av sammenbrudd er særlig store, for eksempel ved atomreaktorer og lagringsanlegg for radioaktivt avfall, store dammer og marine konstruksjoner bør jordskjelvrisikoen vurderes spesielt, eventuelt basert på en risikoanalyse.

Lagertanker for flytende gass og store hydrokarbonførende rørledninger over land er behandlet i NA til NS-EN 1998-4.

[2)] Se veiledende tabell for valg av seismisk klasse for bruer i NA til NS-EN 1998-2.

Table B.4: Importance factor as per seismic class (Table NA.4(901) i EC 8-1)

Seismisk klasse	γ_I
I	0,7
II	1,0
III	1,4
IV	2,0

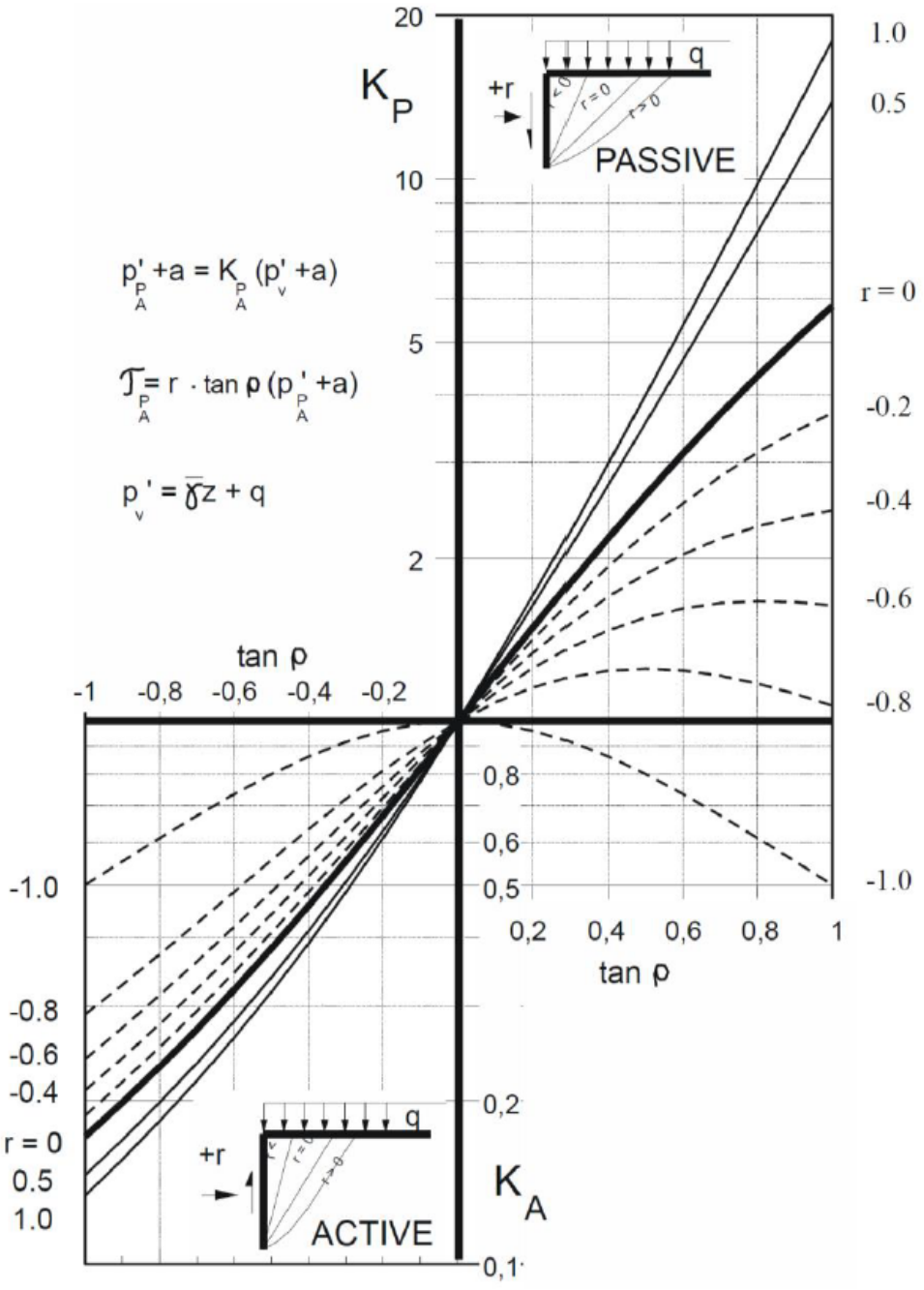

Figure B.1: Earth pressure Coefficients Geotechnical Division NTNU (2014)

Table B.5: Typical Interface Friction angles Kramer (1996)

Interface Materials		Interface Friction Angle δ
Mass concrete against:	clean sound rock	25
	clean gravel, gravel–sand mixtures, coarse sand	29–31
	clean fine to medium sand, silty medium to coarse sand, silty or clayey gravel	24–29
	clean fine sand, silty or clayey fine to medium sand	19–24
	fine sandy silt, nonplastic silt	17–19
Formed concrete against:	medium-stiff and stiff clay and silty clay	17–19
	clean gravel, gravel–sand mixture, well-graded rock fill with spalls	22–26
	clean sand, silty sand–gravel mixture, single-size hard rock fill	17–22
Steel sheet piles against:	silty sand, gravel, or sand mixed with silt or clay	17
	fine sandy silt, nonplastic silt	14
	clean gravel, gravel–sand mixture, well-graded rock fill with spalls	22
	clean sand, silty sand–gravel mixture, single-size hard rock fill	17
	silty sand, gravel, or sand mixed with silt or clay	14
	fine sandy silt, nonplastic silt	11

Table B.6: Amplitude factors for different Boundary conditions

Frequency (f)	ω	ξ (%)	A	r=w/w_n	Boundary Types			
					Viscous, A	Freefield, A	Tied DoF, A	Free lateral
0	0	infinity	1	0	1	1	1	1
0.5	3.141593	0.05	1.412038	0.5	1	1.442	1.448	1.49
1	6.283185	0.03182	20.00691	1	3.248	9.604	18.352	18.342
1.3	8.168141	0.03	2.182905	1.3	4.554	1.328	2.02	2.032
1.5	9.424778	0.03	1.4072	1.5	2.248	1.894	1.328	1.342
2	12.56637	0.03	0.995588	2	0.962	1.14	0.98	0.99
2.5	15.70796	0.033	1.391046	2.5	1.546	2.274	1.452	1.458
3	18.84956	0.038	5.584384	3	3	5.344	5.044	5.088
3.5	21.99115	0.041	1.347409	3.5	1.30508475	1.26836158	1.22	1.224
4	25.13274	0.044	0.963845	4	1.10571429	1.33050847	0.968926554	1.011299435
4.5	28.27433	0.047	1.279978	4.5	1.306	1.34	1.302	1.224
5	31.41593	0.05	2.546479	5	1.1	1.1	error	error

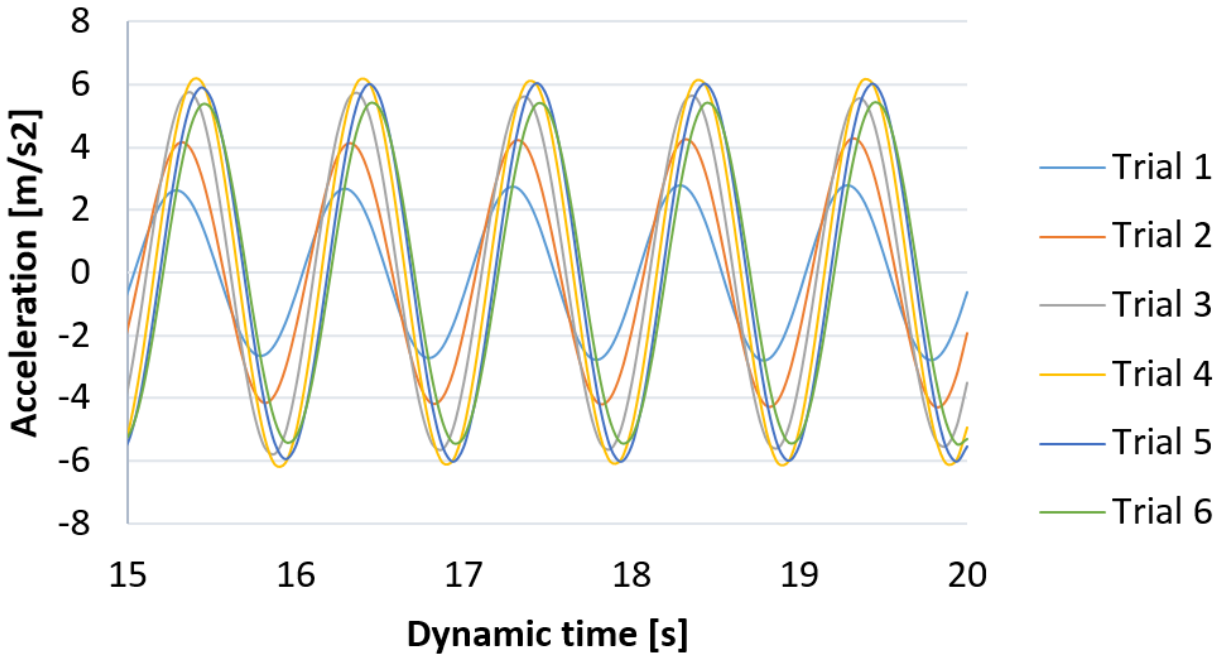

Figure B.2: Acceleration at Point A for different slope test for slope steepness of 1/2 and slope height of 30 m

Table B.7: Total force calculation for different walls

phi backfill	α	Total Force (kN)						
		MO Method	Gravity Wall		Cantilever Wall		Gabion Wall	
			Max	Steady	Max	Steady	Max	Steady
32	0.05	43.98	72.88	53	65.9	47	71.66	54
32	0.1	49.03	82.88	54	67.36	48	81.46	56
32	0.15	55.05	83.85	56	68.52	52	85.54	58
32	0.2	62.37	91.49	59	71.23	54	91.9	63
35	0.05	39.31	71.5	51	65.6	45.21	69	50
35	0.1	44	82.83	50	66.5	46	79.24	54
35	0.15	49.53	82.97	53	68.23	47	83.45	55
35	0.2	56.15	91.93	58	70.52	52	91.1	61
38	0.05	35.01	66.7	46	65.4	45	66.1	47
38	0.1	39.38	82.8	45.7	66	44	78.9	53
38	0.15	44.49	82.47	51	67.65	46	82.45	54
38	0.2	50.56	87.32	57	70.1	50	90.76	58